Staatliche
Materialprüfungsanstalt
Universität Stuttgart

MPA
STUTTGART

IAEA Specialists' Meeting

on

"Irradiation Embrittlement and Ageing
of Reactor Pressure Vessels"

27 - 29 May 1987
Philadelphia, Pa USA

Assurance of the Pressure Vessel Integrity with Respect to Irradiation Embrittlement - Activites in the Federal Republic of Germany

K. Kussmaul
J. Föhl
T. Weissenberg

Staatliche Materialprüfungsanstalt (MPA)
Universität Stuttgart
Stuttgart, Germany F.R.

May 1987

C/2

"Assurance of the Pressure Vessel Integrity with Respect to Irradiation Embrittlement"

Activities in the Federal Republic of Germany (FRG)

K. Kussmaul, J. Föhl, T. Weissenberg

Abstract

Safety research of light water reactor pressure vessels in the Federal Republic of Germany is presently focussed on validation programs based on fracture mechanics concepts, and which study irradiation embrittlement, pressurized thermal shock and cyclic crack growth under operating conditions. Crack initiation values derived from the J_R-curve could be confirmed as reliable material property to enable transferability of results from small specimen testing to complex structures.

For validation of irradiation surveillance practice trepans were taken from a forged shell course of a commercial reactor pressure vessel wall to compare material degradation of the wall with that of the surveillance specimens and to establish properties through the thickness of the wall. The experimentally determined amount of reduction in toughness of the vessel wall depends strongly on the orientation of the specimens with respect to the main forging direction of the hot formed material. The degradation of the material with respect to transition temperature shift and upper shelf energy drop in Charpy impact tests could not be predicted conservatively on the basis of the existing trend curves in the US Code of Federal Register. On the other hand the degree of embrittlement measured in short distances from the inner to the outer surface of the vessel wall is much less and therefore less important than assessed in the proposed revision of the US Code.

Archive material representing the shell course from which the trepans were taken was irradiated in test reactors in the US and the UK. The irradiated archive material shows a lower degradation than the vessel wall of the commercial reactor.

Key words

fracture mechanics, irradiation embrittlement, pressurized thermal shock, cyclic crack growth, neutron exposure, light water reactor, ferritic steel, pressure vessel steel.

Introduction

The previously reported investigations on validation of the integrity of light water reactor pressure vessels have been continued with enhanced efforts. The validation principle relies on verification and validation of calculation codes and mechanistic fracture mechanics, and probabilistic evaluation of non-destructive examination methods. A challenging trial on in-service degradation of pressure vessel wall material of a nuclear power plant is under way. Trepans were taken from the Gundremmingen A (KRB-A) reactor pressure vessel which was shut down in 1977 after 10 years of operation. Investigations with this material and unirradiated reference material are being performed within the scope of a cooperation program between the Staatliche Materialprüfungsanstalt, Universität Stuttgart (MPA), United States Nuclear Regulatory Commission (US NRC), Materials Engineering Associates (MEA), USA, and Atomic Energy Research Establishment Harwell (AERE-Harwell), UK.

To evaluate component failure behavior over a wide toughness range, materials have been selected and treated to achieve properties representing neutron embrittled material state including "worst case" consideration. These materials are available in large quantities and enable testing of large specimens with complex stress fields with respect to initiation and arrest toughness even under pressurized thermal shock condition. The experiments are aimed at providing a general validation of the computational methods and the fracture mechanics concepts on the basis of a modified J-Integral evaluation method and to demonstrate the underlaying principle for transferability.

With regard to irradiation and corrosion assisted crack growth a cyclic experiment was carried out in the VAK power reactor (Boiling Water Reactor) to apply all operational parameters coincidentally. At this time, however, only preliminary results are available.

Safety Assessment According to Present-Approach

The safety assessment of a reactor pressure component is based on five principles, which are quality through production, multiple parties testing, worst case simulation in R & D programs, continuous in-service monitoring and documentation and validation of Codes, fracture mechanics and non-destructive examinations /1/. The first principle is supported by the four other principles which serve as independent redundancies. This strategy provides a sufficiently large safety margin even if there is no guarantee for a 100% effectiveness of each single redundancy.

The most common tests to determine material toughness in a wide temperature range are the Charpy V-notch impact test and the drop-weight test. From these two tests the brittle-ductile transition temperature RT_{NDT} is derived. With the help of the experimentally evaluated fracture toughness reference curve K_{IR} /2, 3, 4/ a lower bound fracture toughness curve for brittle failure can be established, Fig. 1. In comparison with the calculated loading situation of the component in terms of stress intensity a quantitative safety margin with respect to temperature and load can be given on this basis, however, only in the linear-elastic fracture mechanics regime. World wide research work has demonstrated the conservatism of this procedure. Extensive testing in the FRG using CT-specimens up to 500 mm thickness has essentially confirmed the K_{IR}-curve as a lower bound even for degraded materials /5/.

In the elastic-plastic regime the safety against ductile failure is judged from the Charpy upper shelf energy only which does not give quantitative fracture toughness properties and thus no quantitative safety margin against ductile failure or stable crack growth. However, the required minimum upper shelf energy of 68 J (50 ft-lb) has been developed from practical experience in conventional power plant systems and chemical plants. Due to the complex loading situation during pressurized thermal shock the necessity arose to provide quantitative data also for this regime in order to verify the minimum toughness requirements and to define lower bound values.

For design purposes a prediction of the degree of material toughness degradation has to be made which has to be monitored during operation through surveillance programs. The prediction is performed on the basis of trend curves /6, 7, 8/ for both the shift in transition temperature (ΔT_{41J}) and the drop in Charpy upper shelf energy (ΔUSE) as indicated in Fig. 1. With this predicted material state an adjusted fracture toughness curve can be assessed.

The main goal of all the irradiation programs is to either confirm these trend curves for a wide range of materials or to establish modified curves as it is the case with the proposed Rev. 2 of US Reg.Guide 1.99 /8/.

Fracture Mechanics Properties

The given limitations in specimen size for irradiation surveillance programs have forced on the one hand to proceed with the development of quantitative fracture toughness properties from Charpy testing and on the other hand to focus on test and evaluation techniques using small fracture mechanics specimens, e.g. 10 mm thick compact tension specimen CT-10 /9/.

The J-Integral has been proven to be a reliable measure to describe the material behavior in the vicinity of the crack tip. Especially the stable extension of the crack beyond the initiation load can be quantifie as a function of the J-Integral. From the most commonly used unloading compliance test technique to establish a crack resistance curve, crack initiation values are derived by means of different evaluation methods. It becomes evident that the slope of the crack resistance curve (J_R-curve) depends on specimen size and geometry, Fig. 2. Using the ASTM procedure or recommended modifications of that /10, 11/, crack initiation ($J_{0,15}$, $J_{0,2}$) cannot be evaluated independently from specimen size and geometry. If the blunting line, however, is evaluated on the basis of the experimentally determined stretch zone and the J_R-curve is fitted by an adequate polynomial, size and geometry independent crack initiation values J_i (physical initiation values) can be obtained /12, 13/, Fig. 3. In some cases the electrical potential drop method leads to initiation values as low as J_i, whereas from the ASTM procedure values result which can be almost double as high depending on material toughness and specimen geometry.

Transferability of Fracture Mechanics Results

Tremendous efforts have been made to demonstrate the transferability of results for the prediction of component failure on the basis of results from small specimen testing. Large scale specimen testing has been intensified in the past at MPA using for example large scale Double Edge Notched Tension specimens (DENT) of materials with different toughness levels. By comparing different fracture toughness properties it becomes obvious that the crack initiation toughness J_i can be used as transferability criterion for materials in the toughness range from 40 J to 200 J Charpy upper shelf energy. When the experimentally determined J value of the DENT specimen reaches the level of J_i obtained from CT-specimens testing crack, initiation occurs in the large scale specimen experiment; this can be detected by acoustic emission and electrical potential drop measurements and be confirmed by fractography. The results thus obtained show that J_i determined with CT specimens is in good agreement with the initiation value in the DENT specimen, Fig. 4, which is not the case if J_{Ic} (ASTM procedure) or other criteria are applied. The comparison of the calculated load for the initiation point of the DENT specimen with the experimental findings demonstrates that the applied 2 D elastic-plastic calculation of J (plain strain) for the structure and the used fracture toughness value J_i as well are the reliable basis for an adequate fracture mechanics concept.

Although the load at instability and the amount of stable crack growth /5, 14/ depend on the ability of the materials to yield under the applied constraint, failure (instability) of the DENT specimens occurred on a load at initiation which is typical for deeply notched DENT specimens due to the constraint. This behavior was observed for low as well as for high upper shelf Charpy energy materials. Besides a limited amount of stable crack the remaining fracture surface was of a macroscopically brittle appearence.

The large amount of data from Charpy and fracture toughness testing of a variety of materials has provided the basis for a correlation in the Charpy upper shelf regime between upper shelf energy and crack initiation J_i, Fig. 5. This is especially useful for the assessment of fracture toughness properties from surveillance programs where usually only Charpy specimens are available.

Validation of Surveillance Results

Surveillance programs to monitor the degradation of the reactor pressure vessel belt-line material due to neutron irradiation are being performed in each commercial reactor. Irradiation takes place under elevated neutron flux with a lead factor varying from about 2 to 10 or even 15 depending on the vessel design. This involves deviation from the parameters to which the vessel wall is subjected concerning flux density - time for damage and recovery and thus the damage equilibrium - and the neutron energy spectrum.

To validate the surveillance practice according to ASTM E 185 and KTA 3203 a challenging trial was started in cooperation with US NRC, MEA, AERE-Harwell and MPA Stuttgart. US NRC has managed and financed the removal of trepans of the base material (forging) from the reactor pressure vessel of the boiling water reactor Gundremmingen unit A (KRB-A) in Germany, Fig. 6, and has provided those trepans to MPA for investigation. In addition MPA has arranged the removal of trepans from weld material of a near core and off core circumferential weld, Fig. 7. The reliability of surveillance practice will be checked by comparing trepan material with the already existing surveillance results and surveillance specimens still untested and with archive material, which was stored at General Electric Company (GE) - the designer of the plant - and was provided by US NRC. In addition archive material is irradiated in test reactors in the USA and UK so that a wide scenarium of methods is considered in the validation program, Fig. 8. However, the basis for comparison, is rather limited at present since in the surveillance program of KRB-A only Charpy specimens and tensile specimens (Ø 6 mm) from longitudinal direction were investigated. Because of the importance of the results investigation are under way to further confirm the authenticity of the archive material.

The plant KRB-A was designed for a power of 252 MW (el) and was taken out of service after 10 years of operation in 1977. The vessel was fabricated of seamless forged shells, chemical composition Tab. 1, tensile properties, Tab. 2, representing pressure vessel technology in Germany of the early 60's. Therefore the chemical composition and the toughness properties do not exactly meet today's requirements, but might be comparable to the older generation of plants. From measurements of the water temperature and an assumed mixing effect in the downcomer the vessel inner surface temperature during operation was estimated to be in the range of 284° C including a temperature rise by 4 K due to γ- heating.

Besides the comparison of irradiated material and the unirradiated archive material one of the aims of this work is directed to the change in properties through the wall thickness, which will be investigated by means of Charpy, tensile and compact tension specimens as well, Fig. 9. From several trepans (diameter 107 mm) Charpy-V-notch specimens have been removed using electric discharge machining (EDM) to obtain as many specimens as possible and to facilitate the handling of radioactive material. To establish full Charpy energy/temperature curves longitudinal and transverse specimens from two trepans located adjacent to each other in axial direction were combined, example for trepan C and G, Fig. 10. A similar procedure is necessary to measure tensile properties. For the machining of CT-25 and CT-10 compact tension specimens a sufficient number of trepans is available. From archive and trepan material a maximum number of 11 layers of Charpy specimens through the thickness could be machined. The test results obtained at MEA /15, 16/, AERE-Harwell /17/ and MPA for the unirradiated archive material are in good agreement, although testing was performed according to ASTM (MEA, AERE-Harwell) and DIN (MPA) respectively, Fig. 11. In the transverse (weak) direction (T-L) the upper shelf amounts to about 105 J (MPA), in the longitudinal (strong) direction (L-T) to about 145 J.

The absolute neutron exposure (fluence) was calculated with the two-dimensional transport code DOT 4.2 in combination with a (R, ϑ)- and (R, Z)-model to obtain three-dimensional information for the vessel wall /18/. All operating and standstill periods were considered and also the burn-up distribution of the fuel elements at the beginning of each fuel loading cycle. The fission spectrum was assumed to be of the Watt-type according to ENDF/B V for the whole core. The nuclear cross sections were based on the ENDF/B IV library. The neutron exposure was calculated for each trepan, example Fig. 12. Measurements of the Mn-54 activity on chips taken from several trepans /19/ were also used to determine the absolute neutron exposure. Even after a decay time of about 9 years, the agreement between transport calculation and measurement was within $\pm$ 15%. However, the recent calculation leads to much lower neutron exposure than reported earlier /20/ which is due to more advanced computer codes and especially to the more accurate modelling of the 3 D geometry by the application of large computer capacity.

Charpy impact tests with trepan material show a very pronounced drop in upper shelf energy (USE) and shift in transition temperature for the transverse specimens (T-L), example Fig. 13. Longitudinal specimens (L-T) are less sensitive to neutron irradiation, Fig. 14. The low sensitiveness in upper shelf reduction was already indicated by the surveillance specimens irradiated to about $1 \cdot 19^{19}$ cm^{-2} /19/. The fluence level of the surveillance specimens has to be reevaluated according to the present state of the art. Changes in fluence as great as those found in the case of the vessel wall compared with earlier results are not to be expected in this case since the evaluation of the specimens is supported by dosimetry measurements. Compared with specimens of the surveillance program exposed only to temperature but not to neutron irradiation, these longitudinal specimens show a behavior very similar to the trepan material at the low fluence level of about $2{,}4 \cdot 10^{18}$ cm^{-2} see Fig. 14.

The lower part of the two Charpy curves is almost identical. This implies that part of the material change is caused by temperature effects only. From the compilation of Charpy results in layers through the thickness of the wall the near surface quenching effect on transition temperature becomes obvious, Fig. 15 and 16. It is extended over the first 10 mm on both sides and is especially pronounced for the transition temperature of the transverse specimens. The upper shelf energy for archive material is uniform through the thickness and does not exhibit any quenching effects, Fig. 17 and 18.

The compilation of results shows the gradient of material degradation by **neutron irradiation affecting transition temperature and upper shelf energy** of both directions (T-L and L-T), Fig. 15 through 18.

The change in toughness of the transverse (T-L) specimens, Fig. 17, is significant even at the generally low fluence level. However, the longitudinal specimens (L-T), Fig. 18, are insensitive and become even tougher at the outer surface where the fluence is in the range of $1 \cdot 10^{18}$ cm^{-2} which can be attributed to a kind of annealing effect at irradiation temperature and likely insufficient heat treatment of the original material. The USE measured at the outside of the vessel, Fig. 17, gives no indication that the archive material was not correctly identified.

The projection of the change of properties into the trend curves of Reg.Guide 1.99 Rev. 1 /6/ shows that on the basis of the chemical composition (Cu and P) and the calculated local fluence the material behavior cannot be predicted conservatively, neither with respect to the transition shift nor to the drop in upper shelf, Fig. 19 and 20. More recently proposed trend curves (Reg.Guide 1.99 Rev. 2) /8/ which take Cu and Ni into account for the evaluation of shift of transition temperature caused by neutron irradiation are in the same way non-conservative; however, at a fluence below $1 \cdot 10^{18}$ cm^{-2} both trend curves converge. The prediction of upper shelf drop acc. to Rev. 2 remains unaffected because it is still based on the isolated influence of copper.

An important issue is the attenuation of irradiation damage through the wall, Fig. 21. Relative to the inner surface (ferrite/cladding interface) transition temperature the attenuation through the wall is covered conservatively by the Reg.Guide curves Rev. 1 and proposed Rev. 2 when the local fluence is used to determine the shift at any depth. Extremely conservative is the equation proposed in Rev. 2 which assumes a very flat gradient through the wall. This is not in accordance with the measurements obtained from the trepans.

Several questions about material behavior under service conditions in comparison with trend curves or irradiation experiments in test reactors have been raised, since results of irradiation in the United States at MEA /21/ and United Kingdom at AERE-Harwell /17/ indicate less sensitiveness of the archive material (identical chemical composition) even at a neutron exposure three times as high as the trepans, Fig. 22. The continuation of the research work including fracture mechanics testing, metallurgical investigations and annealing studies will give more insight in the prevailing mechanisms and responsible parameters.

With respect to the validation of surveillance results it is necessary that transverse specimens from trepans with the high degradation are directly compared with surveillance specimens. Since only longitudinal specimens were used in the surveillance program of KRB-A, the feasibility of reconstitution of specimens using EB weld technique was checked. From pieces of the archive material as small as 10 x 10 x 10 mm^3 Charpy compound specimen were produced.

The temperature measurement in the specimen center was below irradiation temperature so that annealing of irradiation damage can be excluded. Obviously the residual stresses do not affect the Charpy results inadmissibly as can be seen from the energy/temperature curve in comparision with conventionel Charpy specimens, Fig. 23.

Validation of Fracture Mechanics Concepts under Extreme Loading Situation

The most complex loading situation in a component is acting during pressurized thermal shock. The stress field results from internal pressure and temperature gradients. A large program was started some years ago and is now being completed in which advanced computational methods are used to describe the time dependent stress/strain field in a component-like large specimen under PTS conditions. The fracture mechanics analysis is performed on the basis of K_I and J /22, 23/. For the verification of the calculation tests were performed applying PTS conditions to thick-walled hollow cylinders (ID = 400 mm, OD = 800 mm, length = 1100 mm, circumferential crack), Fig. 24.

A major issue of the experimental investigations was the use of materials with different toughness levels to cover a wide range of materials representing optimized RPV steels (NKS 1 and 2), minimum requirements (NKS 3) and lower bound state according to possible end-of-life degradation including worst case consideration (NKS 4), Fig. 25. Tremendous efforts had to be undertaken to provide these materials matching in both upper shelf Charpy energy and transition temperature. This could only be achieved by combination of selected chemical composition, melting and forging procedure and heat treatment.

In addition to the internal pressure a tension load of up to 100 MN was applied to generate a stress field similar to the real component. During the cool-down phase, as shown for example in the Temperature/Time curve Fig. 26, starting at 300°C (inner surface) the internal pressure and the axial load remained constant. The J-Integral of the specimen was computed on-line during the test based upon the instantaneous test conditions (temperature, pressure, tension load) /24/.

For the assessment of crack extension in the PTS experiment it is assumed that the crack extension characteristics of CT specimens can be applied to the component as well, Fig. 27. This indeed is the case because of the fact that the constraint calculated for the CT-Specimen used to determine the J_R-curve is almost identical with the constraint in the PTS test specimen. The crack extension derived from this comparison is in good agreement with the crack extension determined by ultrasonic testing and fractographical investigation, example Fig. 28. This confirms the reliability of the J calculation of the component and the fracture mechanics concept. The NKS 4 test with an upper shelf energy of about 70 J is presently being evaluated. Other tests will concentrate on a very low upper shelf energy of about 40 J.

On the basis of a validated fracture mechanics concept the safety of a reactor pressure vessel can be assessed quantitatively also for PTS as demonstrated in a parametric study for the nuclear power plant Obrigheim in Germany /25/.

During a PTS transient the maximum load occurs when the temperature of the material at the crack tip is still elevated, i.e. in the upper shelf regime of the Charpy energy/temperature curve. If crack initiation takes place, it will be by a ductile mechanism causing crack tip blunting and subsequent stable crack extension depending on the applied energy (J-integral). After reaching maximum stress intensity or J-integral, respectively, the transient load decreases and the crack tip region is not forced to respond with plastic deformation under tension anymore. Therefore decreasing temperature in combination with decreasing stress intensity cannot cause the specimen to fail even when the load path is intercepting the K_{Ic} failure curve or failure band, respectively /26, 27/. In simulation tests using 50 mm thick CT specimens with 20% side groves, specimens were overstressed in the ductile regime (starting point) and then subjected to different load paths during cool-down including constant load (1), partial (2), total (3) and steady (4) unloading as indicated in Fig. 29 /27/. When the load path intercepted the K_{Ic} scatter band of the material (determined acc. to ASTM E 399) in none of the cases did failure occur. Only when the specimens were reloaded at low temperature, for which brittle failure has to be expected, did the specimens fail but then only at significantly higher load than that applicable to those specimens which had not been overstressed in the upper shelf regime. Failure of the specimens basically occurred at a level above the upper bound of the K_{Ic} scatter band. The so-called "warm prestress effect" is explained by means of a strip yield model which describes the plastic zone at the crack tip and the resulting residual compression forces when unloaded. Supplementary to the validation of the J concept, even for superimposed mechanical and thermal stresses, credit can be taken from the "warm prestress effect" in the safety analysis. This model has been adopted in the safety assessment of the Stade RPV /27/. In addition to the provision of the fracture mechanics assessment, the injection of cooling water into the hot leg during ECC is an important measure to mitigate the PTS situation in the RPV /28/, which has been realized according to requirements of the German Reactor Safety Commission (RSK).

In-Service Crack Growth

In a safety case assessment a postulated crack in the RPV is assumed penetrating into the cladding at the vessel inner surface so that water has access to the ferritic material. In combination with cyclic loading, temperature, neutron and γ- irradiation changes in the materials as well as the flaw state have to be considered according to different mechanisms in consequence of the postulated crack, Fig. 30. The simultaneous action of these different parameters can only be studied in the real environment of a power reactor.

Within the German FKS R & D program an experiment was initiated by the MPA and performed in cooperation with GKSS and the Versuchsatomkraftwerk Kahl (VAK) as reported earlier /28, 29/. Compact tension specimens (CT 40 mm) were loaded cyclically (1 cycle per minute) in an open loop in the VAK power reactor (BWR water chemistry with about 0,4 ppm oxygen) and the crack advancement determined by measuring the crack opening displacement of each specimen. Preliminary evaluation of the measurements by GKSS give no indication of synergistic effects due to the combination of all acting operating parameters. Final results will be reported shortly /30/.

Conclusion

Ongoing R & D programs in the Federal Republic of Germany are focussed on the validation of the existing concepts for stress-strain calculation (computer codes), determination of reliable fracture mechanics material properties, the time-dependent material state as it degrades by operational parameters, and validation of non-destructive examination. Challenging trials in this context are the investigations directed to pressurized thermal shock (PTS) and especially to the investigation of trepans removed from a commercial reactor pressure vessel with respect to Code verification.

The main results of the research work in the Federal Republic of Germany up to now including evaluation of international programs can be summarized as follows

- J integral and an assessment of crack initiation J_i (which differs from the ASTM procedure) is a reliable tool to evaluate onset of crack extension in complex geometries and loading situations even for the combination of mechanical and thermal stresses as acting during PTS

- The amount of stable crack extension depends on the Charpy-V notch upper shelf energy (USE), the existing constraint and the severity of the transient.

  For deep cracks ($\geq$ 1/4 T) the growing crack does not penetrate through the wall even for low USE materials and severe transients. This is due to the gradient of temperature and the resulting stress decreasing in thickness direction. In case of shallow cracks, which can initiate in a brittle mode, further investigations are under consideration with respect to crack arrest and PTS behavior.

- Investigations of trepans from the Gundremmingen reactor pressure vessel in combination with extensive neutron field calculation indicate a strong conservatism of the Code (US NRC Reg.Guide 1.99 proposed Rev. 2) presently in preparation with respect to attenuation of material degradation through the thickness of the vessel wall.

- The material of the Gundremmingen vessel exhibits directionality effects in the initial state and differences in sensitivity against neutron irradiation depending on specimen orientation relative to the main working direction of the forging. Transverse specimens are more sensitive with respect to both upper shelf drop and transition temperature shift. The material degradation of these transverse specimens could not be predicted conservatively by the existing trend curves of the Code.

- The irradiation response of the Gundremmingen reactor pressure vessel material during operation is not in accordance with recently obtained results from irradiation experiments performed with the corresponding archive material in test reactors. The experiments recently performed in the USA and UK show less degradation than the specimens taken from the vessel wall. Reasons might be attributed to the neutron flux level which is about 100 times higher in the test reactor than at the RPV wall and differences in neutron energy distribution.

In the Federal Republic of Germany a safety strategy has been developed on a theoretical and experimental basis including plant specific surveillance programs for monitoring material degradation through irradiation. In combination with operational changes, e.g. reduction of DLT fluence and mitigation of PTS by hot leg water injection, irradiation embrittlement is not considered an aspect that requires restictions for the LWR plants.

Acknowledgment

The authors wish to thank all experts from research establishments and industry involved in this national and partly international R & D work for their willingness to cooperate.

Thanks are due to the Federal Minister for Research and Technology (BMFT) and the Minister for Environment, Protection of Nature and Nuclear Safety (BMU) and their Technical Advisory Committees for continuous scientific, financial and practical support and encouragement.

The authors acknowledge especially the cooperation of Dr. C.Z. Serpan from the US Nuclear Regulatory Commission.

References

/1/ K. Kussmaul
German Basis Safety Concept rules out possibility of catastrophic failure
Nuclear Engineery International
Dec. 1984 p. 41-46

/2/ Protection against nonductile failure
ASME Boiler and Pressure Vessel Code, Section III App. G

/3/ Material Properties
ASME Boiler and Pressure Vessel Code, Section XI App. A 4000

/4/ Komponenten des Primärkreises von Leichtwasserreaktoren: Auslegung, Konstruktion und Berechnung
KTA 3201.2 (1980)

/5/ K. Kussmaul, J. Föhl, E. Roos
Some conclusions with regard to the safety assessment of cracked components drawn from the research program Integrity of Components (FKS) at the present state
12. MPA-Seminar Sicherheit und Verfügbarkeit in der Anlagentechnik
9./10. Oktober 1986, Stuttgart, Germany F.R.
prepared for publication NED (1987)

/6/ Effects of residual elements on predicted radiation damage to reactor vessel materials
U.S. Nuclear Regulatory Commission Regulatory Guide 1.99 Rev. 1/1977

/7/ Überwachung der Strahlenversprödung von Werkstoffen des Reaktordruckbehälters von Leichtwasserreaktoren
KTA 3203 (1984)

/8/ Radiation damage to reactor vessel materials
U.S. Nuclear Regulatory Commission Regulatory Guide 1.99 proposed Rev. 2/1986

/9/ K. Kussmaul, J. Föhl, E. Roos
Application of advanced material, design and computation technologies to enhance safety, reliability and availability
IAEA Specialists' Meeting on "Recent Trends in Development of Reactor Pressure Circuit Technology"
25-28 November 1985, Madrid, Spain
Pressure Vessel and Piping 25 (1986) pp 185-2215

/10/ F.J. Loss et al.
Structural Integrity of water Reactor Pressure Boundary Components
Quaterly Progress Report (April-June 1979)
NUREG/CR 0943, NRC Memorandum Report 4064 (Sept. 1979)

/11/ K.H. Schwalbe, J. Heerens
Vorschlag zur Modifizierung der J_{IC}- Norm ASTM E 813-81
10. MPA-Seminar "Sicherheit und Verfügbarkeit in der Anlagentechnik"
10.-13. Oktober 1984, Stuttgart, Germany F.R.
NED 87 (1985) pp 101-107

/12/ E. Roos, U. Eisele, H. Beyer, R. Gillot
Einordnung und Charakterisierung von Werkstoffen mittels bruchmechanischer Parameter
12. MPA-Seminar "Sicherheit und Verfügbarkeit in der Anlagentechnik"
9./10. Oktober 1986 Stuttgart, Germany F.R.
prepared for publication NED (1987)

/13/ E. Roos, U. Eisele
Remarks concerning the problem of determination of elastic-plastic fracture mechanics materials charakteristics by means of J-Integral crack resistance curves
to be published
ASTM Int. Journal of Testing and Evaluation

/14/ E. Roos, U. Eisele, H. Silcher, F. Spaeth
Einfluß der Werkstoffzähigkeit und des Spannungszustandes auf das Versagensverhalten von Großproben
12. MPA-Seminar "Sicherheit und Verfügbarkeit in der Anlagentechnik"
9./10. Oktober 1986, Stuttgart, Germany F.R.
prepared for publication NED (1987)

/15/ J. R. Hawthorne
Preirradiation Qualification of Materials Identified as KRB-A Archive
MEA report 2095 (1985)
NRC-contract 04-84-102

/16/ J. R. Hawthorne
Through-Thickness Mechanical Properties of KRB-A Archive Steel Forging GEB
MEA report 2159 (1986)

/17/ C. A. English
Compilation of preliminary data from Charpy impact testing on KRB-A Archive in the pre- and post irradiation condition
personal information (1986)

/18/ G. Prillinger
Neutron Spectrum Calculation for the Gundremmingen KRB-A Reactor
NUREG/CR 4791 (1986)

/19/ R. Schröder
Gammaspektrometrische Messungen von Bohrspänen aus den Bohrkernen A, D, G, L und P des RDB Gundremmingen A
Techn. Notiz der KFA-Jülich IRW-TN-24/86

/20/ N. Eickelpasch, R. Seepolt
Experimentelle Ermittlung der Neutronendosis des KRB Druckgefäßes und deren betriebliche Bedeutung
Atomkernenergie Bd. 29 (1977) 2, S. 149-152

/21/ J.R. Hawthorne, A.L. Hiser
Dose Rate Effects on Irradiation Embrittlement and Composition and Temperature Effects on Annealing/Reirradiation Sensitivity
MEA-report 2187 (1986)

/22/ S.K. Iskander, A.W. Sauter, J. Föhl
Reactor Pressure vessel implications of embrittlement to the pressurized thermal shock scenario, "Radiation Embrittlement of Nuclear Reactor Pressure Vessel Steels" (edited by L. Steele), ASTM STP 909 (1986) pp 163-176

/23/ J. Jansky, J. Föhl, A. W. Sauter, S.K. Iskander
Einfluß der Werkstoffzähigkeit auf Schädigung durch Thermoschock
9. MPA-Seminar "Sicherheit der druckführenden Umschließung von Leichtwasserreaktoren" 13./14. Oktober 1983 Stuttgart, Germany F.R.

/24/ K. Kussmaul, A.W. Sauter
Anlagensimulation zur Behandlung der Notkühlproblematik beim Leichtwasser-Druckbehälter
10. MPA-Seminar "Sicherheit und Verfügbarkeit in der Anlagentechnik" 10.-13. Oktober 1984 Stuttgart, Germany F.R.
NED 87 (1985) pp 313-27

/25/ K. Kussmaul, A.W. Sauter, U. Weber, R. Bartsch
Rechnerische Studie zur Thermoschockbelastung des Reaktordruckbehälters im Kernkraftwerk Obrigheim
11. MPA-Seminar "Sicherheit und Verfügbarkeit in der Anlagentechnik" 10./11. Oktober 1985 Stuttgart, Germany F.R.

/26/ F.J. Loss, R.A. Gray, J.R. Hawthorne
Significance of warm prestress to crack initiation during thermal shock
NRL/NUREG Report 8165 (Sept. 1985)

/27/ T. Hollstein, J.G. Blauel, R. Kienzler, G. Nagel
Use of load path dependent material fracture toughness values (WPS) in the safety analysis of RPV Stade
Nuclear Engineering and Design 94 (1986) pp. 233-239

/28/ K. Kussmaul
West German research programs on irradiation effects on reactor pressure vessels
"Radiation Embrittlement and Surveillance of Nuclear Reactor Pressure Vessels: An International Study" (edited by L. Steele), ASTM STP 819 (1983) pp 16-28

/29/ J. Föhl, Ch. Leitz, D. Anders
Irradiation experiments in the Testing Nuclear Power Plant VAK
"Effects of Radiation on Materials" (edited by H.R. Barger and J.S. Perrin), ASTM STP 782 (1982) pp 520-549

/30/ J. Föhl, D. Anders, J. Ahlf
Cyclic crack growth of RPV materials under simultaneous effect of irradiation, corrosion, temperature and cyclic loading;
in preperation for publication

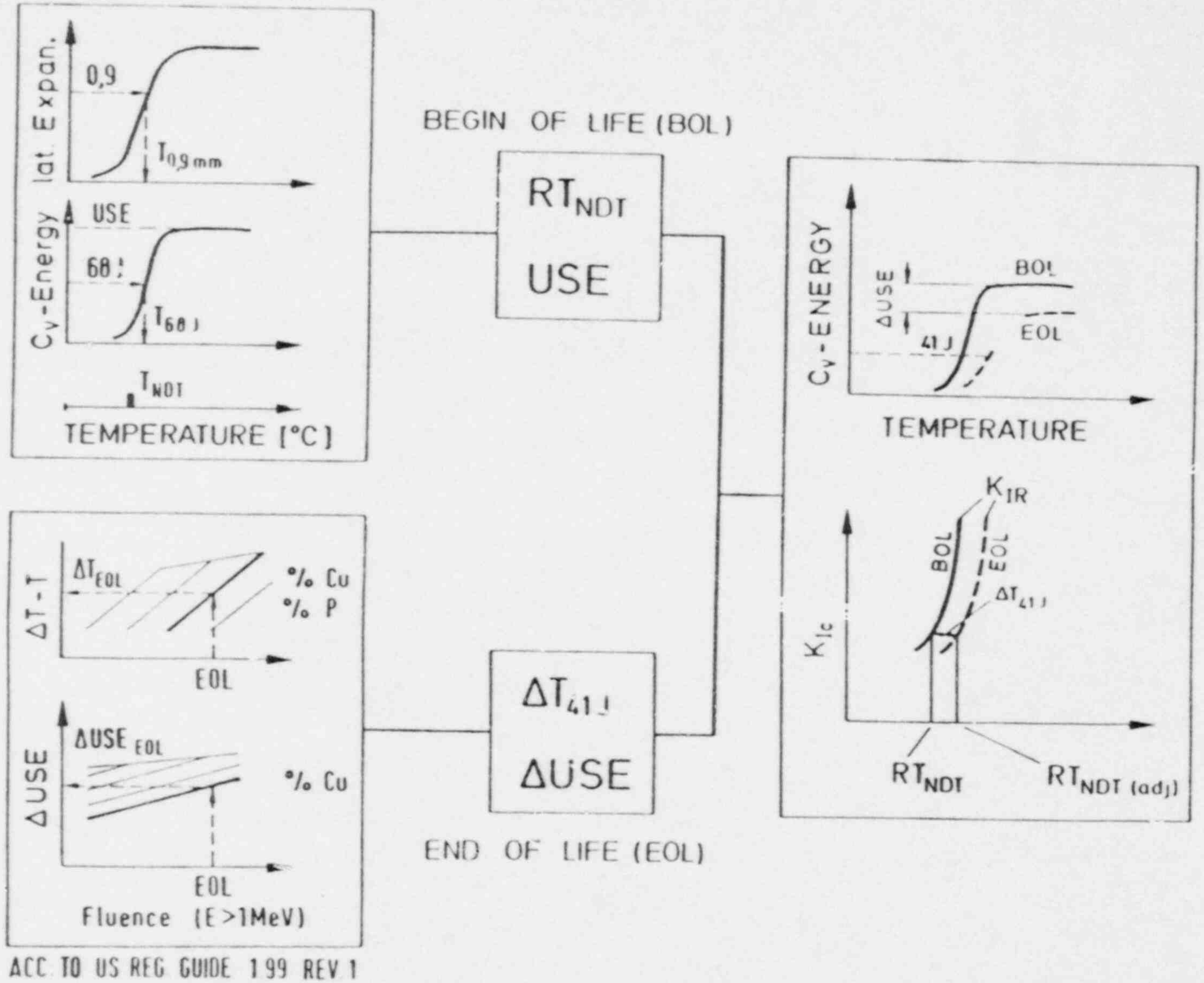

Fig. 1: Code procedure to determine the linear elastic fracture mechanics properties

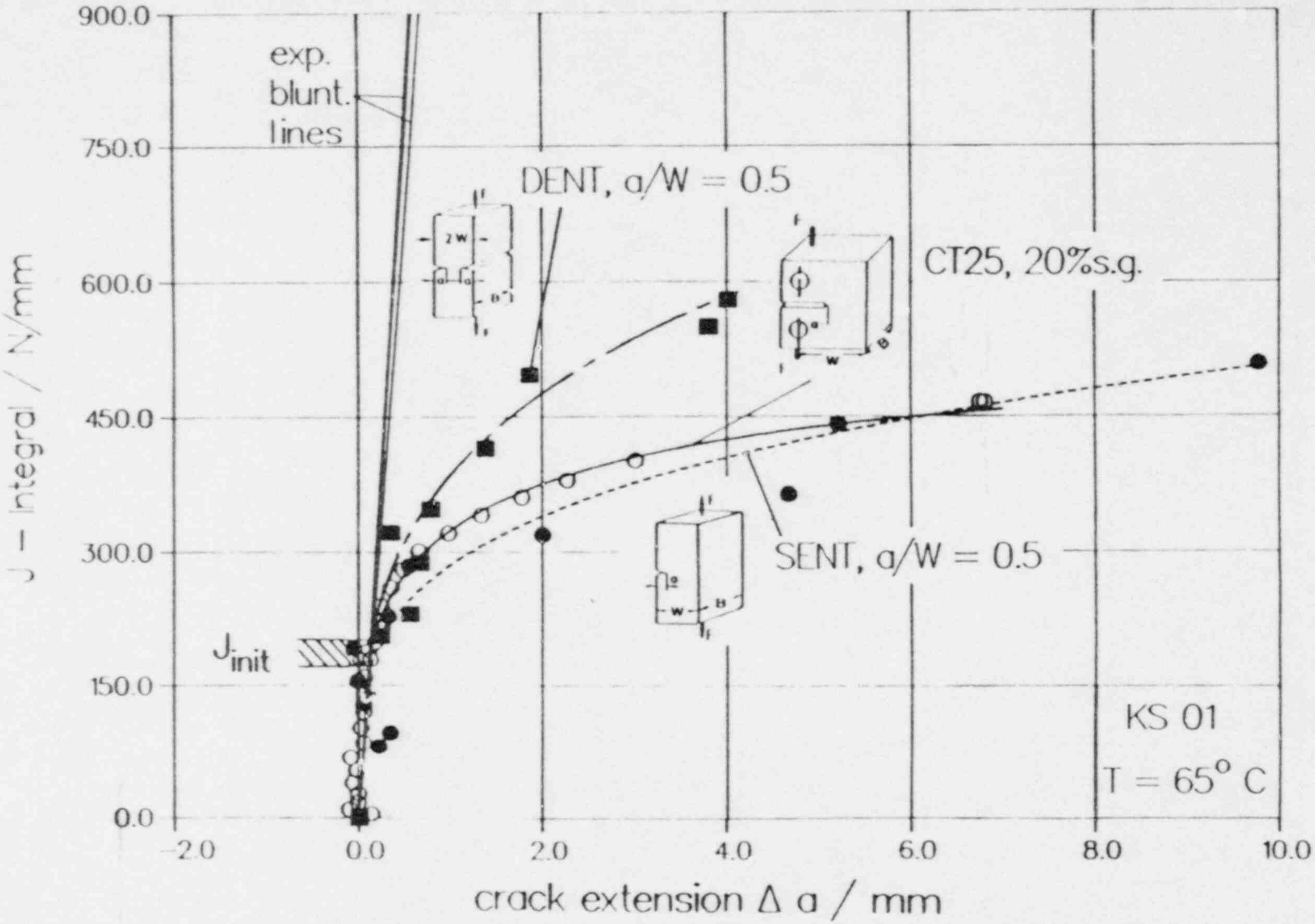

Fig. 2: J_R-curves for different geometries, material 22 NiMoCr 37 similar to A 508 Cl 2, tested at upper shelf temperature, USE   90 J

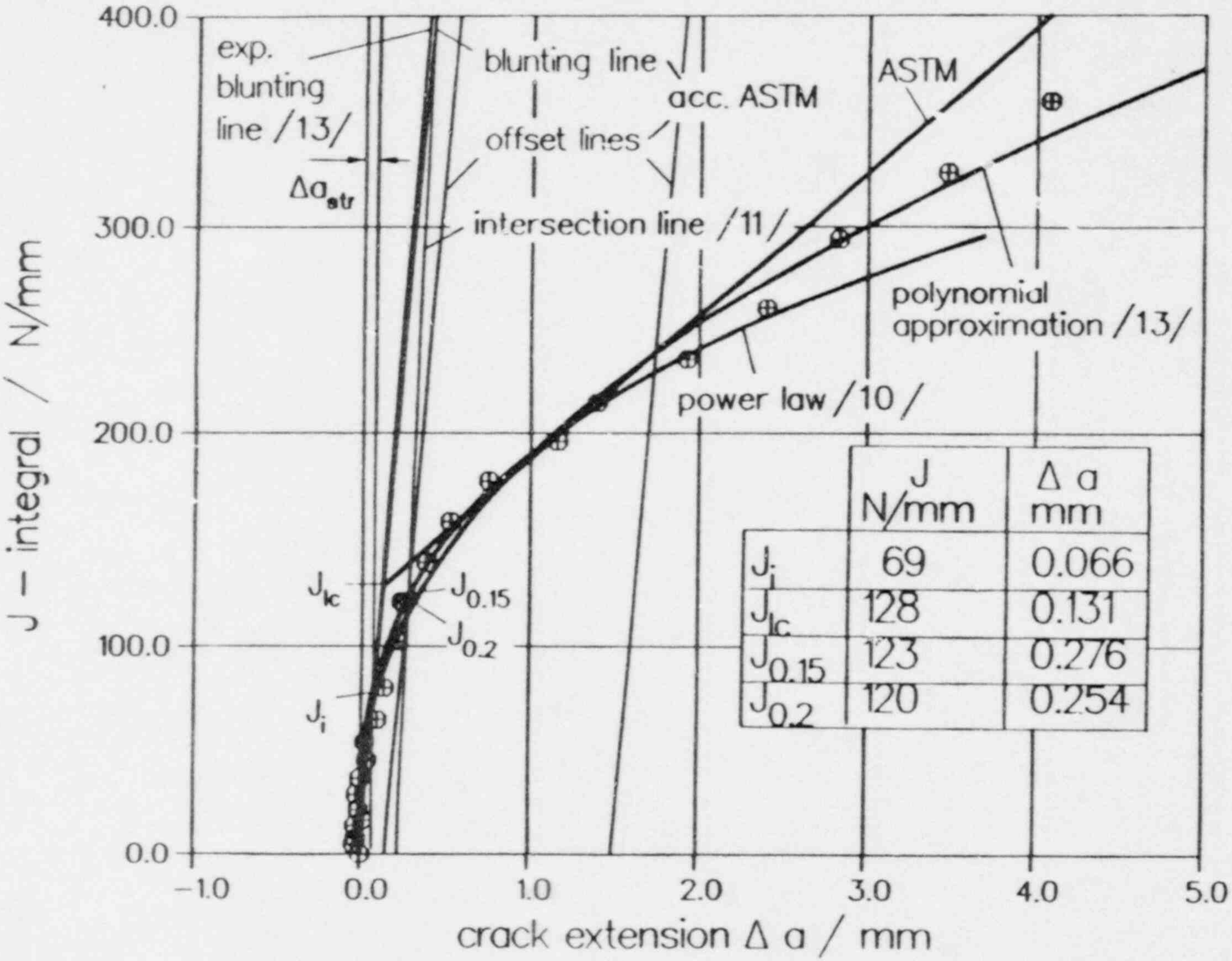

	J N/mm	Δ a mm
J_i	69	0.066
J_{Ic}	128	0.131
$J_{0.15}$	123	0.276
$J_{0.2}$	120	0.254

Fig. 3: Different methods to evaluate initiation toughness, material and testing parameters s. fig. 2

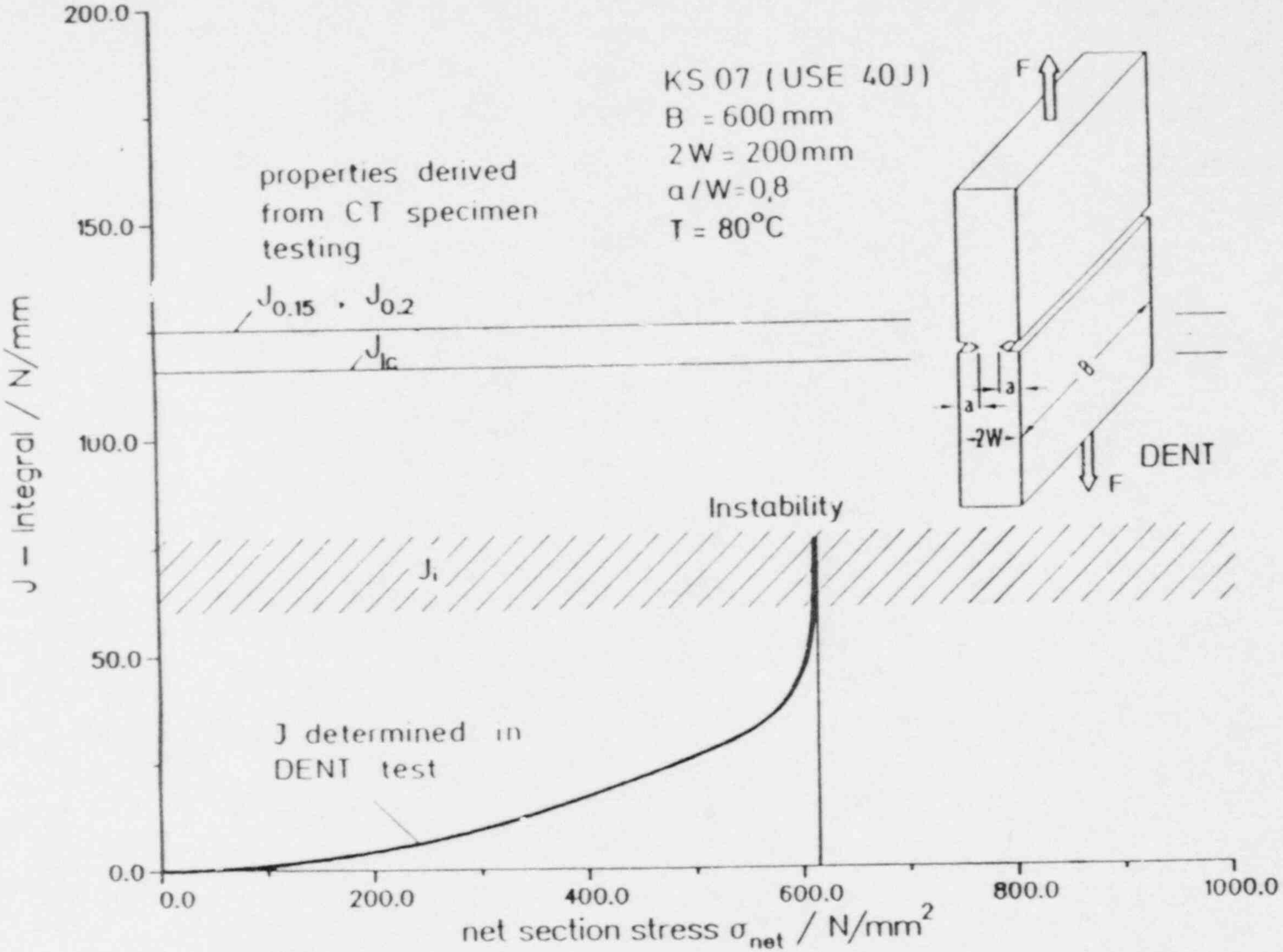

Fig. 4: Application of initiation values from CT testing to predict failure of large components, material 22 NiMoCr 37 similar to A 508 Cl 2, low USE test heat

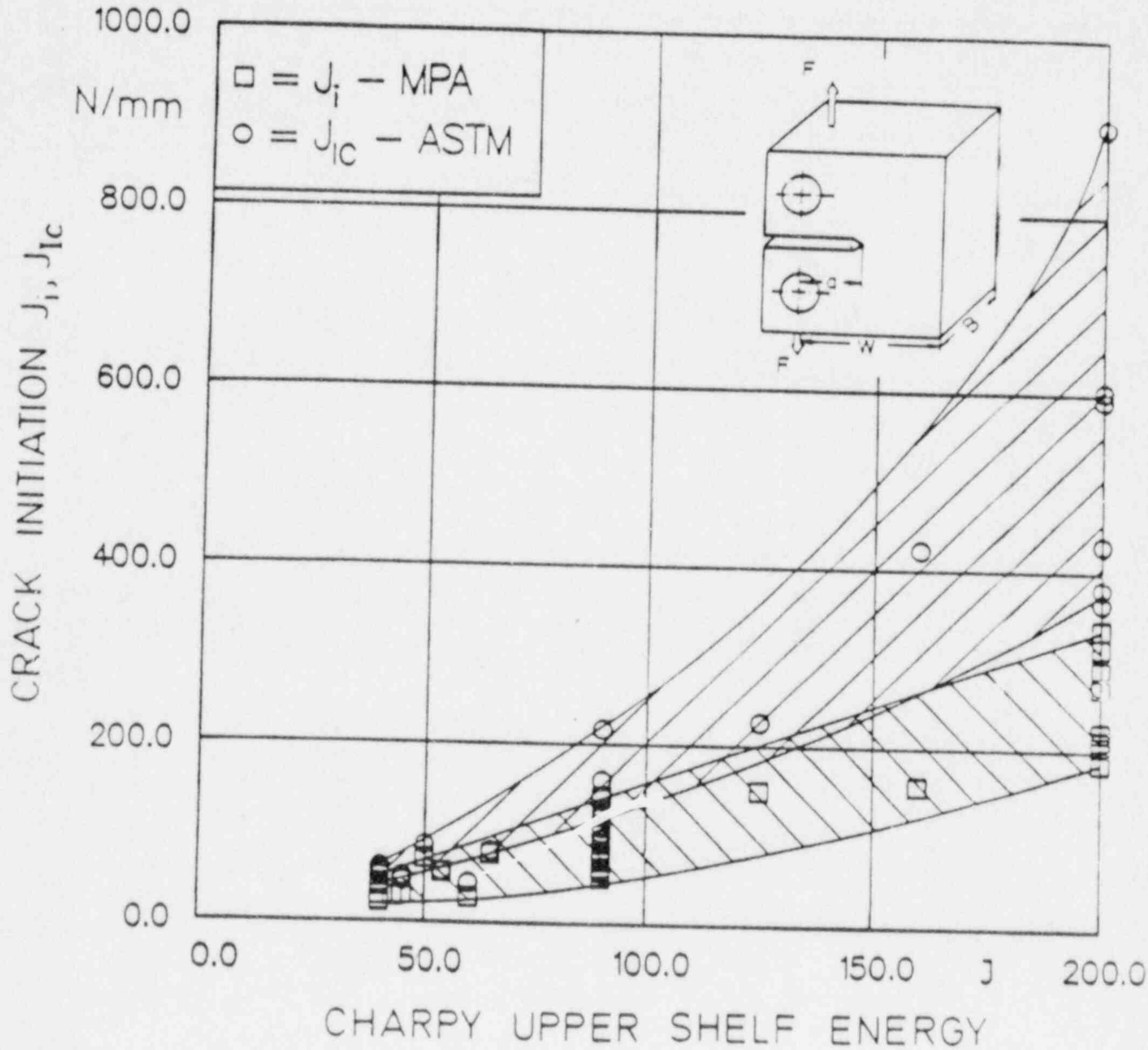

Fig. 5: Correlation of initiation toughness with upper shelf Charpy energy, material base 22 NiMoCr 37 similar to A 508 Cl 2 and 20 MnMoNi 55 similar to A 508 Cl 3

	Yield Strength σy MPa	Ultimate Strength σu MPa	Elongation $A^{2)}$ %	Reduction of Area Z %
axial orientation 1) T	460	620	35	60
circumferential orientation 1) (main working direction) L	475	625	40	70

1) acc. to vessel axis

2) l_0 = 12,7 mm, d_0 = 5,74 mm, l/d = 2,2

Table 2: Tensile properties at room temperature of archive material GEB-1, acc. to MEA

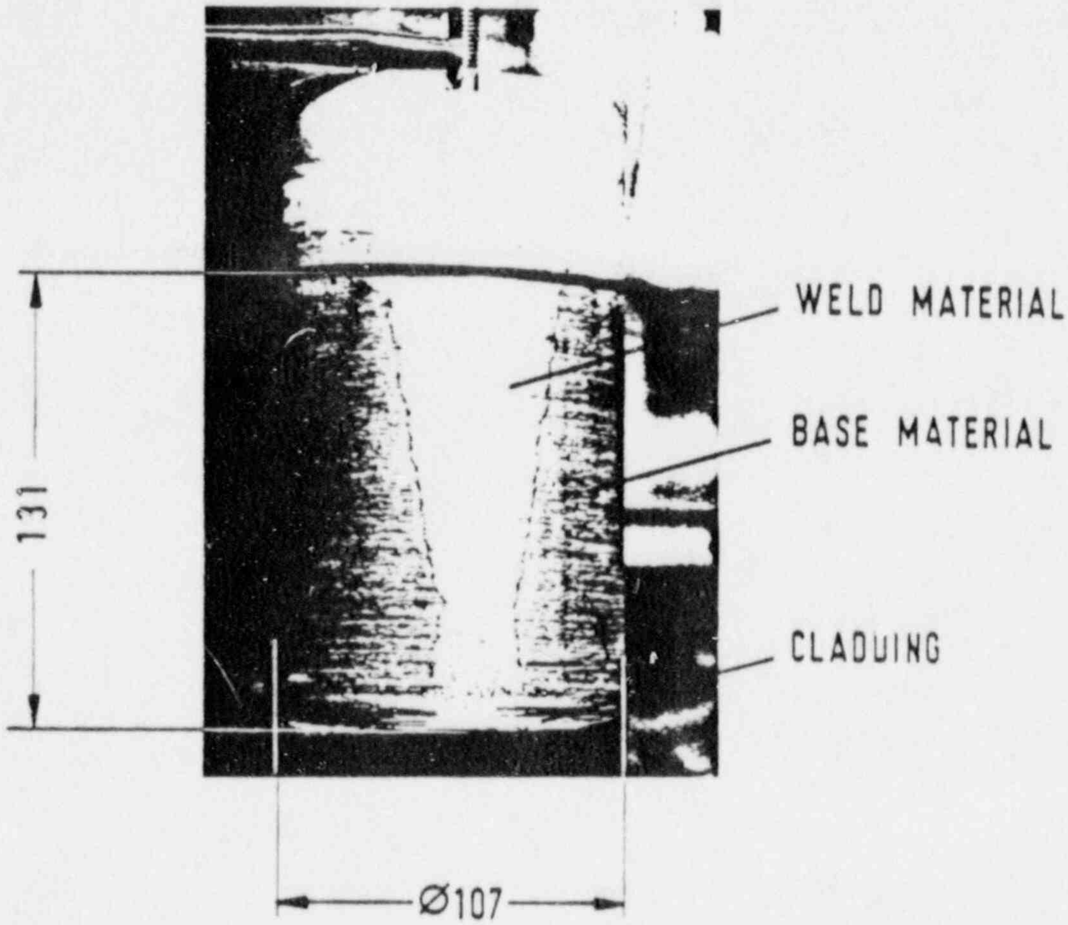

Fig. 7: Trepan Nr. 7 from the circumferential weld 4.1 A of the reactor pressure vessel Gundremmingen A

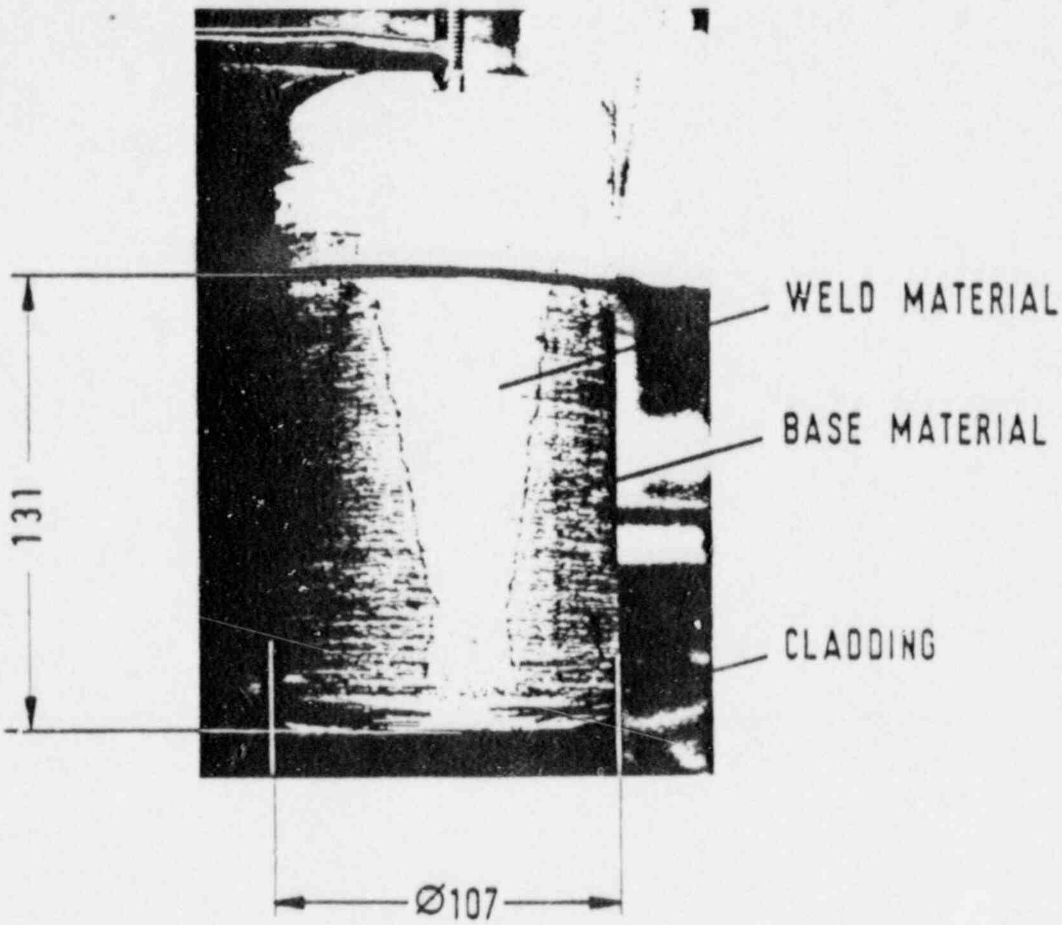

Fig. 7: Trepan Nr. 7 from the circumferential weld 4.1 A of the reactor pressure vessel Gundremmingen A

Chemical Composition (Wt - %)

	base materials 20 NiMoCr 36		weld material
	Archive material GEB 1-I	Trepan G	sample from vessel head flange
C	0.23	0.22	0.05
Si	0.23	0.22	0.17
Mn	0.71	0.71	1.45
P	0.013	0.013	0.009
S	0.012	0.012	0,005
Cr	0.38	0.38	0.10
Mo	0.65	0.62	0.51
Ni	0.75	0.75	0.25
Cu	0.16	0.16	0.28

Table 1: Chemical composition of trepan and archive material 20 NiMoCr 36 similar to A 508 Cl 2

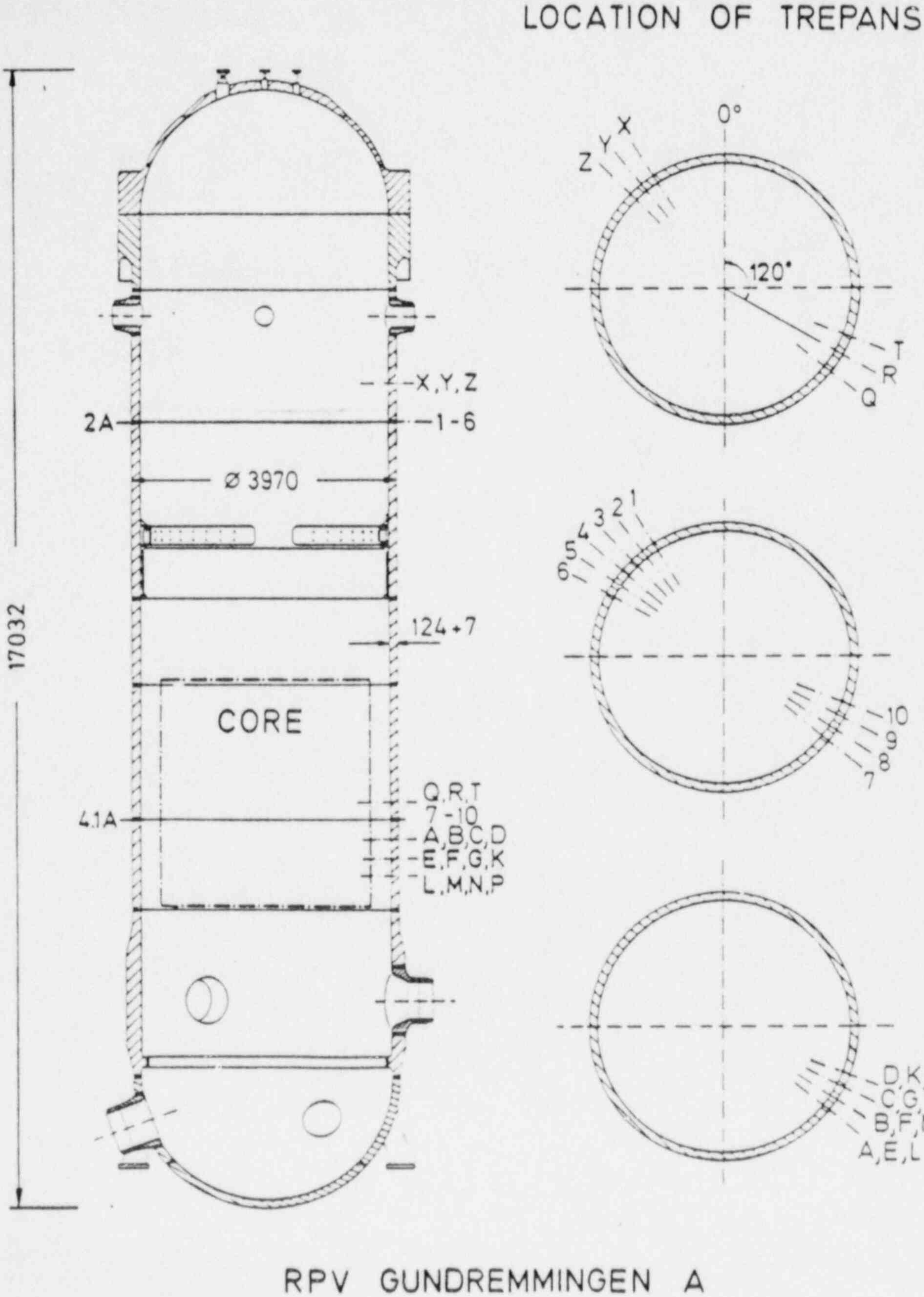

Fig. 6: RPV Gundremmingen A and location of trepans

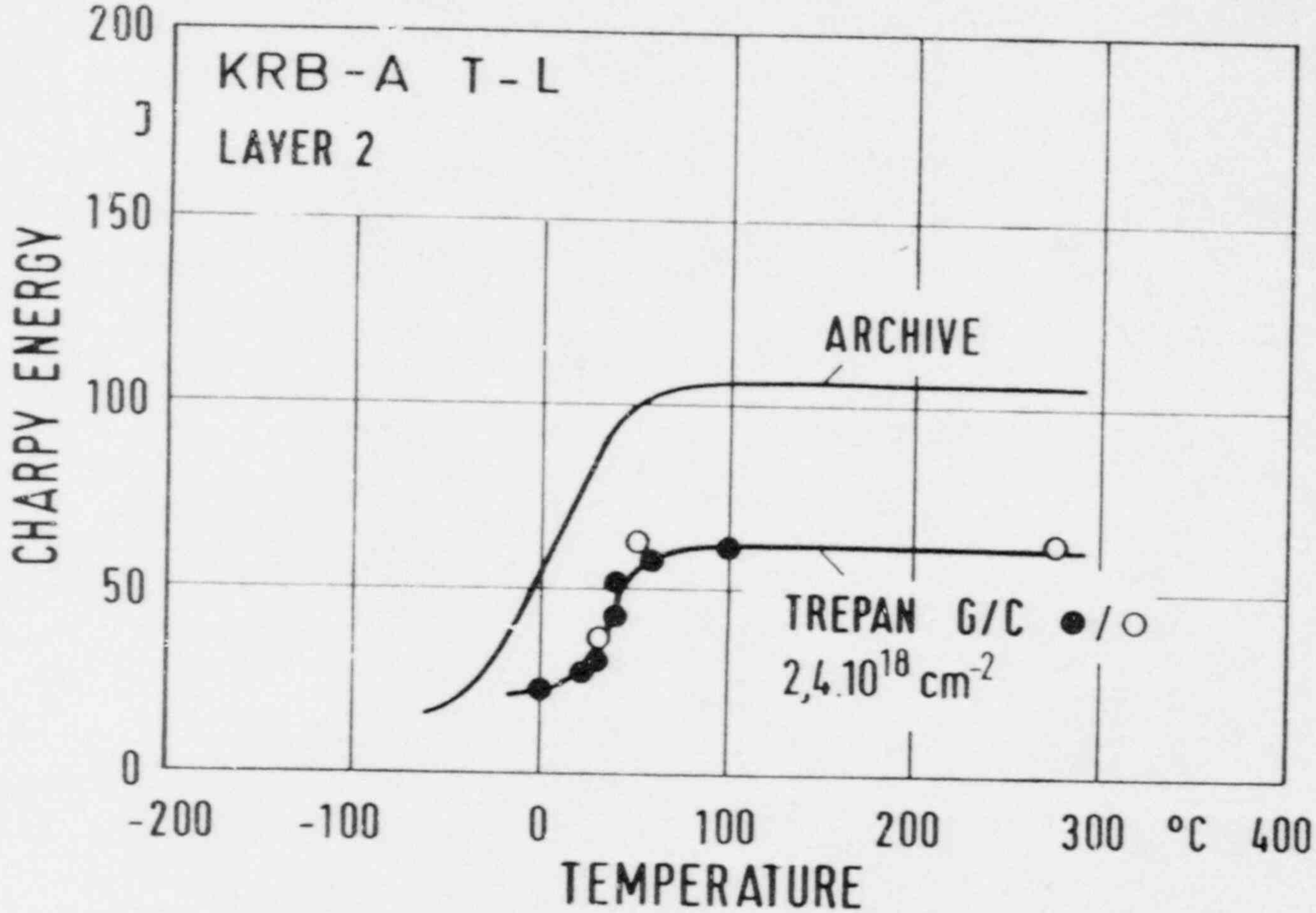

Fig. 13: Charpy results obtained from trepans in comparison with archive material (example) for transverse specimens

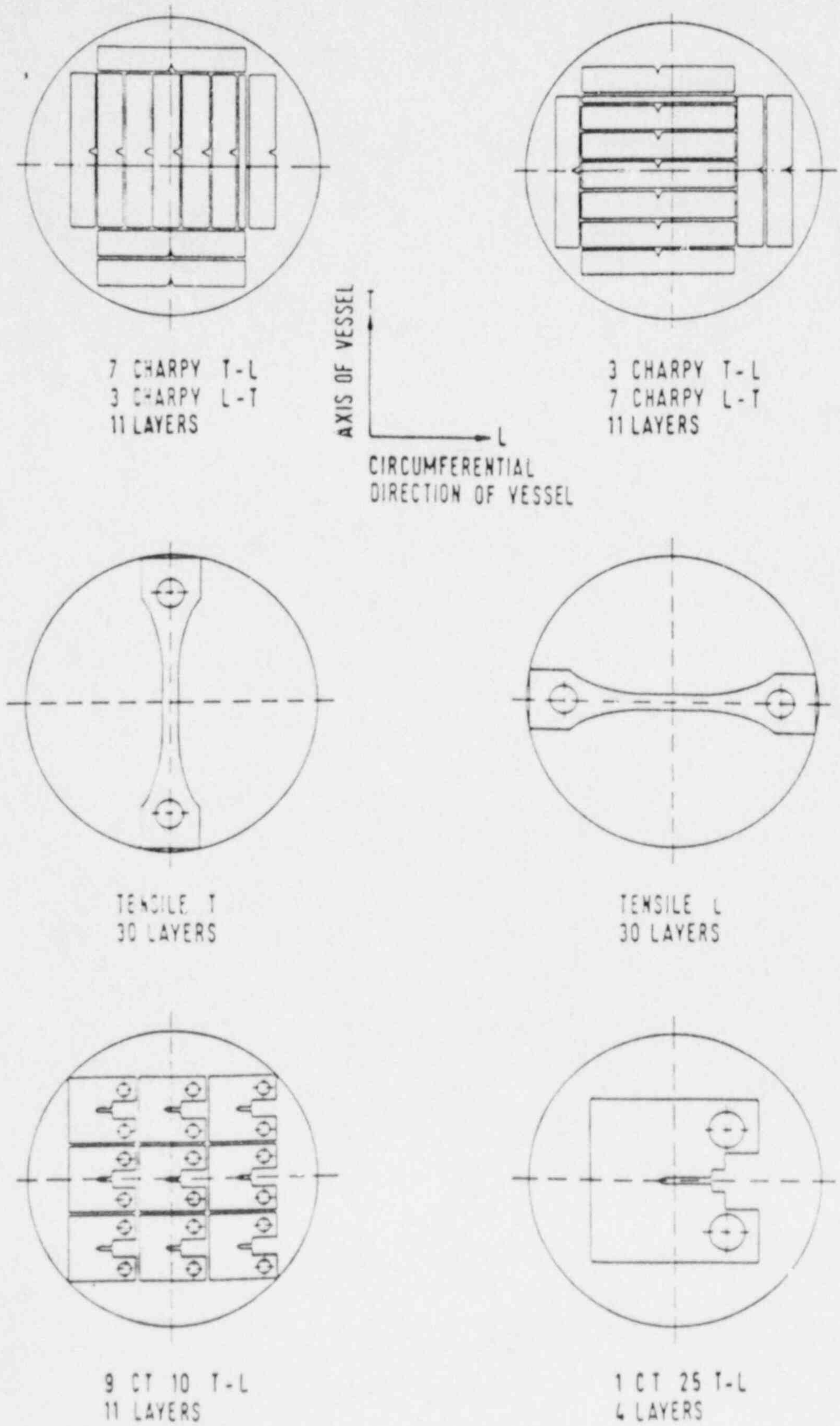

Fig. 10: Cutting scheme of trepans for different specimen types

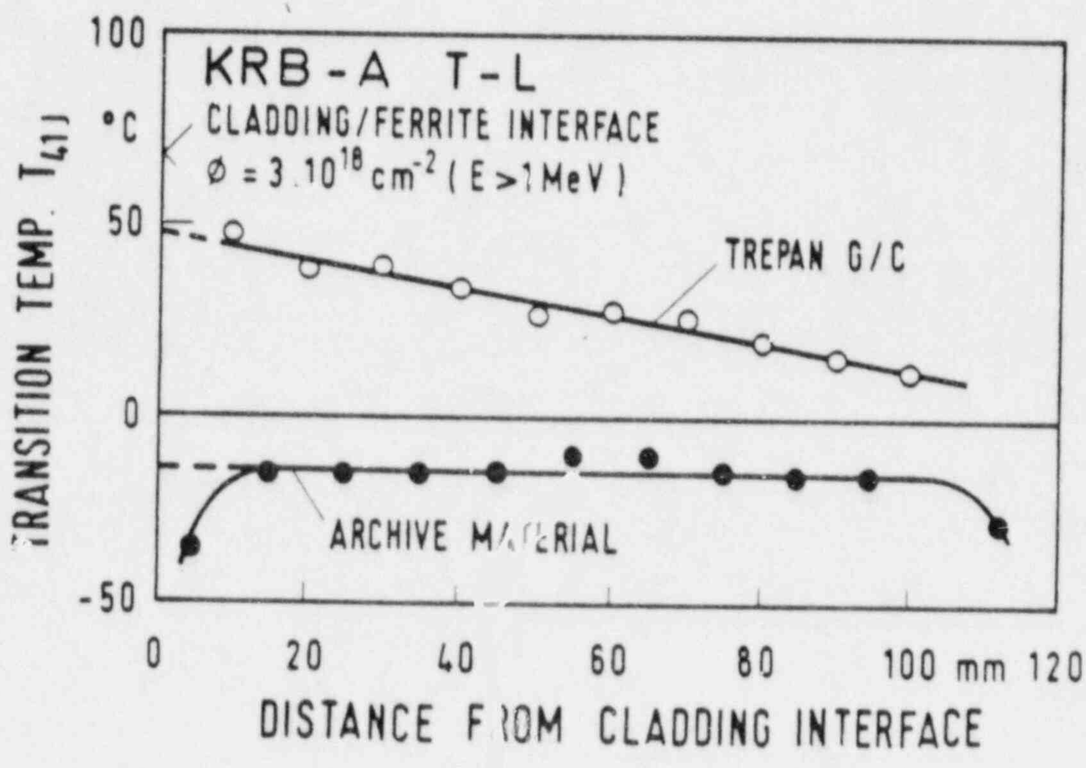

Fig. 15: Transition temperature T_{41J} of transverse specimens (T-L) for archive and trepan material; through thickness properties

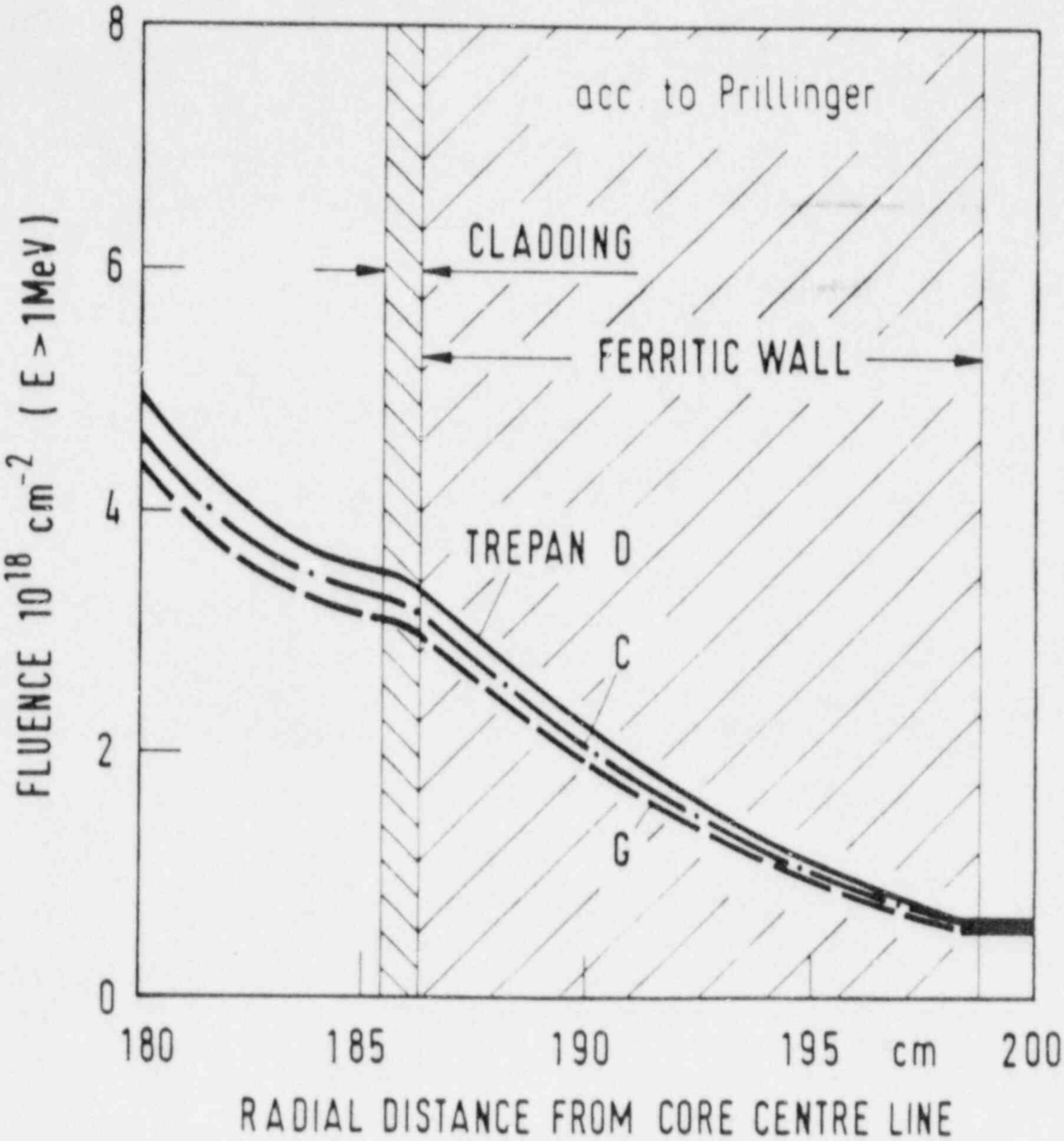

Fig. 12: Fluence claculation for trepans C, D and G

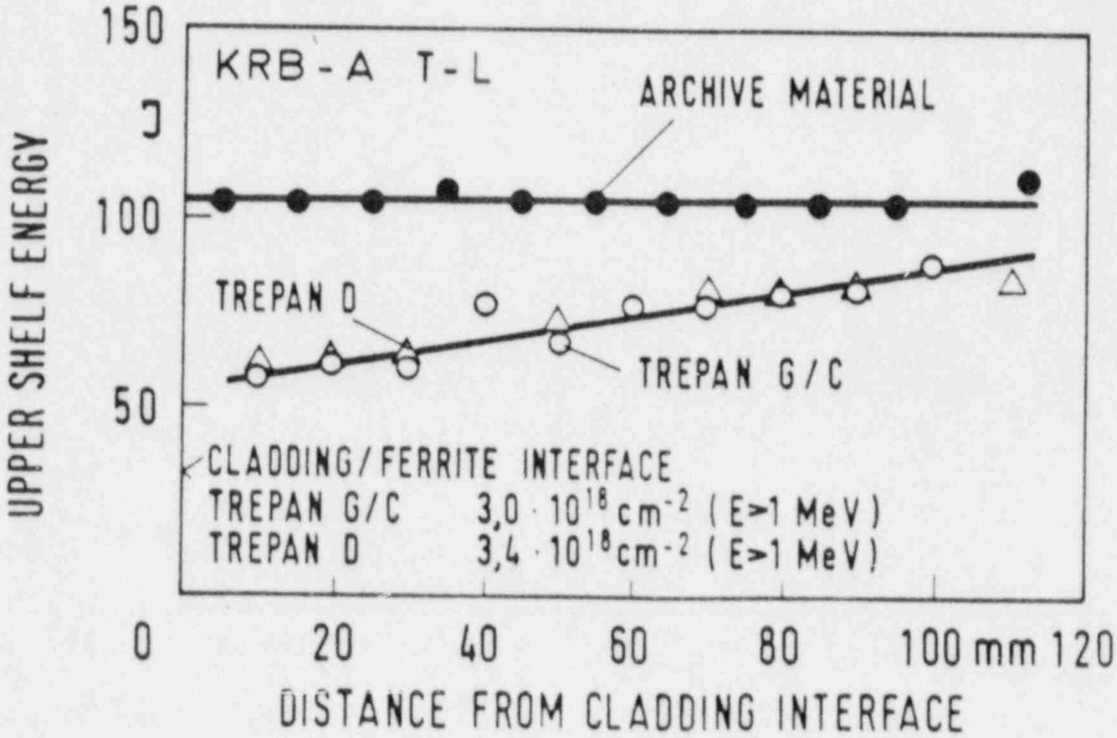

Fig. 17: Upper shelf energy of transverse specimens (T-L) for archive and trepan material; through thickness properties

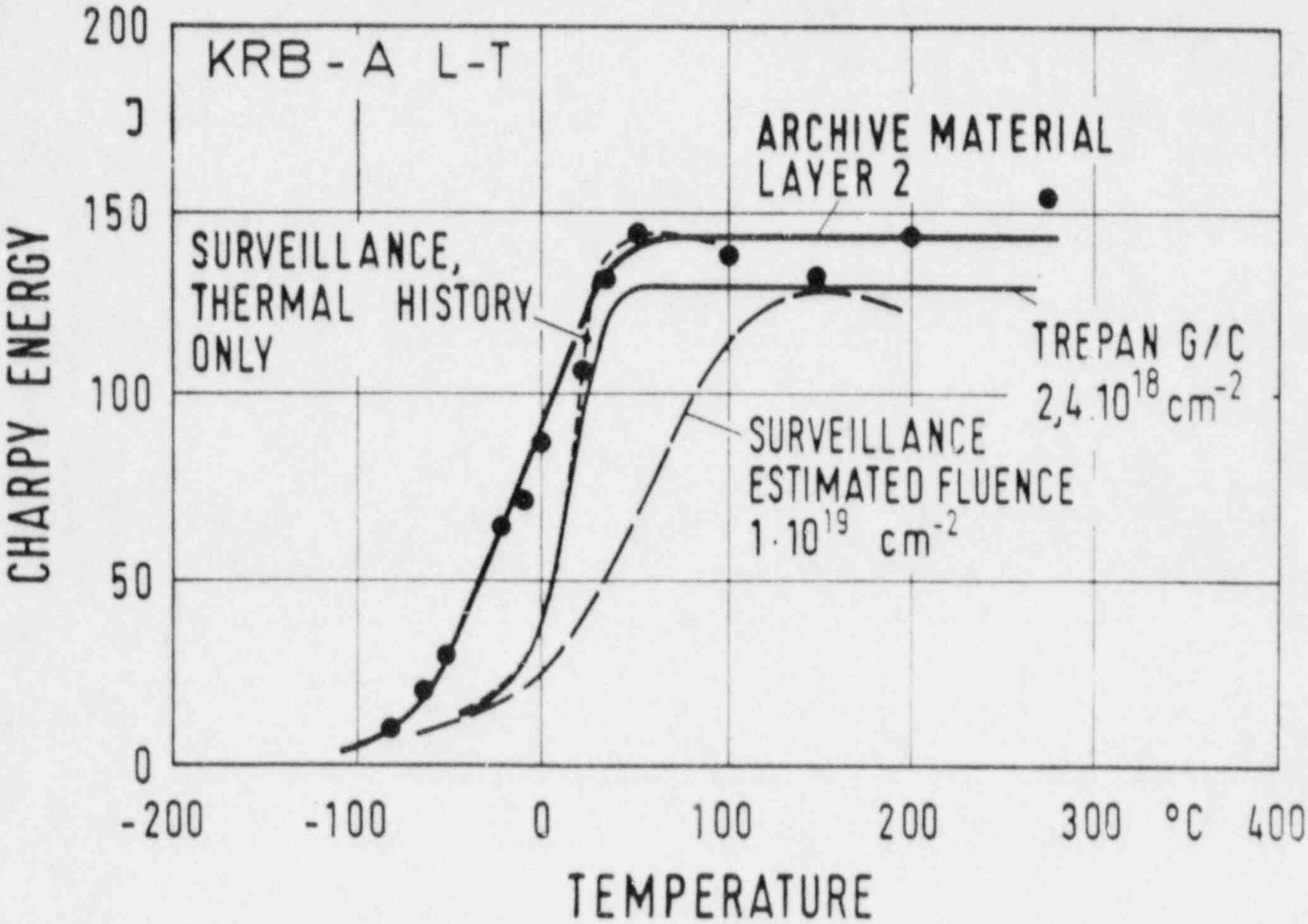

Fig. 14: Charpy results from trepan and archive material in comparison with surveillance results (longitudinal specimens)

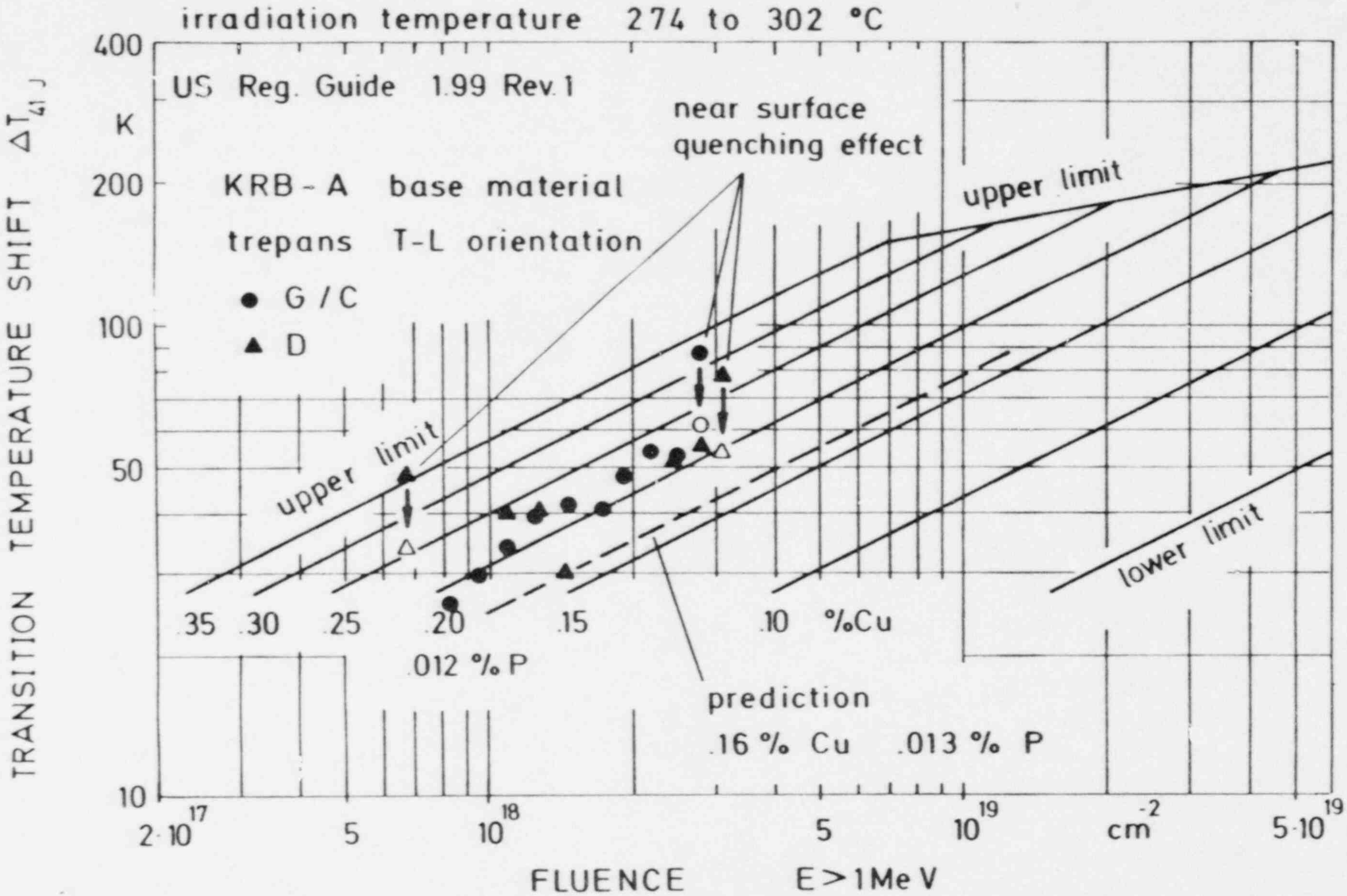

Fig. 19: Comparison of measured transition temperature shift for the Gundremmingen vessel material in comparison with predicted values according to US Reg. Guide 1.99 Rev. 1

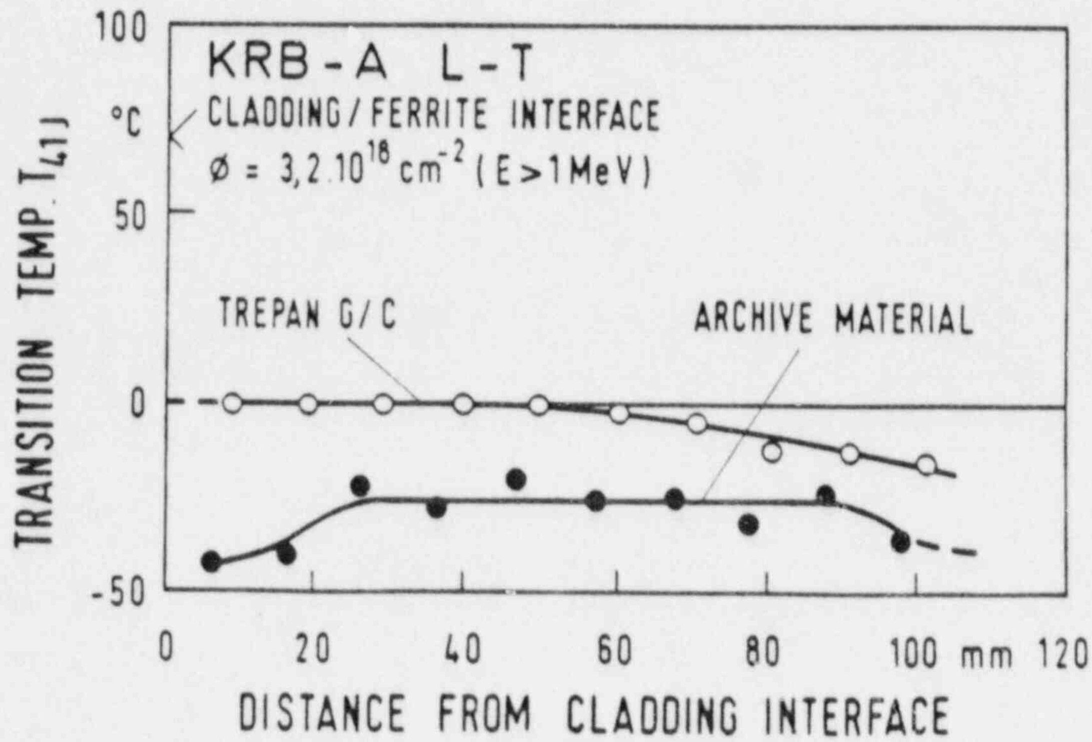

Fig. 16: Transition temperature T_{41J} of longitudinal specimens (L-T) for archive and trepan material; through thickness properties

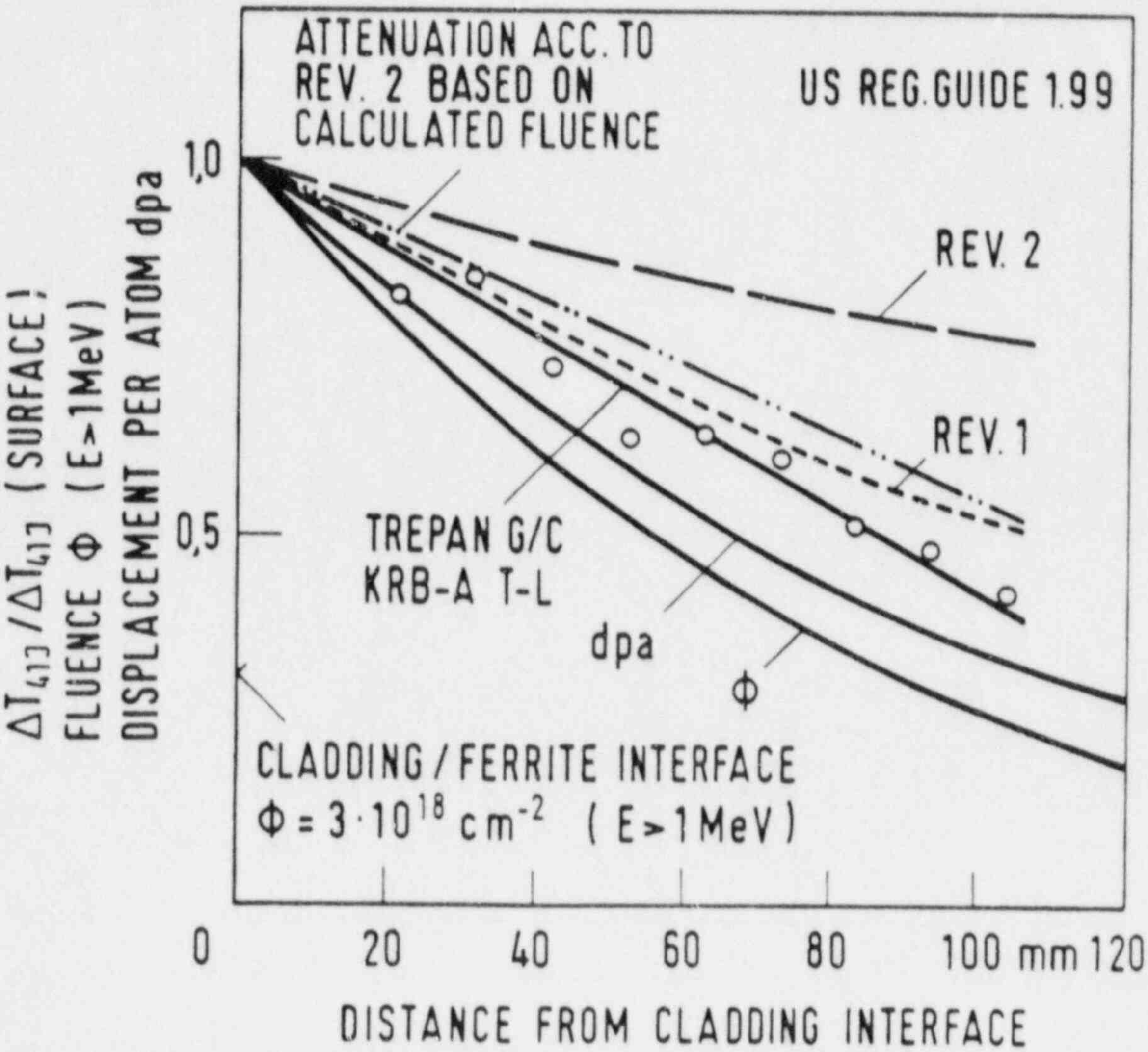

Fig. 21: Relative change of transition temperature through the wall thickness compared with fluence and dpa gradient and Code (Reg. Guide 1.99 Rev. 1 and proposed Rev. 2) prediction

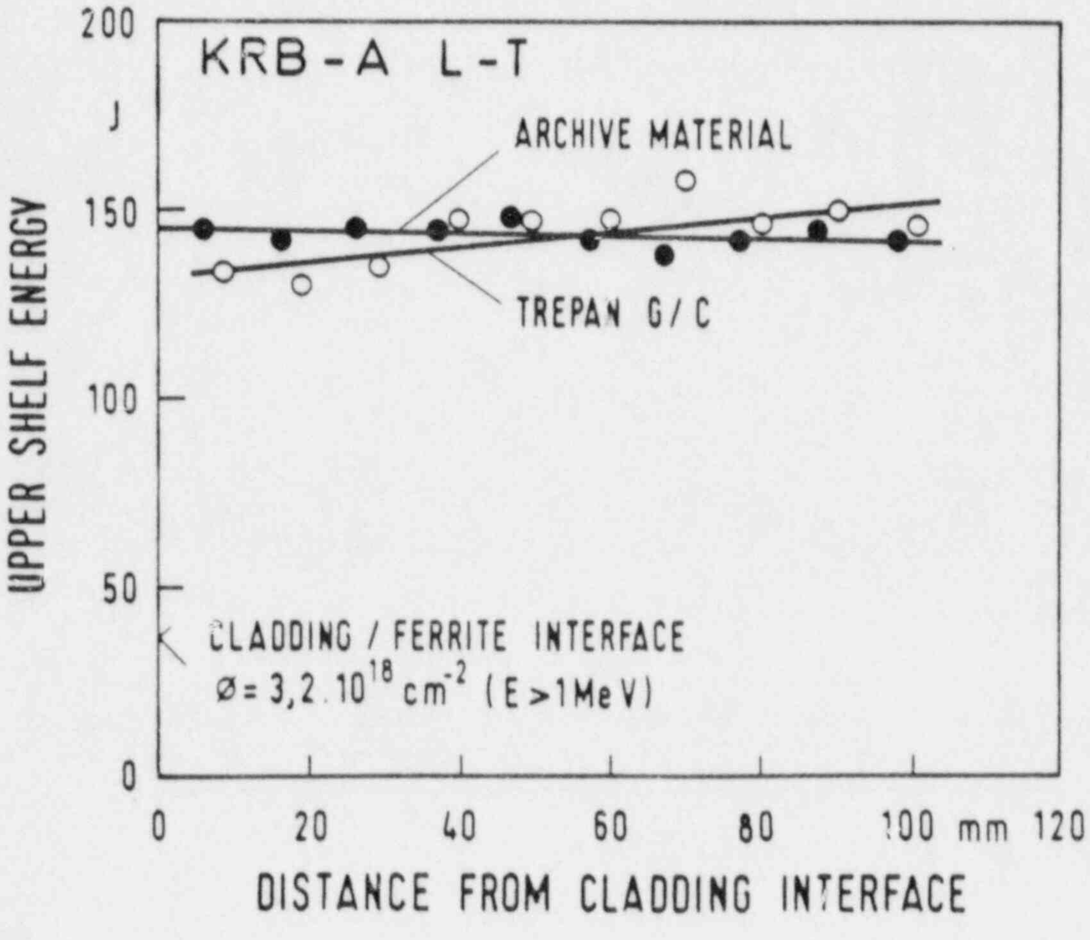

Fig. 18: Upper shelf energy of longitudinal specimens (L-T) for archive and trepan material; through thickness properties

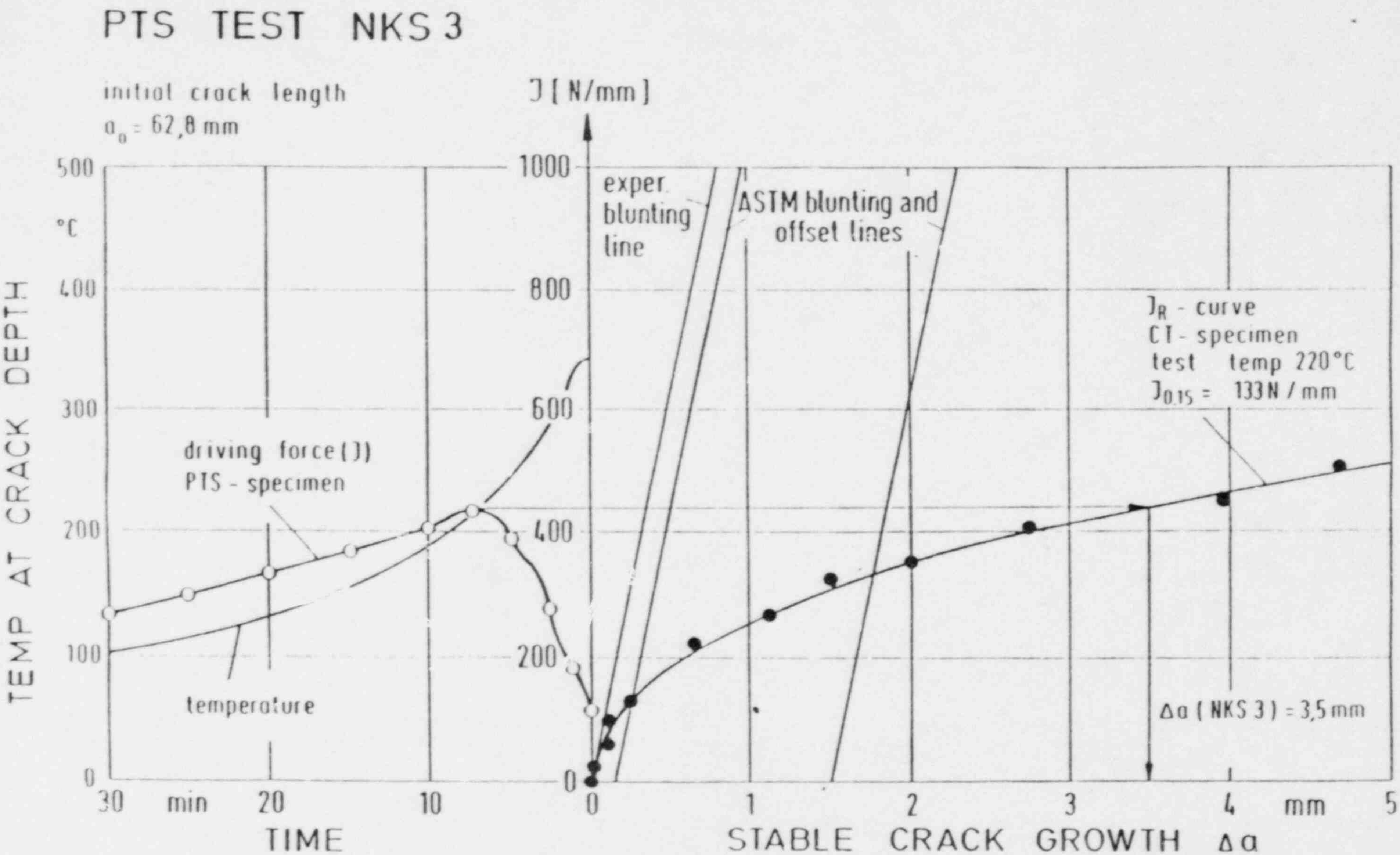

Fig. 27: Material J_R curve and J-Integral for the test specimen in PTS experiment NKS 3

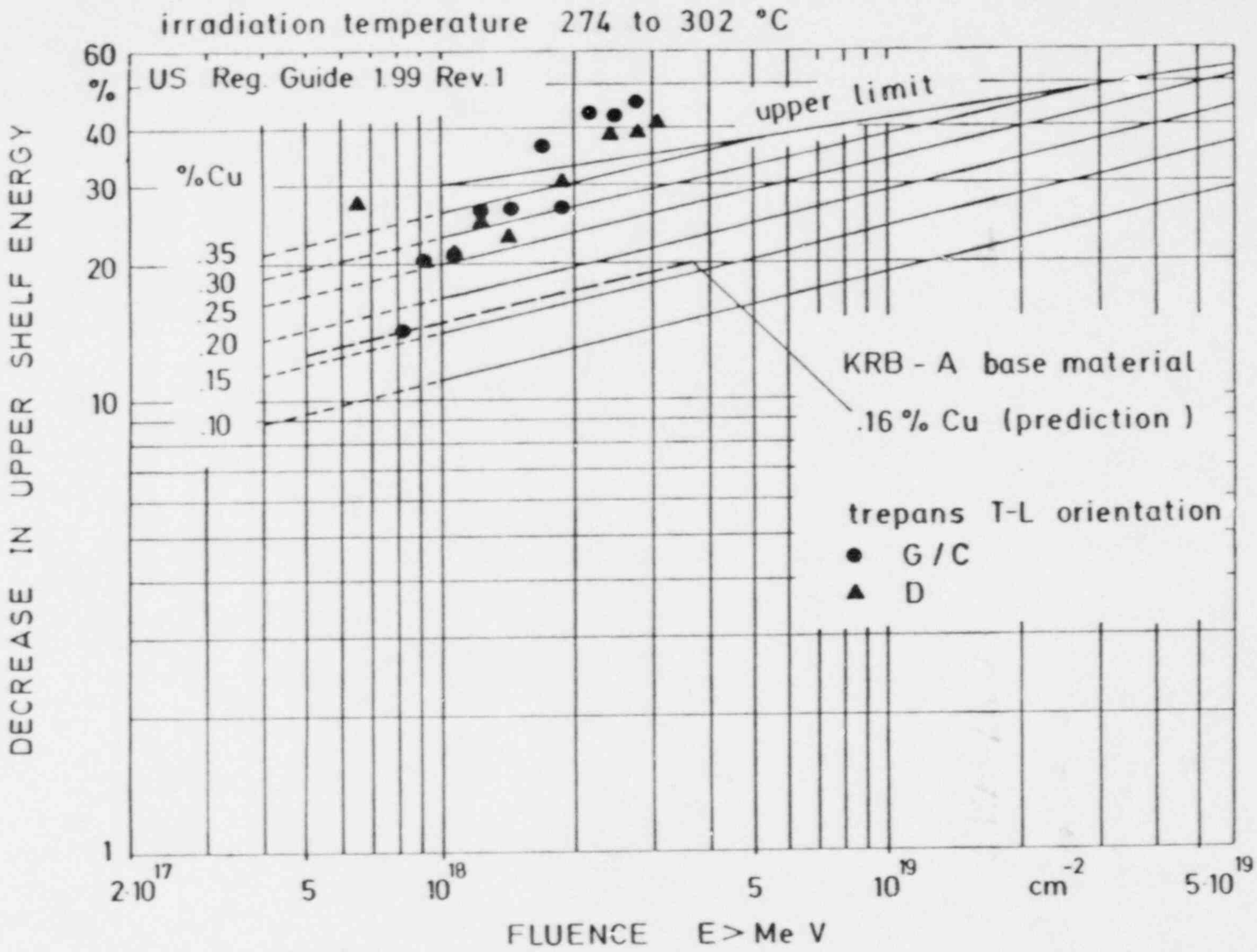

Fig. 20: Comparison of measured upper shelf energy drop for the Gundremmingen vessel material in comparison with predicted values acco:ding to US Reg. Guide 1.99 Rev. 1

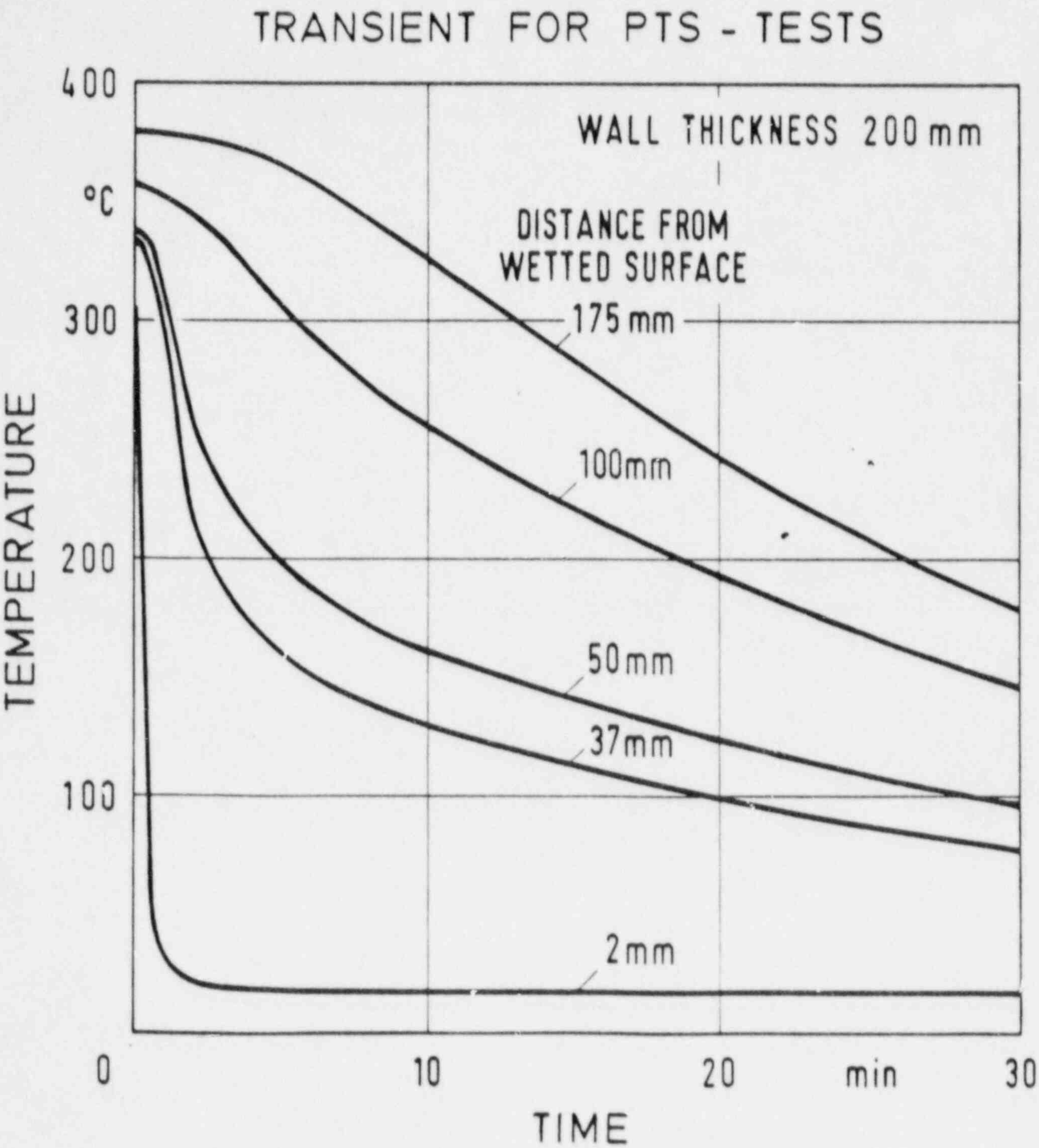

Fig. 26: Temperature/time function for different depth location in the wall during PTS experiment

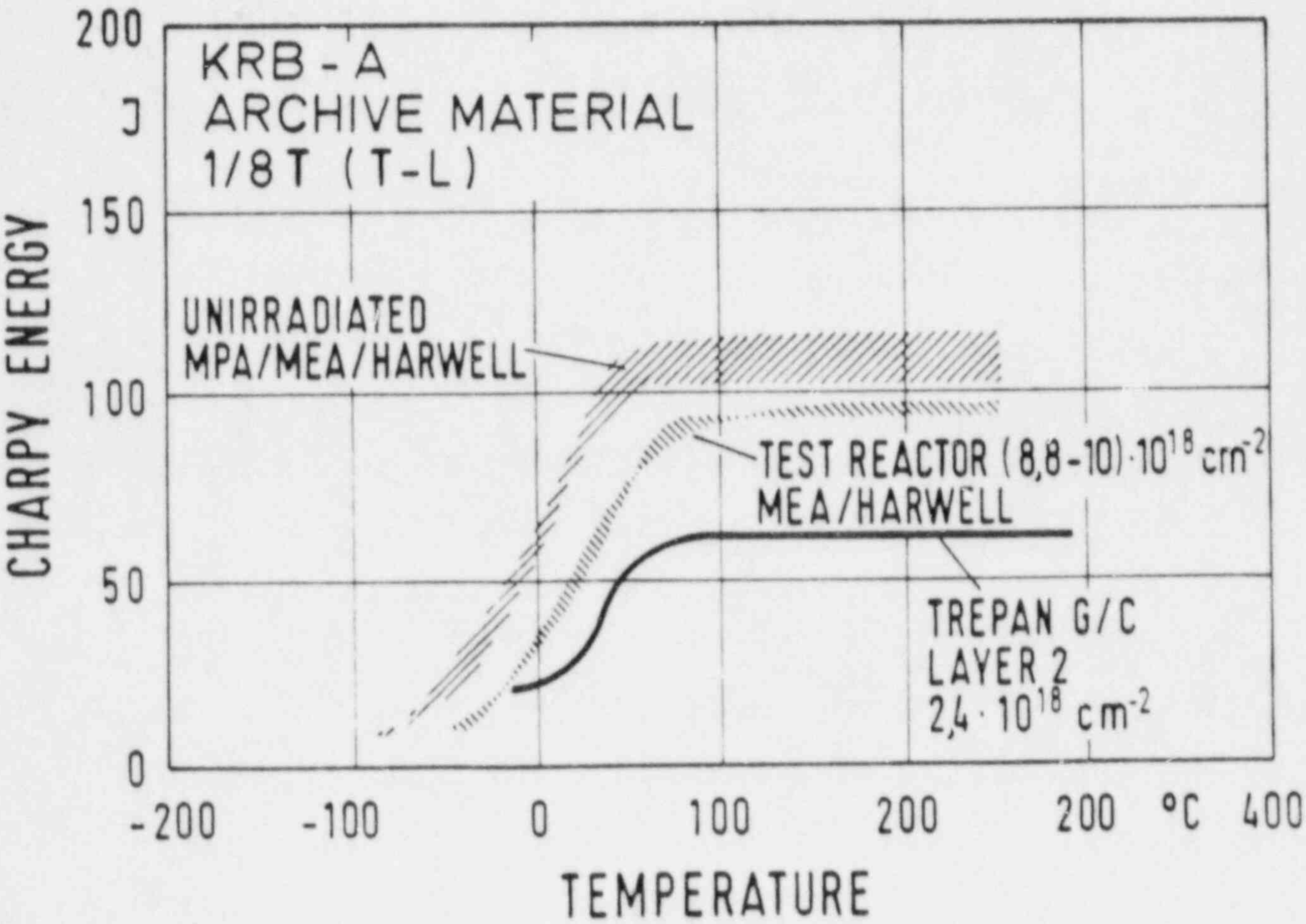

Fig. 22: Comparison of trepan results with results from irradiation experiments (archive material) in test reactors (MEA and Harwell) and unirradiated archive data

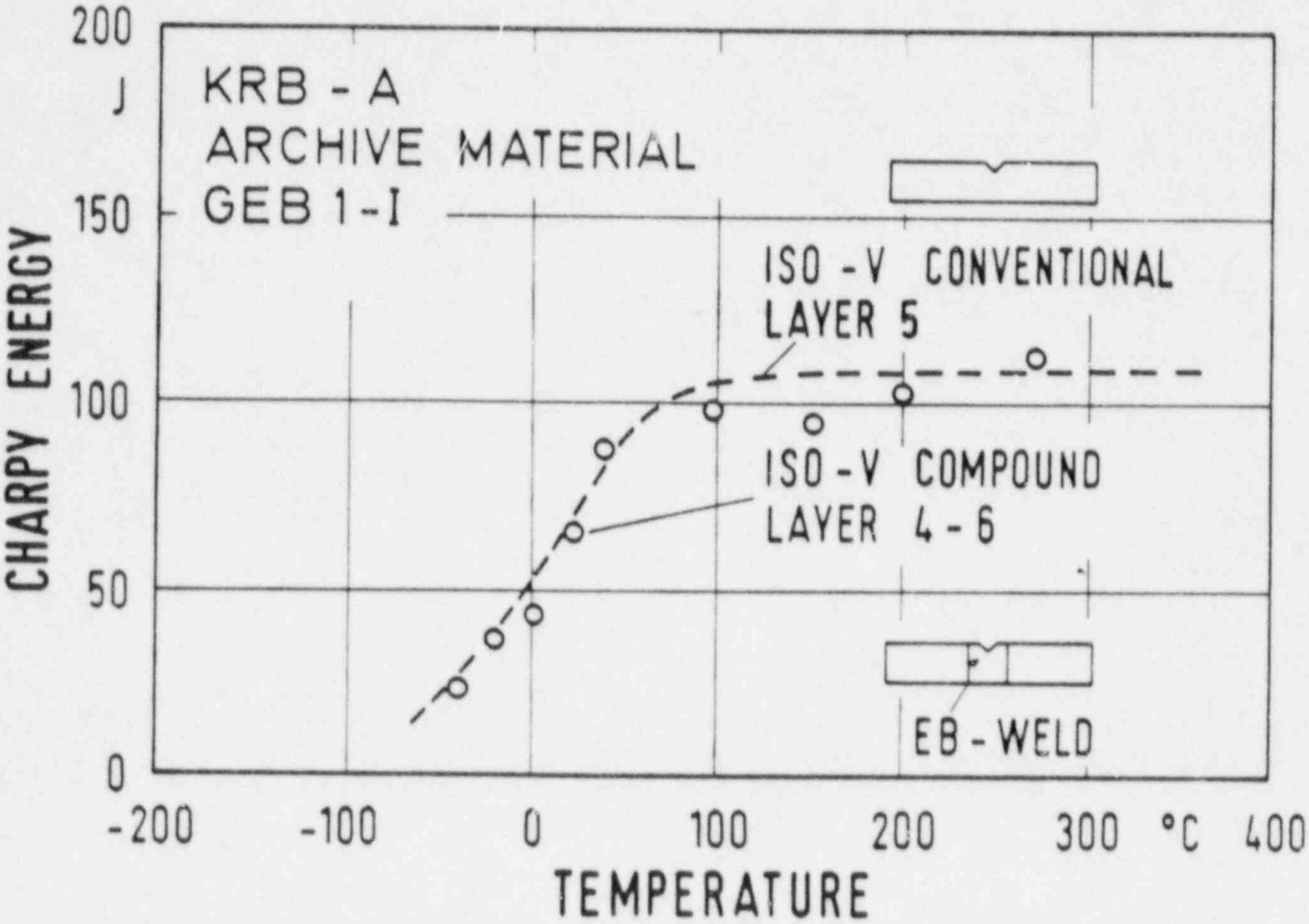

Fig. 23: Results of composite Charpy specimens compared with conventional procedure

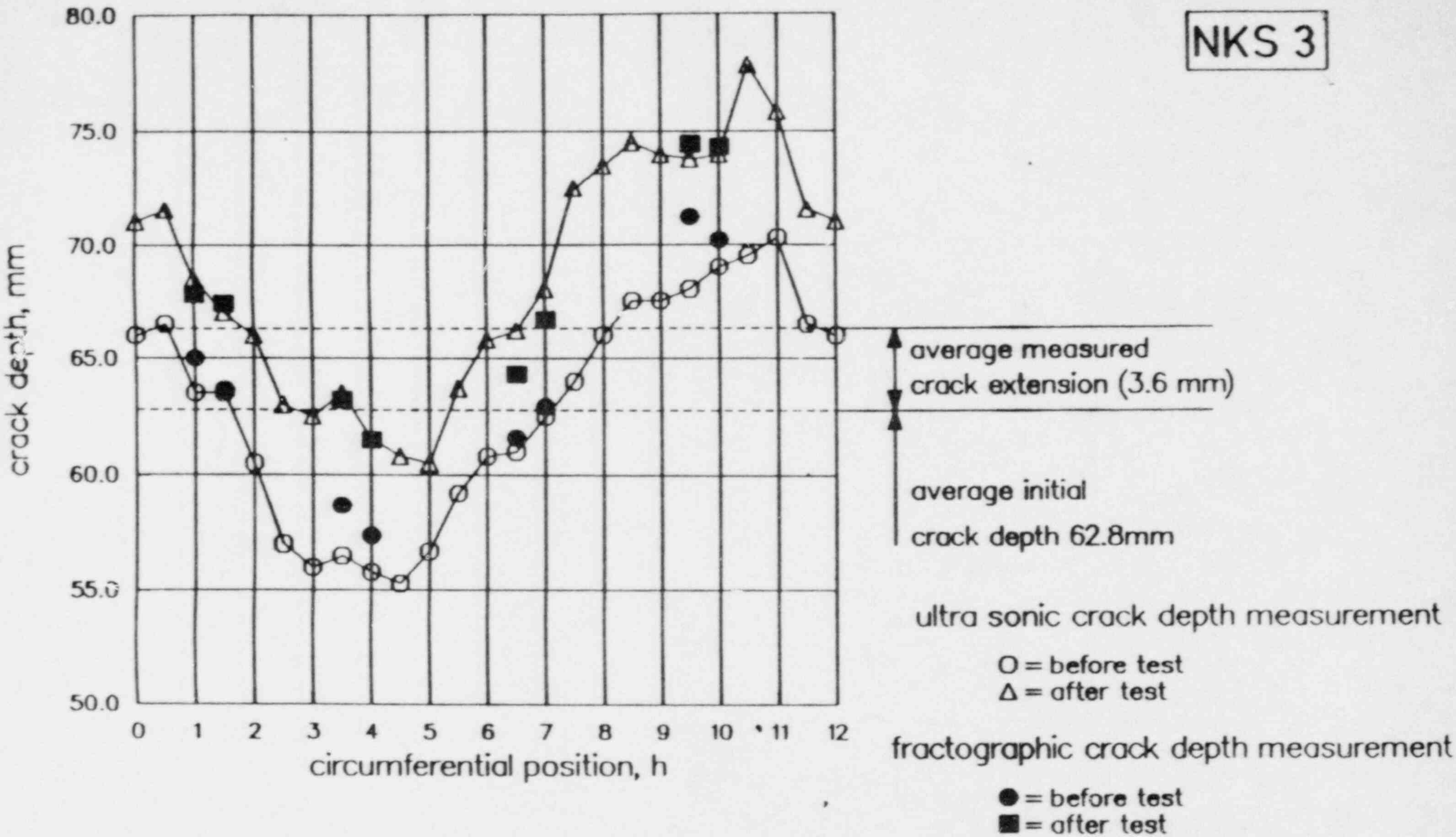

Fig. 28: Stable crack growth during PTS experiment NKS 3

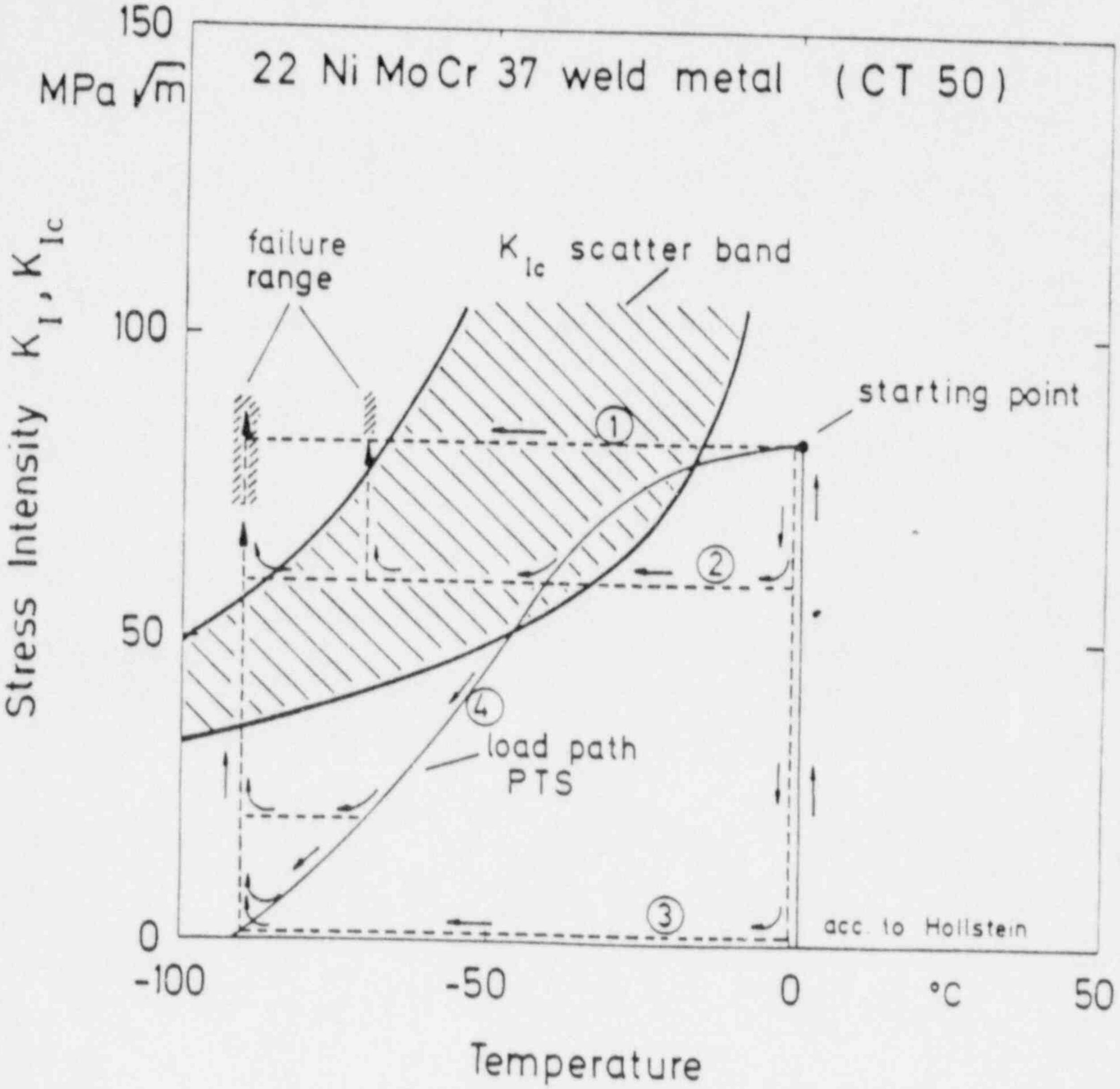

Fig. 29: Experimental verification of warm prestress effect during PTS

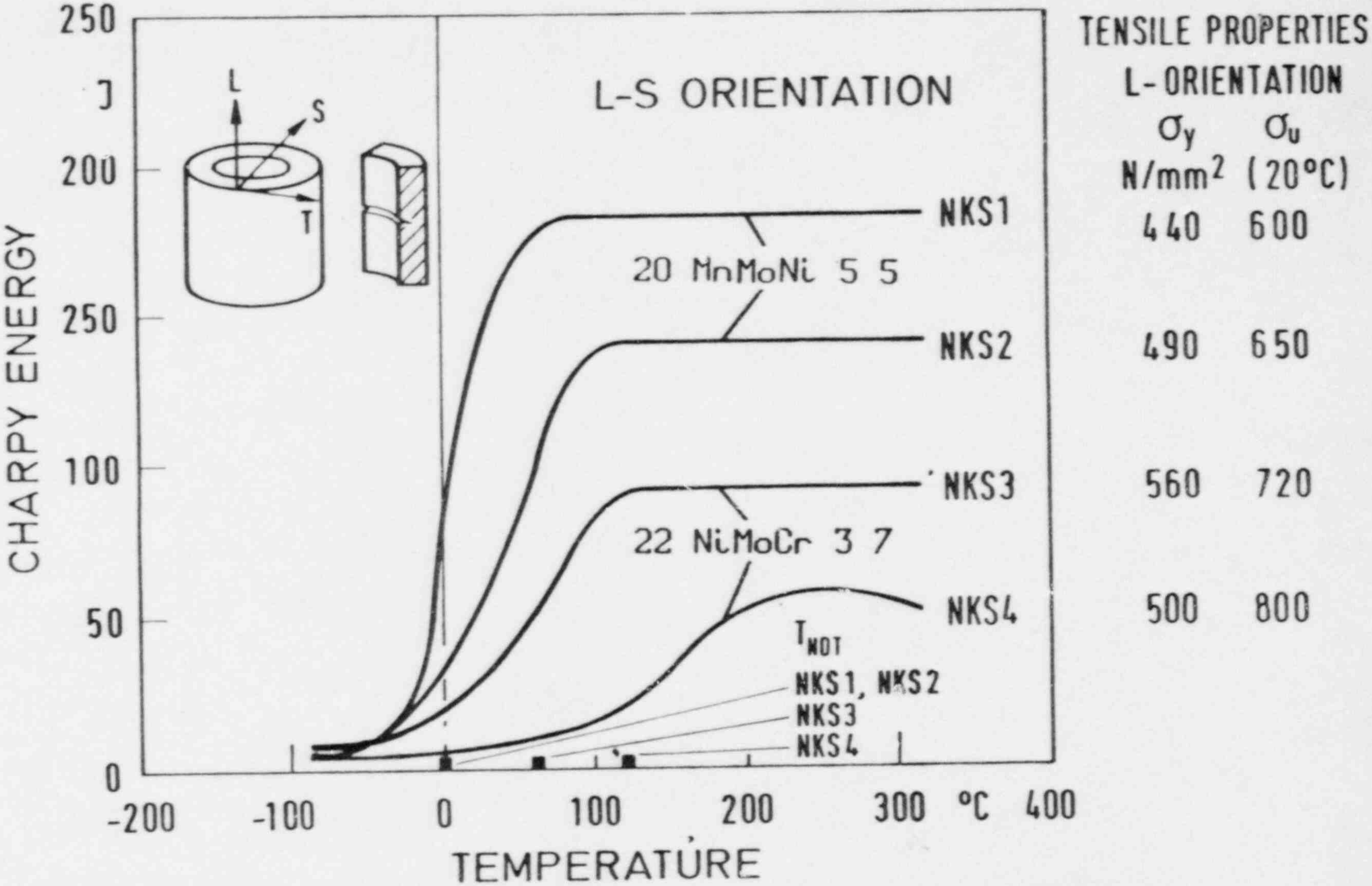

Fig. 25: Material used for PTS investigation ranging from "as specified" to "worst case" condition

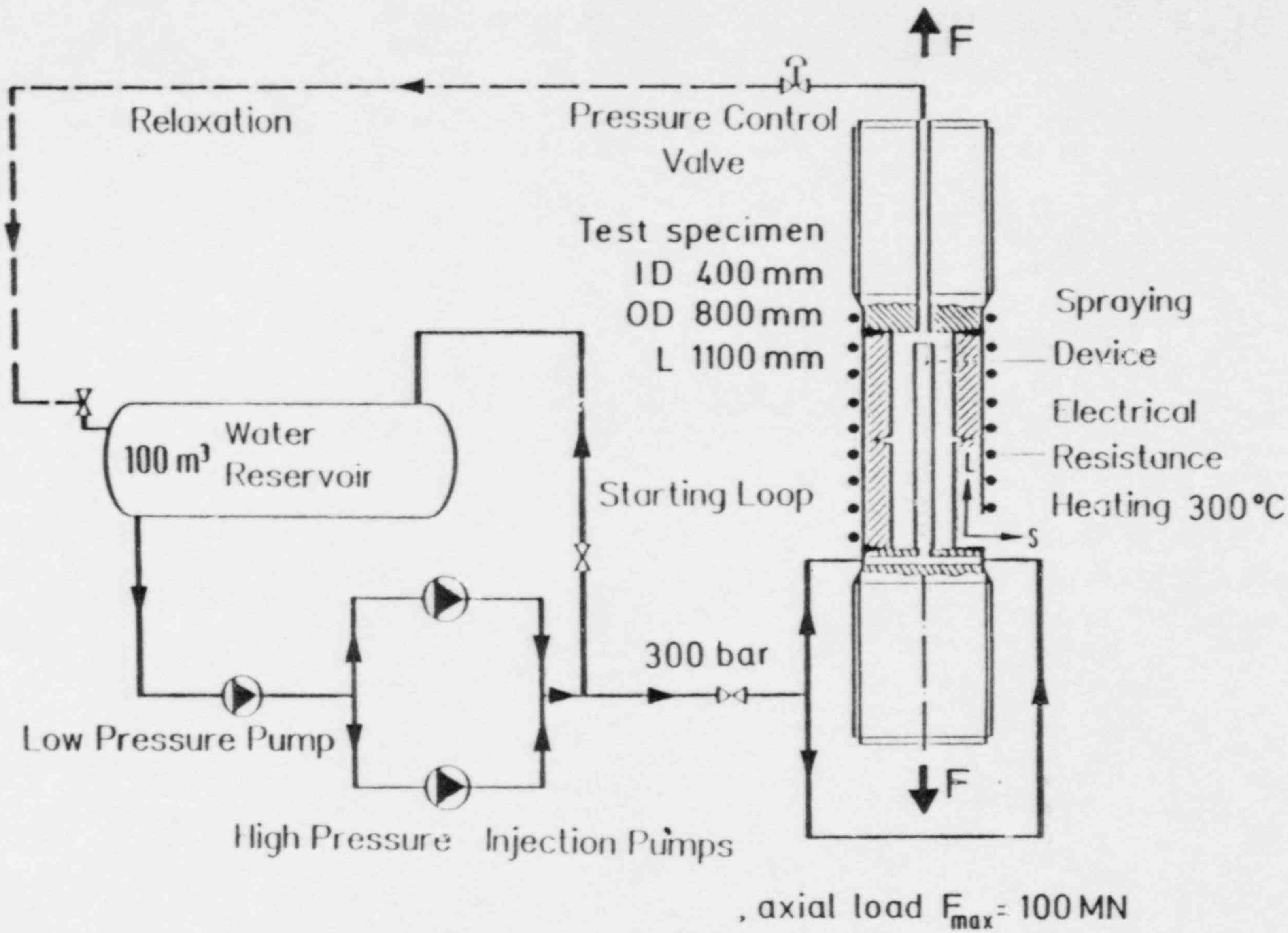

Fig. 24: Test specimen and loop for PTS simulation

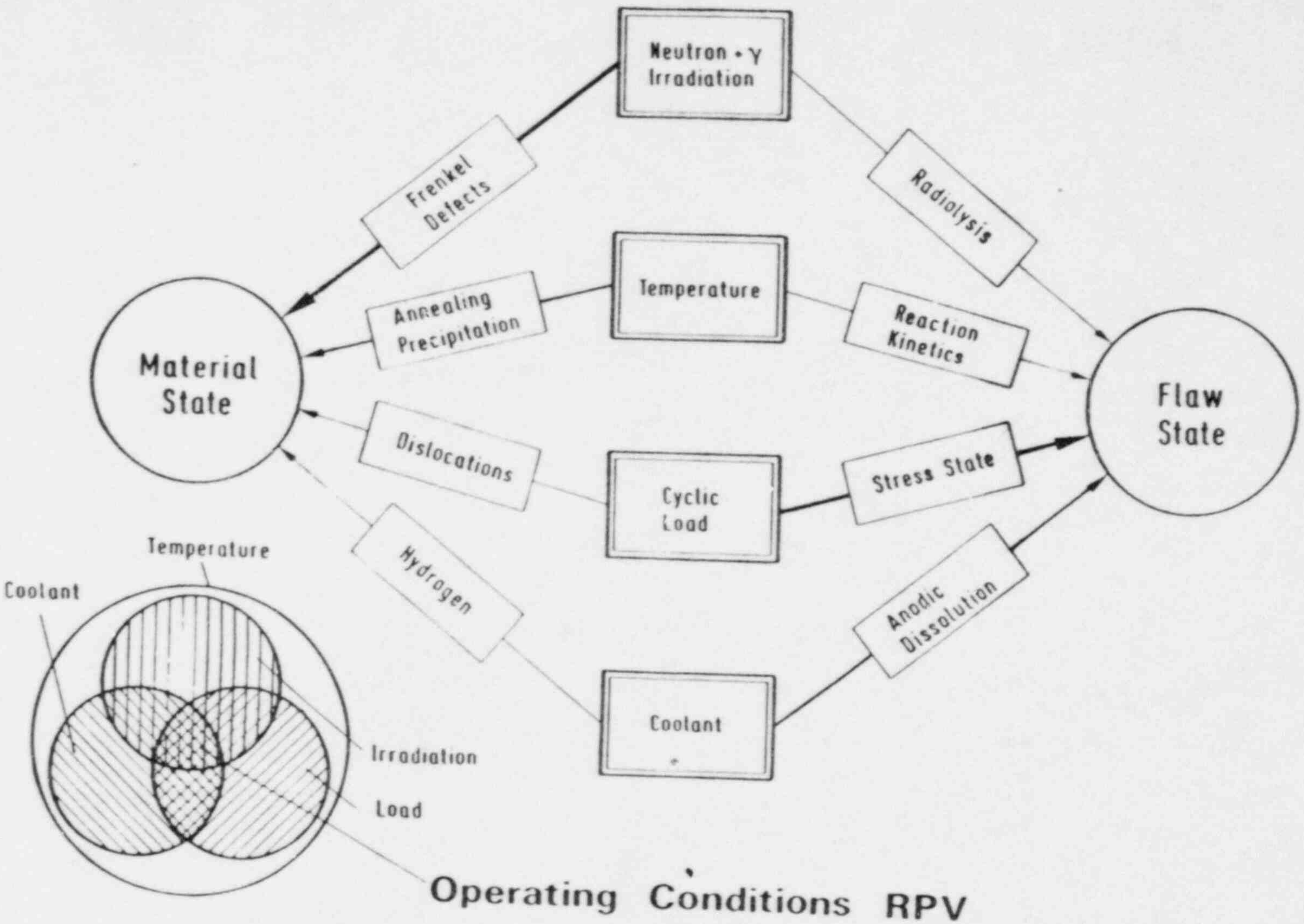

Fig. 30: Superimposed effects by operational conditions on material degradation and crack growth

IKE-6-FB-35
NUREG/CR-4791

NEUTRON SPECTRUM CALCULATION FOR THE GUNDREMMINGEN KRB/A REACTOR

C/3

U.S. Nuclear Regulatory Commission

NOTICE

This report was prepared as an account of work sponsored by an agency of the United States Government. Neither the United States Government nor any agency thereof, or any of their employees, makes any warranty, expressed or implied, or assumes any legal liability of responsibility for any third party's use, or the results of such use, of any information, apparatus, product or process disclosed in this report, or represents that its use by such third party would not infringe privately owned rights.

NOTICE

Availability of Reference Materials Cited in NRC Publications

Most documents cited in NRC publications will be available from one of the following sources:

1. The NRC Public Document Room, 1717 H Street, N.W.
   Washington, DC 20555

2. The Superintendent of Documents, U.S. Government Printing Office, Post Office Box 37082, Washington, DC 20013-7082

3. The National Technical Information Service, Springfield, VA 22161

Although the listing that follows represents the majority of documents cited in NRC publications, it is not intended to be exhaustive.

Referenced documents available for inspection and copying for a fee from the NRC Public Document Room include NRC correspondence and internal NRC memoranda; NRC Office of Inspection and Enforcement bulletins, circulars, information notices, inspection and investigation notices; Licensee Event Reports; vendor reports and correspondence; Commission papers; and applicant and licensee documents and correspondence.

The following documents in the NUREG series are available for purchase from the NRC/GPO Sales Program: formal NRC staff and contractor reports, NRC-sponsored conference proceedings, and NRC booklets and brochures. Also available are Regulatory Guides, NRC regulations in the *Code of Federal Regulations*, and *Nuclear Regulatory Commission Issuances*.

Documents available from the National Technical Information Service include NUREG series reports and technical reports prepared by other federal agencies and reports prepared by the Atomic Energy Commission, forerunner agency to the Nuclear Regulatory Commission.

Documents available from public and special technical libraries include all open literature items, such as books, journal and periodical articles, and transactions. *Federal Register* notices, federal and state legislation, and congressional reports can usually be obtained from these libraries.

Documents such as theses, dissertations, foreign reports and translations, and non-NRC conference proceedings are available for purchase from the organization sponsoring the publication cited.

Single copies of NRC draft reports are available free, to the extent of supply, upon written request to the Division of Technical Information and Document Control, U.S. Nuclear Regulatory Commission, Washington, DC 20555.

Copies of industry codes and standards used in a substantive manner in the NRC regulatory process are maintained at the NRC Library, 7920 Norfolk Avenue, Bethesda, Maryland, and are available there for reference use by the public. Codes and standards are usually copyrighted and may be purchased from the originating organization or, if they are American National Standards, from the American National Standards Institute, 1430 Broadway, New York, NY 10018.

1 INTRODUCTION

To determine neutron exposure of several trepans taken from the pressure vessel of the nuclear power plant Gundremmingen Block A (KRB-A) a three-dimensional neutron spectrum analysis is performed by IKE (Institut für Kernenergetik und Energiesysteme, University Stuttgart). The work, funded by US-NRC, is part of the KRB-A program analysing through vessel wall embrittlement of a real reactor vessel at the end of operation.

The Boiling Water Reactor KRB-A has a nominal thermal power of 801 MW (250 MW electrical). The reactor was put in operation in November 1966 and, until the last shutdown on January 13th, 1977, generated a total of about 16 TWh of electrical power, with an average availability of 75 %.

After decomissioning, 15 trepans have been taken at different axial and azimuthal positions within the 90 to 135 degree octant of the reactor. The axial and azimuthal positions of the trepans named A,B,C,D,E,F,G,K,L,M,N,P,Q,R,T can be seen in Figure 1 and 2. To get accurate assessments of the absolute magnitude of the interested exposure parameters such as fast fluence ($E > 1.0$ MeV), fluence ($E > 0.1$ MeV) or dpa (displacements per atom in iron) the three-dimensional flux distribution has to be calculated using the DOT4.2 /1/ code. This code solves the Boltzmann transport equation in two-dimensional geometry using the discrete ordinates method. Combining the results of a (R,Θ)-and (RZ)-model of the reactor the neutron spectrum is defined with sufficient accuracy /2/. To perform the transport calculations on an absolute scale a complete analysis of the reactor power-time history and of the three-dimensional burnup distributions at start and end of each of the reactor cycles has been performed.

This report describes the method used, summarizes important input data and gives the results of fast fluence ($E > 1.0$ MeV, $E > 0.1$ MeV), displacements per atom in iron (dpa) and total and thermal ($E < 0.414$ eV) fluences for all trepans.

The real attenuation within the vessel wall is discussed in context with formulae proposed in Regulatory Guide 1.99 Revision 1 and 2.

To confirm the results of the transport calculations calculated and measured Mn-54 activities of the trepans have been compared. Additionally dosimetry results from surveillance capsule 128 have been analysed. Since a surveillance capsule is not modeled in the transport calculation this comparison can only be a rough estimate. A detailed analysis of the capsule perturbation effects should follow.

2 METHOD OF ANALYSIS AND INPUT DATA

2.1 3D-Reactor Physics Calculation

In the analysis of the neutron environment outside the reactor core the three-dimensional flux distribution has been calculated with the help of a flux synthesis for each energy group G of the form

$$\Phi^G(R,\theta,Z) = \Phi_1^G(R,\theta) \cdot F^G(R,Z)$$

$$F^G(R,Z) = \Phi_2^G(R,Z) / \Phi_3^G(R)$$

where

$\Phi^G(R,\theta,Z)$ .... neutron fluence at point R,Z,θ for energy group G

$\Phi_1^G(R,\theta)$ .... solution of (R,θ)-calculation

$\Phi_2^G(R,Z)$ .... solution of (R,Z)-calculation

$\Phi_3^G(R)$ .... solution of one-dimensional axial infinite (R)-calculation

Φ_1^G, Φ_2^G and Φ_3^G have been calculated with the DOT4.2 /1/ code applying S_8/P_3 approximation. In the (R,θ)-model shown in Figure 2 the neutron source is calculated from axial averaged burnup distributions. In the (R,Z)-model axial variation of the burnup as well as moderator density is taken into account. In the (R,Z) analysis the reactor core is treated as an equivalent volume cylinder with 137,4 cm radius (Fig. 2). To obtain the relative axial variation $F^G(R,Z)$ the radial-axial neutron flux distribution $\Phi_2^G(R,Z)$ must be devided by the one-dimensional axial-infinite solution $\Phi_3^G(R)$.

The perturbation of the neutron field by surveillance capsules is not taken into account. Neutron fluxes have been stored at appropriate R-boundaries for detailed surveillance capsule analysis in the future.

2.2 Material Data

Specific material data for KRB-A are given in Table 1. The atomic compositions of material zones modeled in the transport calculation are summarized in Table 2. For the water zones in the downcomer and reflector in front of the trepans a temperature of 279 °C was assumed. The inlet temperature into the reactor core is 265,6 °C. For the homogenized core zone data in Table 2, saturated water with 285,8 °C has been assumed. These core data are only used in the (R,Θ)- calculations. In the (R,Z)-model 16 core zones with axial increasing void content have been taken into account.

2.3 Determination of the Neutron Source

The whole time-power history as well as burnup distributions per fuel element at start and end of each cycle are available for the KRB-A reactor. On the basis of these data total neutron source densities have been calculated taking into account burnup dependent energy and number of neutrons per fission. Since the burnup tables are only available per fuel elements, the shape of the power distribution within the outer fuel elements has been determined by means of theoretical curves. The calculated source densities have been transformed finally to the (R,Θ) space mesh (shown in Figure 1) conserving number of neutrons.

For the (R,Z)-transport calculations, the axial-radial dependent source densities have been obtained from axial burnup given at 12 axial modes of the fuel elements around the 120 degree Theta direction. An energy spectrum for thermal fission of U235 (Watt-type, ENDF/BV) has been assumed for the whole core. Only few Plutonium fuel elements situated at inner positions have been used during the whole reactor operation time.

2.4 Cross-section Data Used

For the two-dimensional transport calculation a special library with 35 neutron energy groups has been generated. Energy boundaries are given in Table 3. Group cross-section weighting has been performed with fine-group spectra calculated for KRB-A in one-dimensional geometry.

The fine-group library is based on ENDF/B IV data /3/ and has been compared with the VITAMIN/C /4/ library giving equivalent results /2/.

With this procedure higher accuracy can be achieved compared to the use of more general libraries like CASK /5/ or SAILOR /6/. The SAILOR library is specially designed for large Light Water Power reactors of the 1000 MW_{el}-class. Nevertheless, differences should be small if correct treatment of the resonance region especially in iron and temperature corrected thermal cross-section are guaranteed.

3 RESULTS OF TRANSPORT CALCULATIONS

Using the flux synthesis method described in Chapter 2 the neutron spectra is defined at each space mesh point of our KRB-A-model.

The maximum fluence value at the OT vessel position is $5,96 \times 10^{18}$ neutrons/cm² near the axial midplane of KRB/A at Z = 130 cm and 90 degree Theta direction.

The azimuthal variation of the fluence (E > 1 MeV) is within 55 percent of the maximum fluence value as it can be seen in Figure 3.

The axial shape function as a ratio of the two-dimensional (R,Z)- and the one-dimensional (R)-calculation is shown in Figure 4.

The neutron energy spectra in 35 energy group structure defined in Table 3 are given at the OT, 1/4 T, 1/2 T, 3/4 T and 1 T positions of the pressure vessel in Tables 4 to 7. Each table represents one Theta direction (see Figure 2). The values must still be multiplied with appropriate axial form factors from Figure 4 to get absolute values for each trepan.

3.1 Trepan Fluences E > 1 MeV and E > 0.1 MeV

The axial variation of the fast fluences E > 1 and E > 0.1 MeV within the cylindrical trepans, which is equivalent to attenuation of the fast neutrons through vessel wall, is shown in Figures 5 to 8. Each figure compares the fluences of trepans of the same axial level in the vessel. Z and Θ coordinated can be found in Figures 1 and 2. The radial variation of neutron exposure within one trepan (radius = 5.35 cm) can be neglected.

From the curves a maximum E > 1 MeV fluence value of about 4.3×10^{18} neutrons/cm² can be seen at the inner vessel surface. E > 0.1 MeV fluence at that location is a factor of two higher. For the attenuation through the vessel one gets a fluence ratio of about 5.6 for E > 1 MeV and 2.5 for E > 0.1 MeV. The ratio of the two exposure quantities within the vessel is plotted in Figure 9. In all figures the curves start at 180 cm radius to give first estimates also for the surveillance position nearest to the vessel (capsules 126, 127, 128 and 129).

3.2 Displacements per Atom in Iron

To calculate total displacements per atom in iron the ASTM E693 cross-section has been used. The 35 energy group values are listed in Table 8.

The resulting dpa exposure values for the fifteen trepans are shown in Figures 10 to 13. The increase of the dpa to E > 1 MeV fluence ratio within the vessel is demonstrated in Figure 14.

3.3 Total and Thermal Fluences

Finally the total and thermal (E < 0.414 eV) fluences have been calculated and plotted for all trepans in Figures 15 - 18. The thermal fluence fall off very strongly in the iron vessel down to a minimum of about 10^{17} neutron/cm². After 1/2 T depth it rises again due to the high thermal flux level in the concrete shield. The ratios of total to thermal and thermal to E > 1 MeV fluence are given in Figures 19 and 20.

3.4 Comparison of through Vessel Wall Attenuation

The attenuation of the different neutron exposure quantities within the pressure vessel together with the material property changes is of primary interest in the KRB/A trepan investigation. In Figure 21 the fluence E > 1 MeV and E > 0.1 MeV and dpa are compared with two pure exponential functions proposed in U.S. NRC Regulatory Guide 1.99, Revision 1 and 2.

The Rev. 1 curve

$$f = f_{surface} \cdot \exp(-0.33 \cdot x) \quad ,$$

where x is the wall depth in inches fits well the E > 1 MeV fluence curve. The 'dpa equivalent' attenuation formula with an exponent factor 0.24 proposed in Revision 2 seems to be too conservative for the small KRB/A reactor with only a 5 in thick vessel wall.

4 COMPARISON OF CALCULATED AND MEASURED ACTIVITIES

4.1 Mn-54 Activity of Trepans

Two independent measurements of the Manganese-54 activity one on 1st May 1984, the other on 22nd January 1986 have been made by KfA Jülich /7/. The measured activities of drillings taken from trepan A (1984) and trepan A, D, G, L. P (1986) are listed in Table 9 together with their radial position in the vessel measured from the vessel- clad interface.

The calculated specific activity A is determined using the relationship

$$A = A_{sat} \cdot \sum_{m=1}^{n} P_m (1-e^{-\lambda \cdot T_m})(e^{-\lambda t_m}),$$

where

P_m = fractional power for the operating period m,
λ = decay constant for the activation product $[d^{-1}]$
$\lambda = 2{,}218 \times 10^{-3}$ for Mn-54,
T_m = number of operating days for period m,
t_m = decay time after operating period m in days.

The saturated activity A_{sat} is determined by the macroscopic Fe-54(n,p)Mn-54 reaction cross-section and by the neutron flux spectra at appropriate space mesh intervalls.

Table 10 summarizes parameters for 14 operation time periods. For the activity calculations monthly averaged data have been used.

Considering the high statistical errors especially for the second measurement the agreement between calculated and measured activities is reasonably well.

4.2 Surveillance Capsule 128 Dosimetry Results

In the KRB-A surveillance program ten capsules have been irradiated at various locations within the vessel which can be seen in Figure 22. For the trepan investigation capsule 128 is the most adequate for comparison with the theoretical analysis. These capsule installed at an azimuthal position $\Theta = 140°$ and a radius R = 183 cm at the core midplane was irradiated during the whole time of reactor operation. The dimensions of the capsule which has the form of a basket are 5/8 x 6 7/8 x 10 1/8 in. For dosimetry purpose iron, nickel and copper wires have been irradiated together with the samples. The activation monitors as well as the Mn-54 activity of the material samples have been measured independently from two laboratories /8/. The measured Co-60 from the Cu-63(n,α)-reaction and Mn-54-activities from Fe-54(n,p) are summarized in Table 11. The cross-sections for Cu-63(n,α) and Mn-54(n,p) are given in Table 8.

Since the surveillance capsule is not modeled in the transport calculation caution should be exercised in comparing the measured and calculated activities which have been summarized also in Table 11. Nevertheless, one can assume that the capsule perturbation effect should rather improve the C/E-values.

There are plans for a detailed analysis of the perturbation effect together with a reevaluation of all the other capsules.

BIBLIOGRAPHY

/1/ W.A. Rhoades, D.B. Simpson, R.L. Childs and W.E. Engle, 'The DOT-IV Two Dimensional Discrete Ordinates Transport COde with Space-Dependent Mesh and Quadrature', ORNL/TM-6529, (1979)

/2/ G. Prillinger and G. Pfister, 'The Necessity of Detailed Multi-Dimensional Transport Calculations in LWR Pressure Vessel Surveillance and for MTR Irradiation', Sixth International Conference on Radiation Shielding (ICRS), May 16-20, 1983 Tokyo Japan,

/3/ M. Mattes, 'EURLIB-4, a coupled Neutron and Gamma Multigroup Cross Section Library based on ENDF/BIV, IKE 6-121 (1979)

/4/ R.W. Roussin, C.R. Weisbin, J.E. White, N.M. Green, R.Q. Weight, and J.B. Weight, 'VITAMIN/C, The CTR Processed Multigroup Cross Section Library for Neutronics Studies', ORNL/RSIC-37

/5/ CASK-40-Group Coupled Neutron and Gamma Ray Cross-Section Data, RSIC-DLC-23, Radiation Shielding Inf. Center, Oak Ridge, TN

/6/ SAILOR, RSIC Data Library Collection DLC-76, 'Coupled, Self-Shielded, 47 Neutron, 29 Gamma Ray, P_3, Cross-Section Library for Light Water Reactors

/7/ R. Schröder, 'Gammaspektroskopische Untersuchung von Bohrspänen aus den Bohrkernen A,D,G,L und P des RDB Gundremmingen. KFA-Jülich, IRW-TN-24/86, Feb. 1986

/8/ G. Lörcher, NIS-Hanau, private communications, June 1986

Table 1: Material data

Zone	Shield thickness [cm]	Density [g/cm³]	Comment
core			
reflector	20.1 *)	0.753	water
barrel	2.54	7.86	ASTM-A240, Typ 304 X5CrNi189
downcomer	25.36	0.753	water
clading	0.8	7.8	
vessel	12.7	7.86	20NiMoCr26
reactor cavity	21.1		
liner	0.3	7.85	St34
concrete	129.7		

*) equivalent core radius is 137.4 cm

Table 2: Material compositions in atoms $cm^{-3} \cdot 10^{-24}$

	core	reflector	barrel	downcomer	clading	vessel	liner	concrete
H	2.97E-2	5.03-2	-	5.03-2	-	-	-	9.62E-3
C	-	-	3.15E-4	-	8.99E-5	9.06E-4	6.69E-4	3.81E-3
O	2.71E-2	2.52-2	-	2.52-2	-	-	-	4.65E-2
Al	-	-	-	-	-	-	-	9.75E-4
Si	-	-	-	-	-	-	-	1.47E-2
Ca	-	-	-	-	-	-	-	9.68E-4
Cr	-	-	1.64E-2	-	1.87E-2	3.37E-4	-	-
Mn	-	-	8.62E-4	-	1.01E-3	6.03E-4	-	-
Fe	-	-	5.81E-2	-	5.51E-2	8.18E-2	8.45E-2	1.41E-3
Ni	-	-	9.68E-3	-	9.20E-3	6.37E-4	-	2.60E-6
Zr	3.70E-3	-	-	-	-	-	-	-
Mo	-	-	-	-	-	3.01E-4	-	-
U^{35}	1.49E-4	-	-	-	-	-	-	-
U^{38}	6.01E-3	-	-	-	-	-	-	-

Table 3: 35 group energy structure

Nr	Energy boundaries	Nr	Energy boundaries
1	10.000 - 14.917 MeV	18	183.16 - 301.97 KeV
2	8.187 - 10.000 MeV	19	111.09 - 183.16 KeV
3	6.703 - 8.187 MeV	20	52.475 - 111.09 KeV
4	6.065 - 6.703 MeV	21	31.829 - 52.475 KeV
5	4.966 - 6.065 MeV	22	26.050 - 31.829 KeV
6	3.679 - 4.966 MeV	23	24.788 - 26.050 KeV
7	3.011 - 3.679 MeV	24	15.034 - 24.788 KeV
8	2.466 - 3.011 MeV	25	5.531 - 15.034 KeV
9	2.346 - 2.466 MeV	26	1.585 - 5.531 KeV
10	2.231 - 2.346 MeV	27	0.454 - 1.585 KeV
11	1.653 - 2.231 MeV	28	101.3 - 454.0 eV
12	1.353 - 1.653 MeV	29	37.267 - 101.3 eV
13	1.003 - 1.353 MeV	30	10.677 - 37.267 eV
14	0.748 - 1.003 MeV	31	5.044 - 10.677 eV
15	550.23 - 747.74 KeV	32	1.855 - 5.044 eV
16	368.83 - 550.23 KeV	33	0.625 - 1.855 eV
17	301.97 - 368.83 KeV	34	0.414 - 0.625 eV
		35	10^{-5} - 0.414 eV

Table 4: Calculated neutron spectra [n/cm²] in KRB-A vessel, (R,θ)-model, θ = 111.4°

Energy Group	0T	1/4 T	1/2 T	3/4 T	1 T
1	2.41768E+16	1.43527E+16	8.38085E+15	4.88476E+15	3.08149E+15
2	5.62619E+16	3.30369E+16	1.89338E+16	1.08325E+16	6.78702E+15
3	1.10246E+17	6.32407E+16	3.52255E+16	1.96076E+16	1.21180E+16
4	9.92484E+16	5.58647E+16	3.04234E+16	1.65725E+16	1.01098E+16
5	2.10192E+17	1.15203E+17	6.16436E+16	3.31748E+16	2.03497E+16
6	3.39282E+17	1.86751E+17	1.00426E+17	5.45103E+16	3.40013E+16
7	2.17273E+17	1.28243E+17	7.30518E+16	4.15435E+16	2.64497E+16
8	3.10179E+17	1.96755E+17	1.16720E+17	6.82597E+16	4.36974E+16
9	1.00749E+17	6.62852E+16	4.02394E+16	2.39138E+16	1.53463E+16
10	9.89759E+16	6.87723E+16	4.32205E+16	2.62453E+16	1.66785E+16
11	4.90015E+17	3.76694E+17	2.54545E+17	1.61530E+17	1.01738E+17
12	3.37462E+17	2.78920E+17	1.98786E+17	1.31830E+17	8.70057E+16
13	5.06696E+17	4.80317E+17	3.82142E+17	2.74386E+17	1.86695E+17
14	4.90634E+17	4.84540E+17	4.08514E+17	3.16911E+17	2.42286E+17
15	6.14426E+17	6.96054E+17	6.37209E+17	5.18860E+17	3.87985E+17
16	5.30812E+17	5.74140E+17	5.18347E+17	4.17060E+17	3.10754E+17
17	3.22621E+17	3.84789E+17	3.65565E+17	3.05860E+17	2.31745E+17
18	5.34131E+17	6.23447E+17	6.11935E+17	5.36628E+17	4.40809E+17
19	4.28984E+17	4.70318E+17	4.50478E+17	4.01038E+17	3.43745E+17
20	4.55521E+17	5.03236E+17	4.89237E+17	4.34632E+17	3.64917E+17
21	2.07089E+17	1.89201E+17	1.75132E+17	1.59594E+17	1.52231E+17
22	5.24154E+16	2.16577E+16	1.85767E+16	1.72208E+16	3.05688E+16
23	6.65682E+16	7.34628E+16	6.87382E+16	6.17854E+16	5.18504E+16
24	2.36961E+17	2.55189E+17	2.50693E+17	2.32096E+17	2.06234E+17
25	2.90592E+17	1.87602E+17	1.49569E+17	1.49043E+17	1.89050E+17
26	4.11806E+17	3.32365E+17	2.84175E+17	2.59541E+17	2.56399E+17
27	3.65412E+17	2.71778E+17	2.27399E+17	2.07795E+17	2.14629E+17
28	4.31474E+17	2.86123E+17	2.20362E+17	2.00766E+17	2.18479E+17
29	2.99563E+17	2.10059E+17	1.59433E+17	1.39029E+17	1.39693E+17
30	3.60056E+17	2.43072E+17	1.79262E+17	1.52125E+17	1.54803E+17
31	2.09619E+17	1.35310E+17	9.74863E+16	8.14947E+16	8.39455E+16
32	2.64431E+17	1.53175E+17	1.02667E+17	8.70480E+16	9.72583E+16
33	2.57275E+17	1.21847E+17	7.26021E+16	6.34031E+16	8.47533E+16
34	8.77455E+16	3.47868E+16	1.88619E+16	1.70732E+16	2.67774E+16
35	5.22009E+18	7.53018E+17	1.19058E+17	1.39774E+17	6.81937E+17

Table 5: Calculated neutron spectra [n/cm²] in KRB-A vessel, (R,Θ)-model, Θ = 117.1°

Energy Group	OT	1/4 T	1/2 T	3/4 T	1 T
1	2.36707E+16	1.40815E+16	8.23095E+15	4.79855E+15	3.02542E+15
2	5.48520E+16	3.22704E+16	1.83056E+16	1.03845E+16	6.62477E+15
3	1.06906E+17	6.14298E+16	3.42243E+16	1.90376E+16	1.17514E+16
4	9.59955E+16	5.41162E+16	2.94723E+16	1.60416E+16	9.77419E+15
5	2.00897E+17	1.10179E+17	5.89474E+16	3.17112E+16	1.94525E+16
6	3.19834E+17	1.75946E+17	9.46263E+16	5.13886E+16	3.21286E+16
7	2.03027E+17	1.19980E+17	6.83596E+16	3.89528E+16	2.48825E+16
8	2.88737E+17	1.83485E+17	1.08891E+17	6.37980E+16	4.10184E+16
9	9.35957E+16	6.16894E+16	3.74725E+16	2.23092E+16	1.43846E+16
10	9.18727E+16	6.39470E+16	4.02084E+16	2.44620E+16	1.56146E+16
11	4.54114E+17	3.50095E+17	2.36666E+17	1.50590E+17	9.52221E+16
12	3.12185E+17	2.59128E+17	1.84670E+17	1.22906E+17	8.14737E+16
13	4.68780E+17	4.46233E+17	3.54887E+17	2.55838E+17	1.74842E+17
14	4.54140E+17	4.50282E+17	3.79398E+17	2.95725E+17	2.27762E+17
15	5.69504E+17	6.46951E+17	5.92412E+17	4.84415E+17	3.64518E+17
16	4.90700E+17	5.32947E+17	4.82447E+17	3.90040E+17	2.93118E+17
17	2.98768E+17	3.57598E+17	3.40482E+17	2.86096E+17	2.18420E+17
18	4.94695E+17	5.79749E+17	3.71276E+17	5.03501E+17	4.17676E+17
19	3.97203E+17	4.38216E+17	4.21445E+17	3.77195E+17	3.26383E+17
20	4.22293E+17	4.69443E+17	4.58378E+17	4.09507E+17	3.47247E+17
21	1.91646E+17	1.76295E+17	1.64056E+17	1.50696E+17	1.45323E+17
22	4.84653E+16	2.01694E+16	1.73796E+16	1.62832E+16	2.92685E+16
23	6.18905E+16	6.85764E+16	6.44557E+16	5.82216E+16	4.91177E+16
24	2.20444E+17	2.38857E+17	2.35520E+17	2.19253E+17	1.96238E+17
25	2.68652E+17	1.74728E+17	1.39740E+17	1.41503E+17	1.81366E+17
26	3.80192E+17	3.09062E+17	2.65292E+17	2.46254E+17	2.45670E+17
27	3.36519E+17	2.52413E+17	2.11779E+17	1.97544E+17	2.05758E+17
28	3.93783E+17	2.63767E+17	2.04795E+17	1.90945E+17	2.09452E+17
29	2.73164E+17	1.93594E+17	1.47948E+17	1.32248E+17	1.33857E+17
30	3.29815E+17	2.25203E+17	1.66299E+17	1.44647E+17	1.48321E+17
31	1.92475E+17	1.25523E+17	8.99631E+16	7.75309E+16	8.07077E+16
32	2.43331E+17	1.41187E+17	9.56125E+16	8.27251E+16	9.35008E+16
33	2.35886E+17	1.12130E+17	6.76681E+16	6.03733E+16	8.20635E+16
34	8.02721E+16	3.19043E+16	1.76278E+16	1.62828E+16	2.59090E+16
35	4.74429E+18	6.75047E+17	1.09130E+17	1.34128E+17	6.64238E+17

Table 6: Calculated neutron spectra [n/cm²] in KRB-A vessel, (R,Θ)-model, Θ = 122.9°

Energy Group	0T	1/4 T	1/2 T	3/4 T	1 T
1	2.42230E+16	1.43294E+16	8.32906E+15	4.83026E+15	3.03044E+15
2	5.67713E+16	3.32187E+16	1.89454E+16	1.07795E+16	6.71087E+15
3	1.12256E+17	6.41765E+16	3.55574E+16	1.96699E+16	1.20609E+16
4	1.01272E+17	5.68311E+16	3.07877E+16	1.66663E+16	1.00807E+16
5	2.15998E+17	1.18085E+17	6.28431E+16	3.33988E+16	2.03929E+16
6	3.51515E+17	1.92838E+17	1.03091E+17	5.55580E+16	3.41928E+16
7	2.25836E+17	1.32640E+17	7.50145E+16	4.23596E+16	2.65740E+16
8	3.24350E+17	2.04565E+17	1.20360E+17	6.97978E+16	4.39844E+16
9	1.05598E+17	6.90249E+16	4.15484E+16	2.44788E+16	1.54637E+16
10	1.03667E+17	7.15373E+16	4.45785E+16	2.68471E+16	1.68137E+16
11	5.10980E+17	3.89984E+17	2.61281E+17	1.64633E+17	1.02285E+17
12	3.50862E+17	2.88036E+17	2.03538E+17	1.34056E+17	8.71063E+16
13	5.23348E+17	4.92793E+17	3.88574E+17	2.77476E+17	1.86354E+17
14	5.04994E+17	4.94943E+17	4.12982E+17	3.18244E+17	2.39844E+17
15	6.27697E+17	7.04879E+17	6.39571E+17	5.17785E+17	3.83078E+17
16	5.41596E+17	5.82153E+17	5.20763E+17	4.15875E+17	3.05464E+17
17	3.27256E+17	3.87599E+17	3.65266E+17	3.03693E+17	2.27718E+17
18	5.41082E+17	6.26676E+17	6.09370E+17	5.30210E+17	4.30786E+17
19	4.34528E+17	4.70988E+17	4.46683E+17	3.94683E+17	3.34919E+17
20	4.63619E+17	5.03738E+17	4.84887E+17	4.26832E+17	3.55015E+17
21	2.12428E+17	1.90464E+17	1.74064E+17	1.56484E+17	1.47539E+17
22	5.40266E+16	2.17967E+16	1.84842E+16	1.68771E+16	2.95047E+16
23	6.73913E+16	7.34548E+16	6.80493E+16	6.06196E+16	5.04780E+16
24	2.38611E+17	2.53440E+17	2.46829E+17	2.26881E+17	2.00247E+17
25	2.98328E+17	1.89696E+17	1.48074E+17	1.45315E+17	1.82369E+17
26	4.22865E+17	3.36299E+17	2.82331E+17	2.54427E+17	2.47687E+17
27	3.77676E+17	2.75925E+17	2.26340E+17	2.03990E+17	2.07215E+17
28	4.48193E+17	2.91072E+17	2.20346E+17	1.97113E+17	2.10790E+17
29	3.11801E+17	2.14201E+17	1.59737E+17	1.36895E+17	1.34869E+17
30	3.76289E+17	2.48405E+17	1.80026E+17	1.50393E+17	1.49480E+17
31	2.19234E+17	1.38569E+17	9.76873E+16	8.05767E+16	8.12420E+16
32	2.74915E+17	1.56952E+17	1.03925E+17	8.59208E+16	9.40134E+16
33	2.67688E+17	1.25420E+17	7.35681E+16	6.25211E+16	8.20858E+16
34	9.14943E+16	3.58580E+16	1.91996E+16	1.68168E+16	2.59160E+16
35	5.48344E+18	7.80187E+17	1.22025E+17	1.37523E+17	6.61608E+17

Table 7: Calculated neutron spectra [n/cm²] in KRB-A vessel, (R,Θ)-model, Θ = 128.6°

Energy Group	0T	1/4 T	1/2 T	3/4 T	1 T
1	2.60094E+16	1.54349E+16	8.98264E+15	5.20993E+15	3.26161E+15
2	6.14715E+16	3.60861E+16	2.06053E+16	1.17212E+16	7.27043E+15
3	1.22867E+17	7.04700E+16	3.90824E+16	2.16031E+16	1.31700E+16
4	1.11182E+17	6.25919E+16	3.39382E+16	1.83538E+16	1.10261E+16
5	2.40182E+17	1.31543E+17	6.99714E+16	3.73183E+16	2.24126E+16
6	3.97460E+17	2.17951E+17	1.16235E+17	6.23655E+16	3.77914E+16
7	2.57876E+17	1.50841E+17	8.49759E+16	4.76864E+16	2.93841E+16
8	3.72461E+17	2.34065E+17	1.37107E+17	7.89549E+16	4.88031E+16
9	1.21632E+17	7.91851E+16	4.74387E+16	2.77496E+16	1.71903E+16
10	1.19468E+17	8.20756E+16	5.08985E+16	3.04375E+16	1.87183E+16
11	5.89280E+17	4.46634E+17	2.97598E+17	1.86140E+17	1.13645E+17
12	4.04996E+17	3.29852E+17	2.31626E+17	1.51264E+17	9.63023E+16
13	6.00347E+17	5.61680E+17	4.40037E+17	3.11573E+17	2.05513E+17
14	5.77234E+17	5.61735E+17	4.65030E+17	3.54430E+17	2.61216E+17
15	7.12568E+17	7.93542E+17	7.14360E+17	5.72563E+17	4.16083E+17
16	6.16042E+17	6.56884E+17	5.81038E+17	4.58341E+17	3.28678E+17
17	3.69653E+17	4.33709E+17	4.05080E+17	3.33172E+17	2.45142E+17
18	6.10534E+17	6.99216E+17	6.71003E+17	5.76503E+17	4.57692E+17
19	4.88261E+17	5.22693E+17	4.88171E+17	4.26080E+17	3.53333E+17
20	5.21583E+17	5.58087E+17	5.28193E+17	4.58890E+17	3.71748E+17
21	2.40392E+17	2.12034E+17	1.89853E+17	1.67459E+17	1.52770E+17
22	6.15953E+16	2.42650E+16	2.02189E+16	1.80640E+16	3.02675E+16
23	7.53943E+16	8.10866E+16	7.40847E+16	6.50146E+16	5.33418E+16
24	2.65270E+17	2.77153E+17	2.66094E+17	2.41527E+17	2.09386E+17
25	3.39467E+17	2.11623E+17	1.61776E+17	1.53638E+17	1.86751E+17
26	4.81343E+17	3.75272E+17	3.09267E+17	2.69837E+17	2.54744E+17
27	4.30504E+17	3.08756E+17	2.48601E+17	2.16045E+17	2.12945E+17
28	3.13032E+17	3.26946E+17	2.41684E+17	2.08622E+17	2.15920E+17
29	3.57026E+17	2.40701E+17	1.75719E+17	1.45114E+17	1.38605E+17
30	4.28737E+17	2.79586E+17	1.98750E+17	1.59941E+17	1.53428E+17
31	2.51229E+17	1.55983E+17	1.08242E+17	8.56882E+16	8.32569E+16
32	3.14985E+17	1.77665E+17	1.14737E+17	9.14001E+16	9.59391E+16
33	3.07335E+17	1.42819E+17	8.14279E+16	6.63271E+16	8.34136E+16
34	1.05167E+17	4.09181E+16	2.12340E+16	1.77864E+16	2.62928E+16
35	6.39590E+18	9.03400E+17	1.40627E+17	1.43300E+17	6.65654E+17

Table 8: dpa, Fe-54(n,p) and Cu-63(n,α) cross-sections [barn]

Energy Group	dpa	Fe-54(n,p)	Cu-63(n,α)
1	0.2437E+04	0.4626E+00	0.5206E-01
2	0.2195E+04	0.4771E+00	0.3499E-01
3	0.2025E+04	0.4728E+00	0.1429E-01
4	0.1910E+04	0.4669E+00	0.7690E-02
5	0.1785E+04	0.4263E+00	0.3108E-02
6	0.1588E+04	0.3107E+00	0.5620E-03
7	0.1369E+04	0.1985E+00	0.4137E-04
8	0.1273E+04	0.1073E+00	0.5129E-05
9	0.1159E+04	0.5623E-01	0.8647E-06
10	0.1041E+04	0.4575E-01	0.6338E-06
11	0.9229E+03	0.1856E-01	0.1236E-06
12	0.8085E+03	0.2815E-02	0.0000E+00
13	0.5591E+03	0.6977E-03	0.0000E+00
14	0.4366E+03	0.3308E-04	0.0000E+00
15	0.3283E+03	0.5158E-06	0.0000E+00
16	0.3758E+03	0.2073E-07	0.0000E+00
17	0.2112E+03	0.1273E-07	0.0000E+00
18	0.1975E+03	0.9138E-08	0.0000E+00
19	0.1422E+03	0.5328E-08	0.0000E+00
20	0.1097E+03	0.3027E-08	0.0000E+00
21	0.7174E+02	0.1588E-08	0.0000E+00
22	0.2839E+03	0.1101E-08	0.0000E+00
23	0.2929E+02	0.9659E-09	0.0000E+00
24	0.7096E+01	0.7486E-09	0.0000E+00
25	0.1738E+02	0.3659E-09	0.0000E+00
26	0.4702E+01	0.1210E-09	0.0000E+00
27	0.1749E+01	0.3464E-10	0.0000E+00
28	0.1207E+00	0.8983E-11	0.0000E+00
29	0.2223E+00	0.2452E-11	0.0000E+00
30	0.3903E+00	0.8194E-12	0.0000E+00
31	0.6349E+00	0.2916E-12	0.0000E+00
32	0.9846E+00	0.1249E-12	0.0000E+00
33	0.1653E+01	0.4435E-13	0.0000E+00
34	0.2406E+01	0.1988E-13	0.0000E+00
35	0.4033E+01	0.9450E-14	0.0000E+00

Table 9: Comparison of measured and calculated Mn 54 activities of trepans

Trepan	Date of measurement	Distance [cm] from vessel-clad interface	Spec. activity [Bq/g] measured	Spec. activity [Bq/g] calculated	C/E
A	1.5.1984	0.30	2035±	2586.2	1.27
A	22.1.1986	0.65	568.8±28.8%	578.4	1.02
D	"	0.55	403.2±36.3%	493.6	1.22
G	"	0.80	405.3±36.0%	437.8	1.08
L	"	0.80	440.2±41,1 %	470.6	1.07
P	"	0.60	429.1±36.5 %	406.8	0.95

Table 10: Parameters used for activity calculation

	Operation period	T_m	t_m *)	Fractional power
1	15.11.66-15.07.67	242	6132	0.403
2	15.09.67-15.01.68	123	5948	0.826
3	15,02.68-15.05.68	90	5827	0.859
4	01.06.68-30.09.68	122	5689	0.506
5	25.11.68-31.05.69	188	5447	0.559
6	25.08.69-31.05.70	280	5082	0.969
7	27.07.70-15.06.71	324	4702	0.986
8	15.07.71-30.04.72	290	4383	0.987
9	01.07.72-05.05.73	309	4013	0.988
10	15.06.73-15.10.73	123	3850	0.974
11	15.11.73-04.05.74	171	3649	0.962
12	15.06.74-11.05.75	331	3277	0.971
13	15.06.75-07.05.76	327	2915	0.955
14	02.10.76-13.01.77	104	2664	0.952

*) for date of measurement 1st May, 1984

Table 11: Comparison with dosimetry results from surveillance Capsule 128

	Date of measurement	Spec. activity [Bq/g] measured	Spec. activity [Bq/g] calculated	C/E
Co-60 in copper wire (Cu-63(n,α))	1. 1.82 [1] 22.12.81 [2]	81 400 88 800	95 056 95 336	1.168 1.074
Mn-54 in iron wire (Fe-54(n,α))	1. 1.82 [1] 22.12.81 [2]	15 540 24 420	25 534 26 162	1.643 1.071
Mn-54 in material sampel	1. 1.82 [1]	22 500	25 534	1.135

[1]) measurement performed by Bundesgesundheitsamt, Institut für Strahlenhygiene, D-8042 Neuherberg

[2]) measurement performed by KRB-Gundremmingen

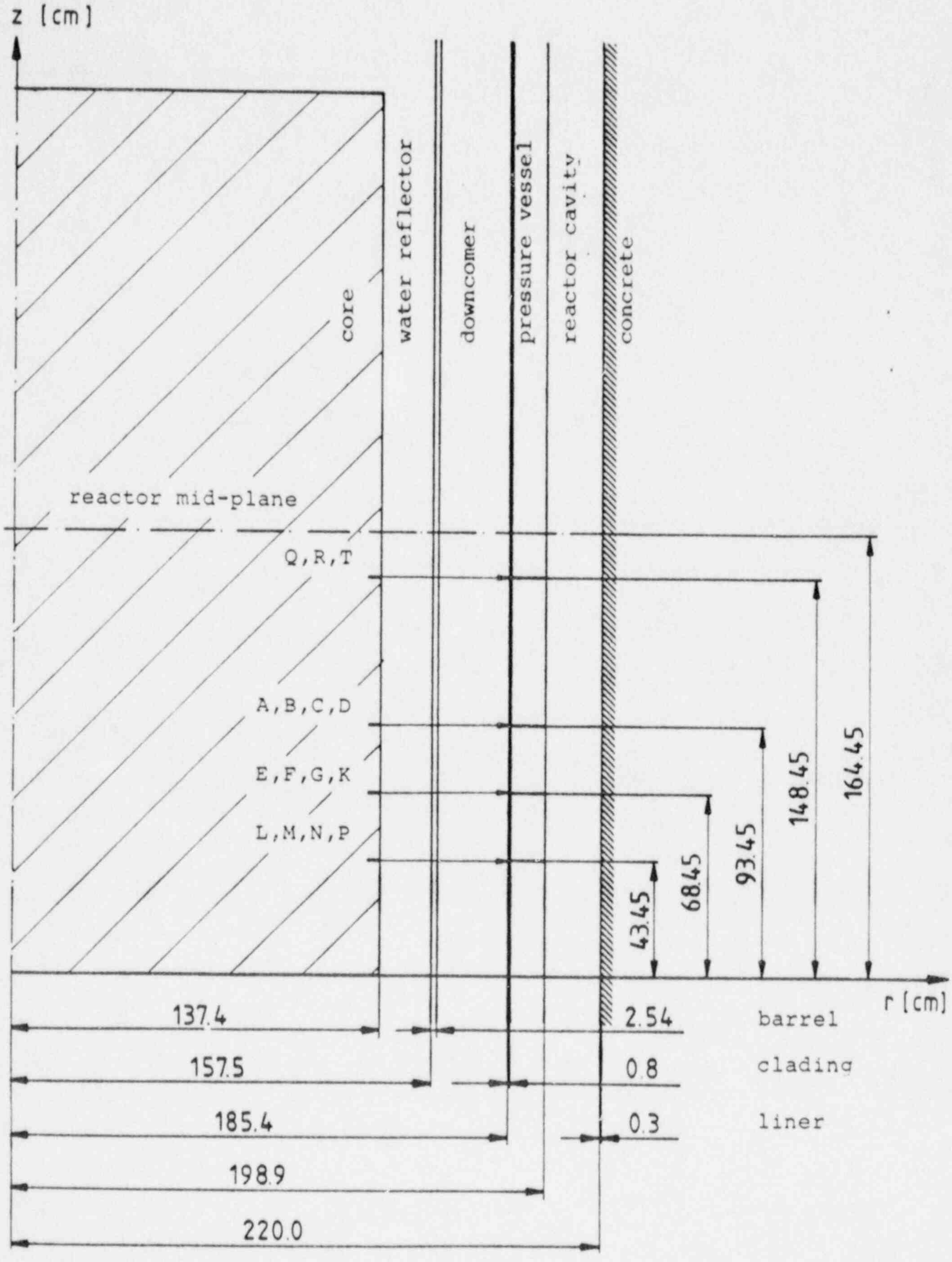

Fig. 1: (R-Z)-Geometry for KRB-A reactor with trepan positions

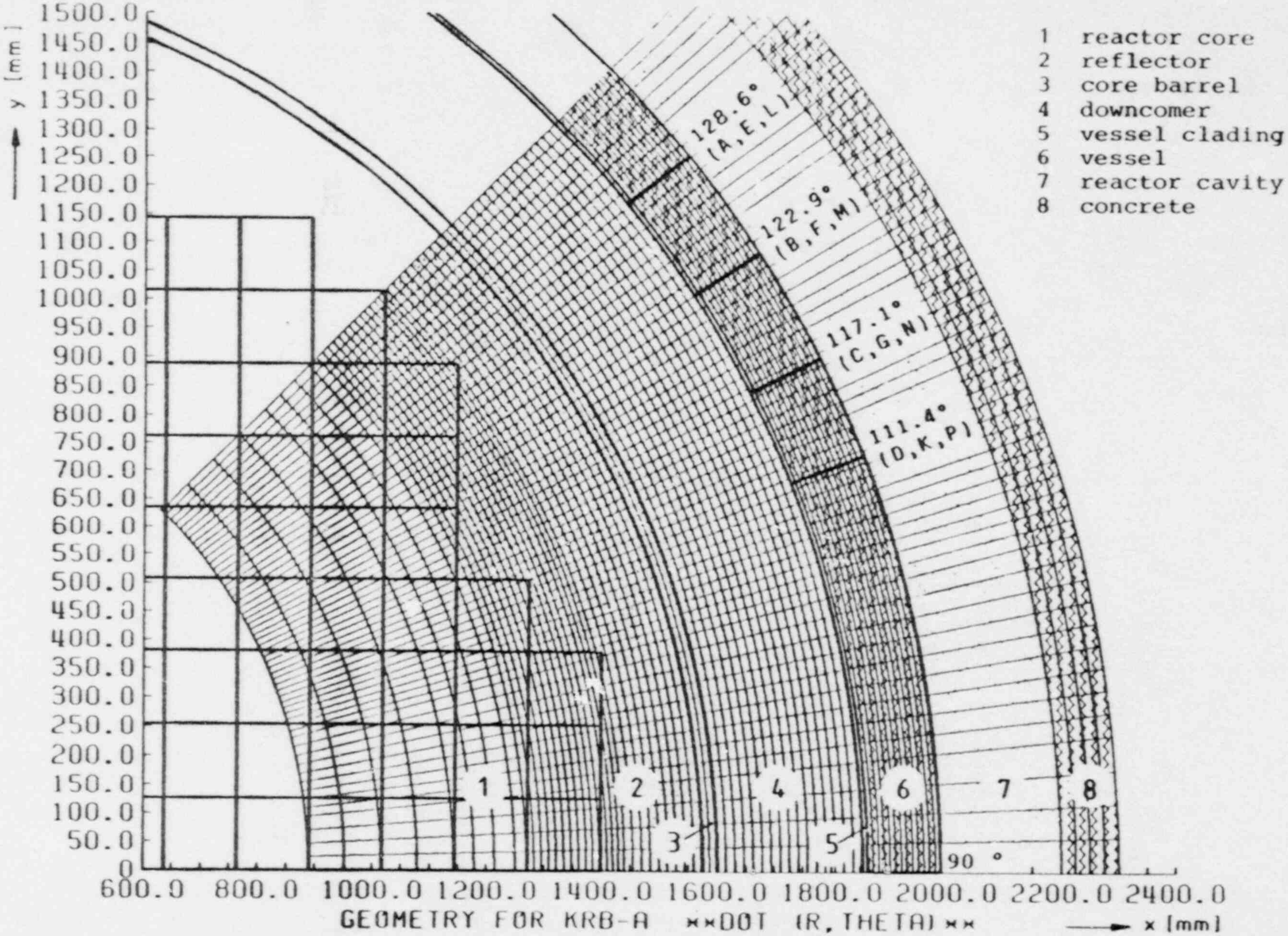

<u>Fig. 2:</u> (R-θ)-geometry for KRB/A reactor with trepan positions

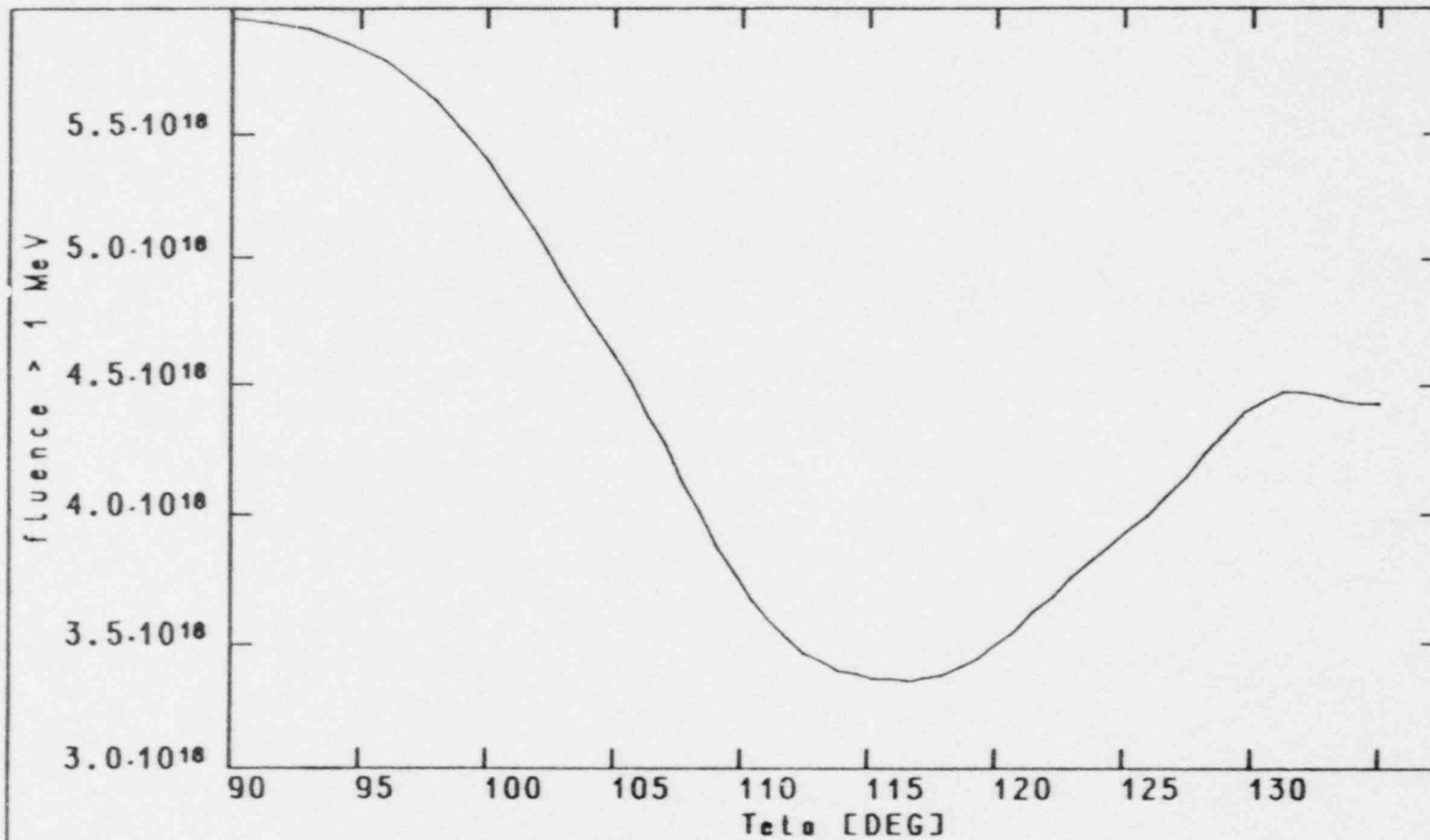

Fig. 3 : KRB/A, fluence E > 1 MeV azimuthal variation
PV-clad., Z=164 cm

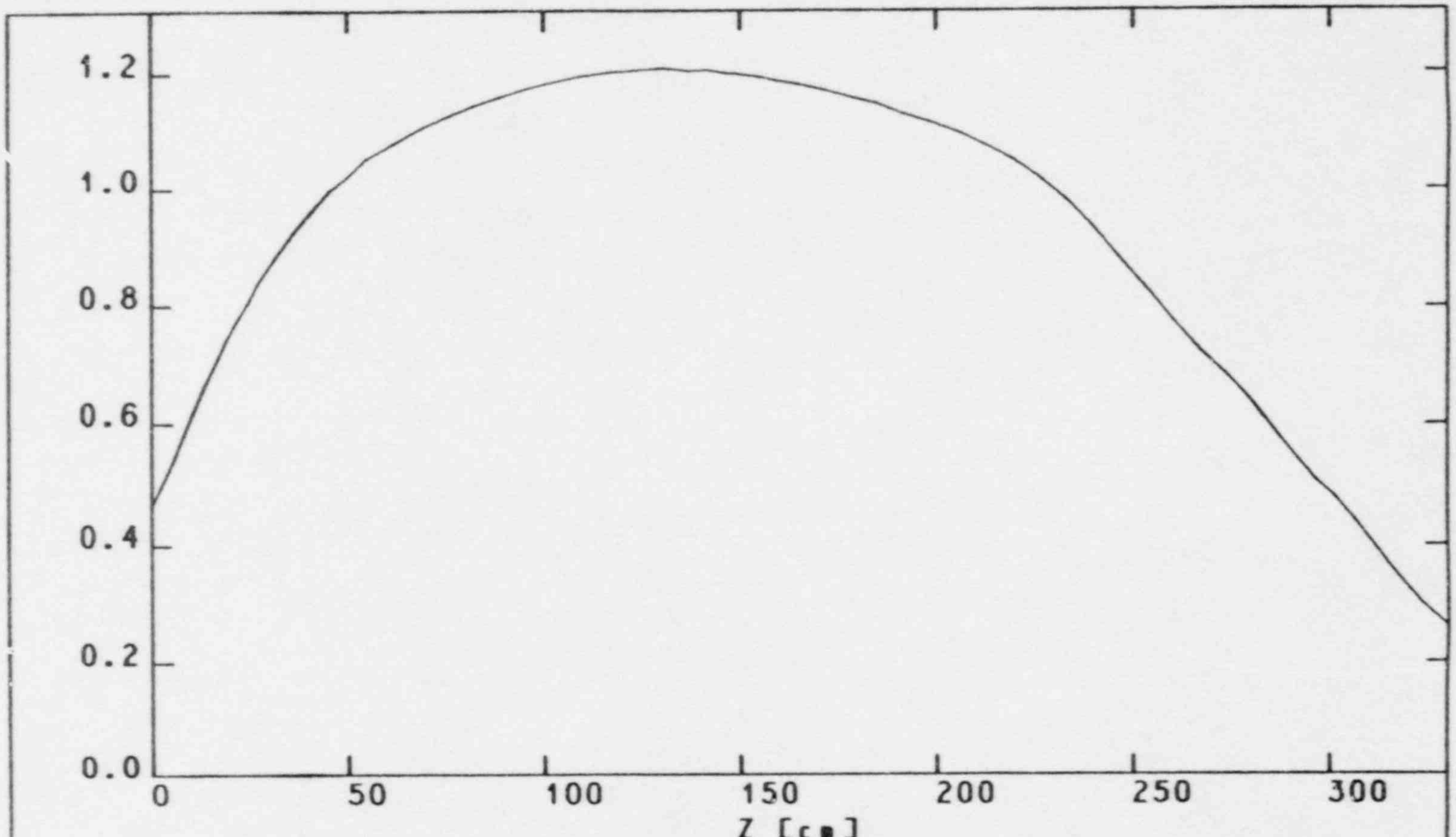

Fig. 4 : axial formfactor at inner vessel surface
(fluence E>1 MeV)

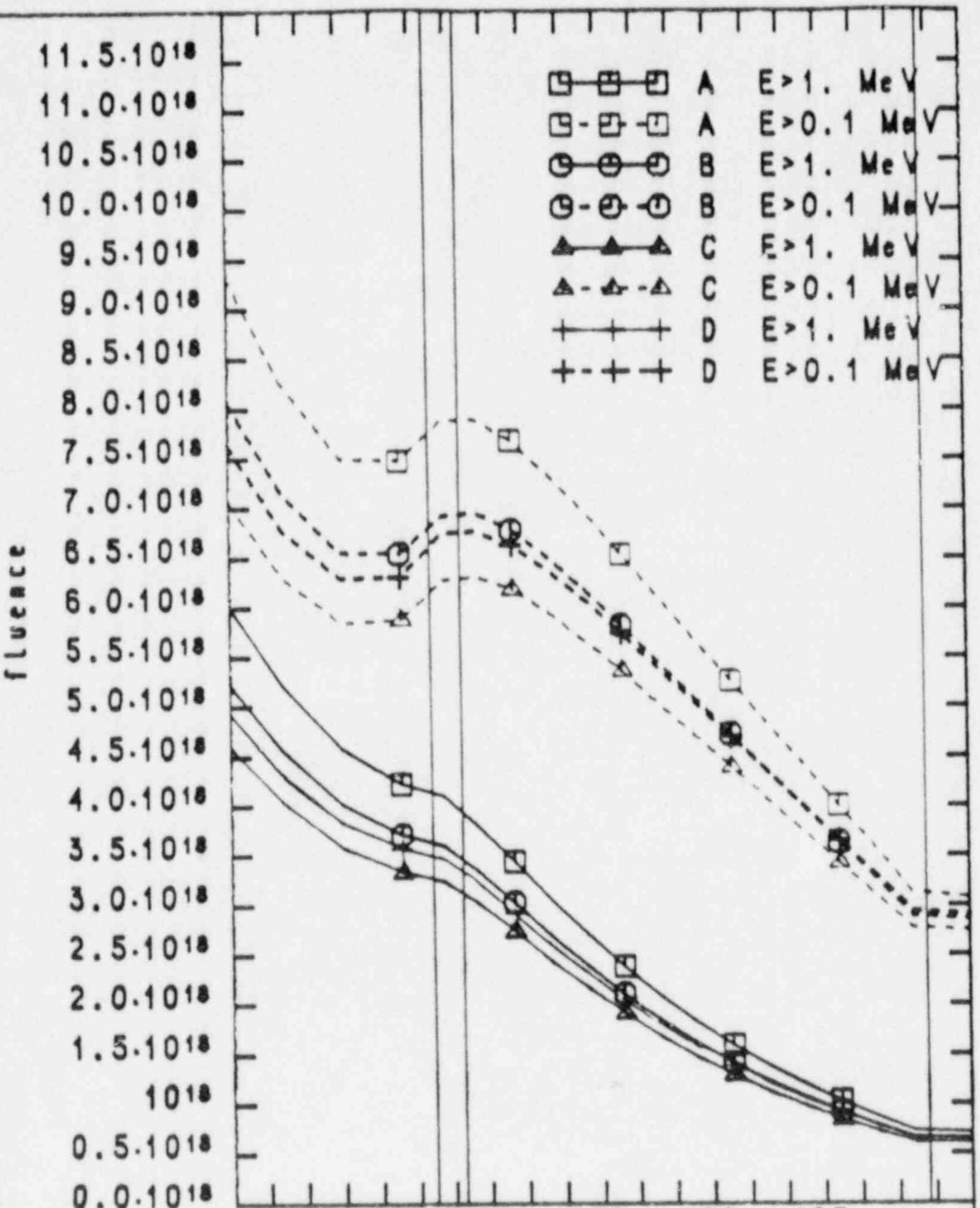

Fig.5 : fluence E>1. and E>0.1 MeV,
trepan A,B,C,D

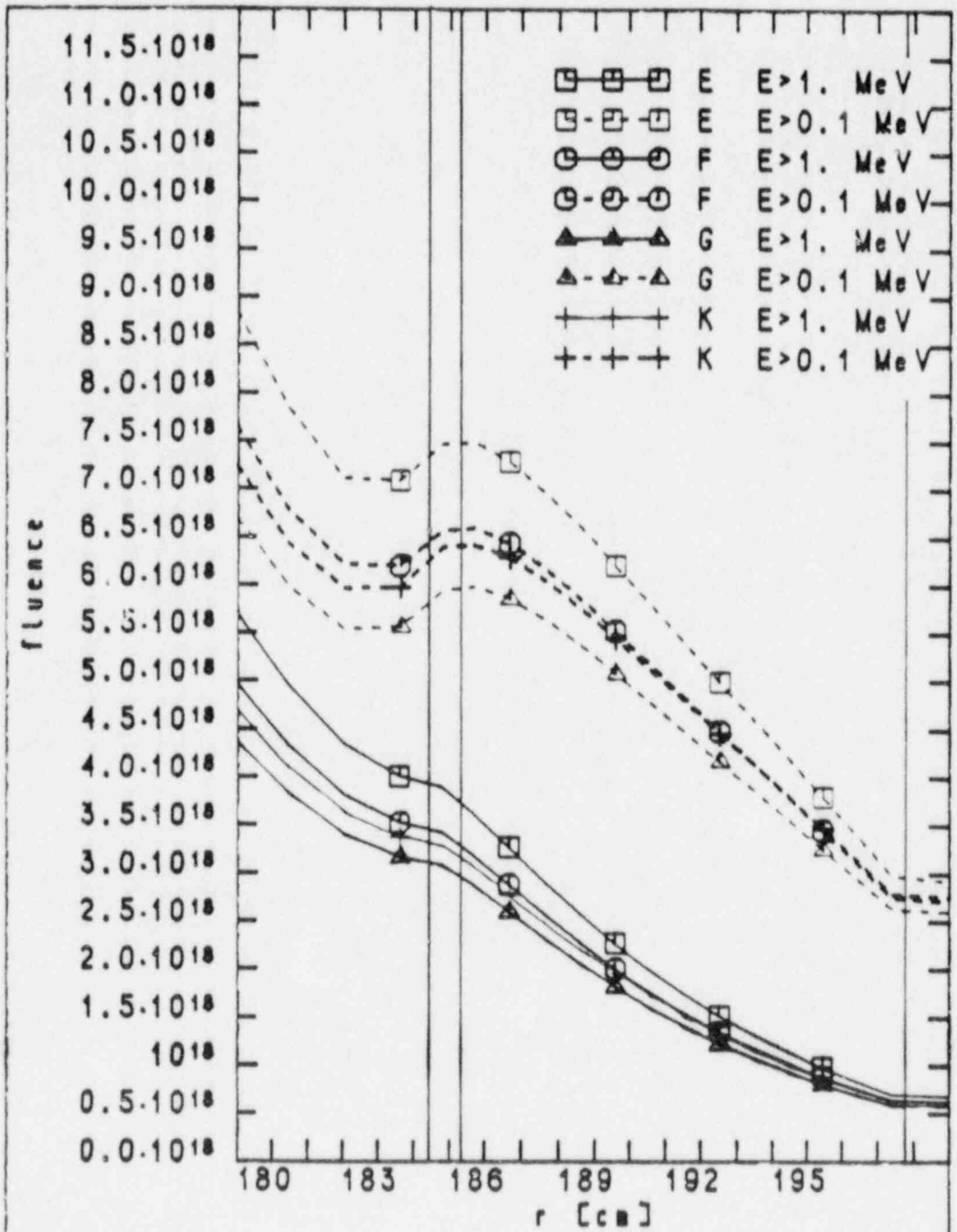

Fig.6 : fluence E>1. and E>0.1 MeV, trepan E,F,G,K

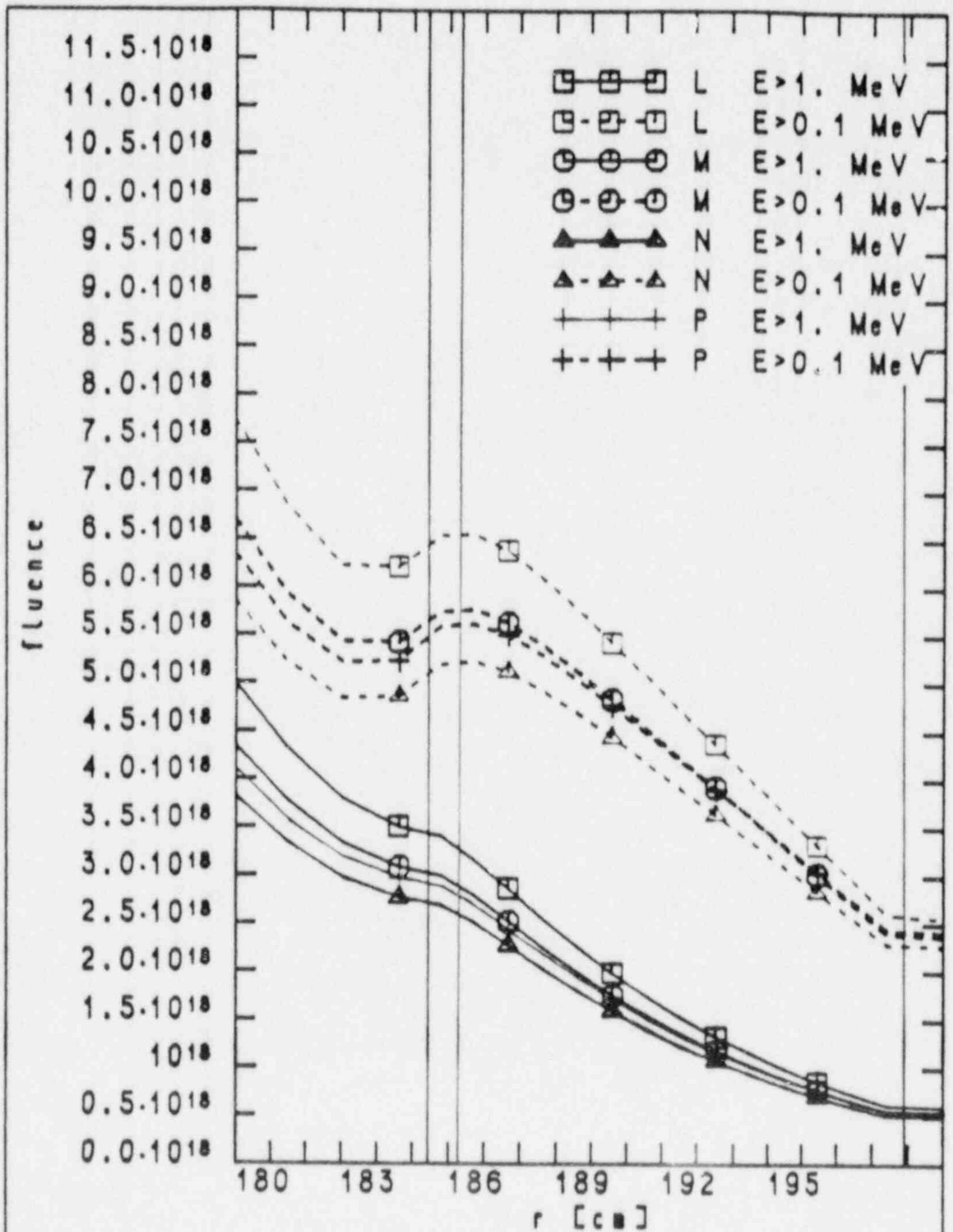

Fig.7 : fluence E>1. and E>0.1 MeV,
trepan L,M,N,P

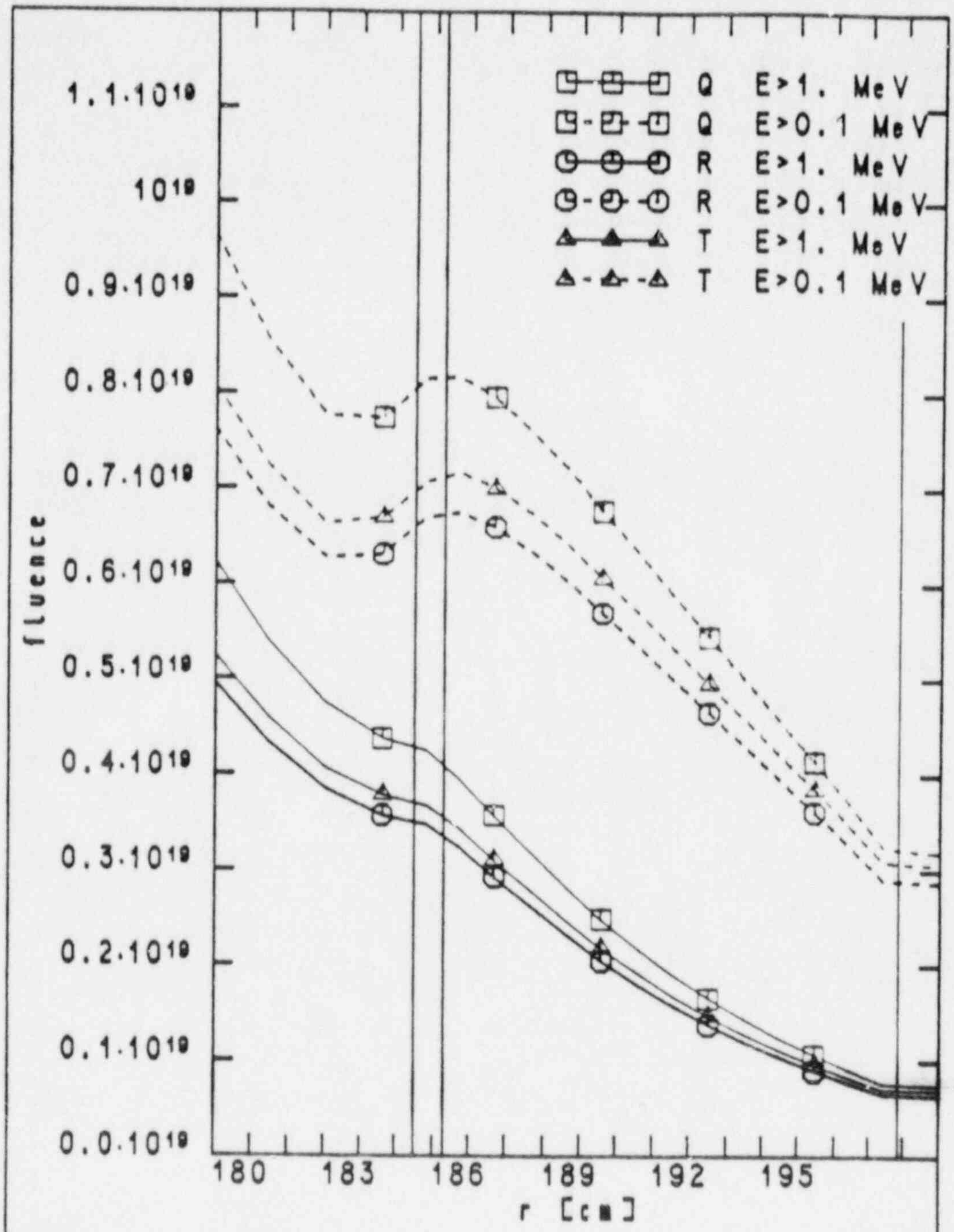

Fig.8 : Fluence E>1. and E>0.1 MeV, trepan Q,R,T

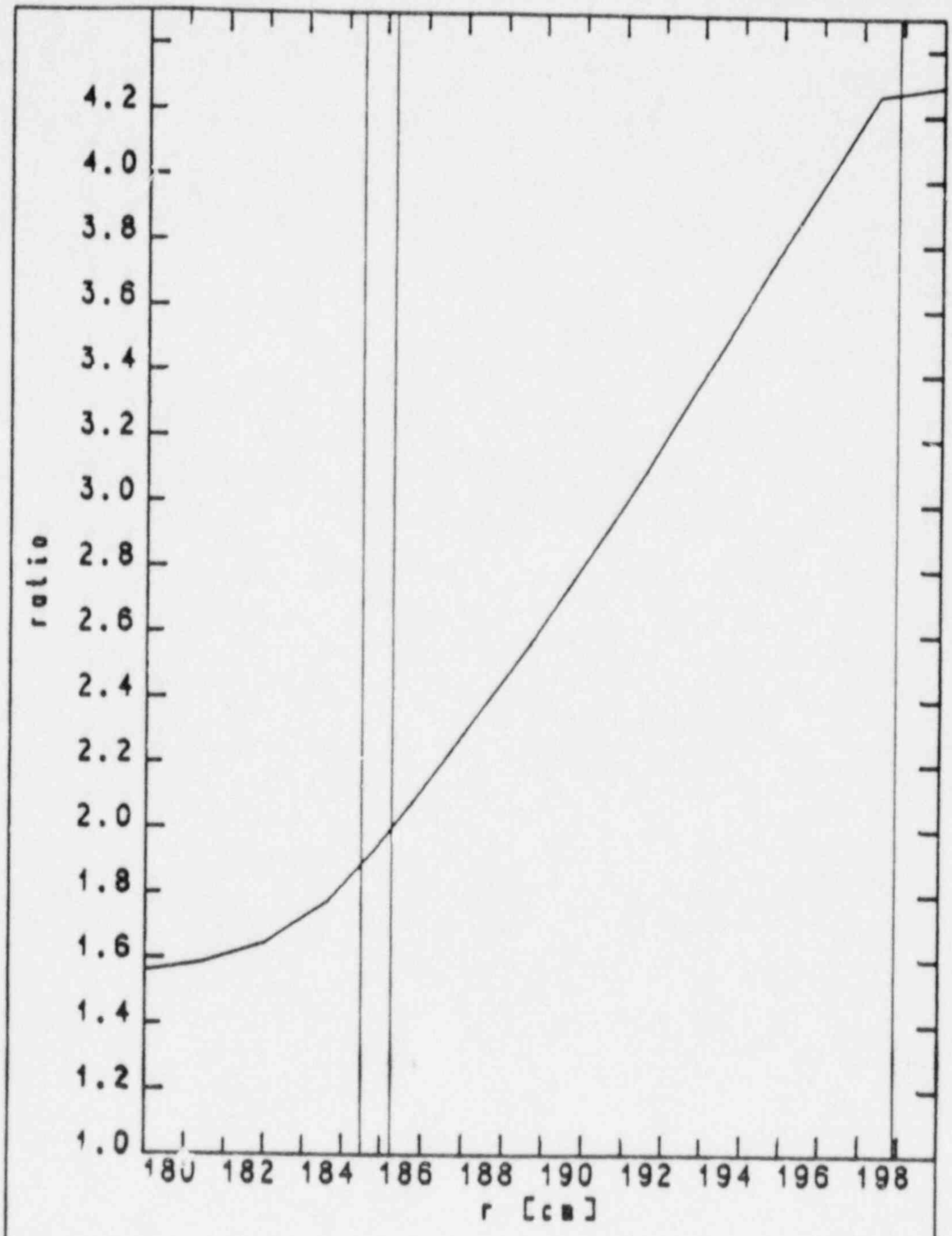

Fig.9 : E>0.1 to E>1. MeV fluence ratio (trepan A)

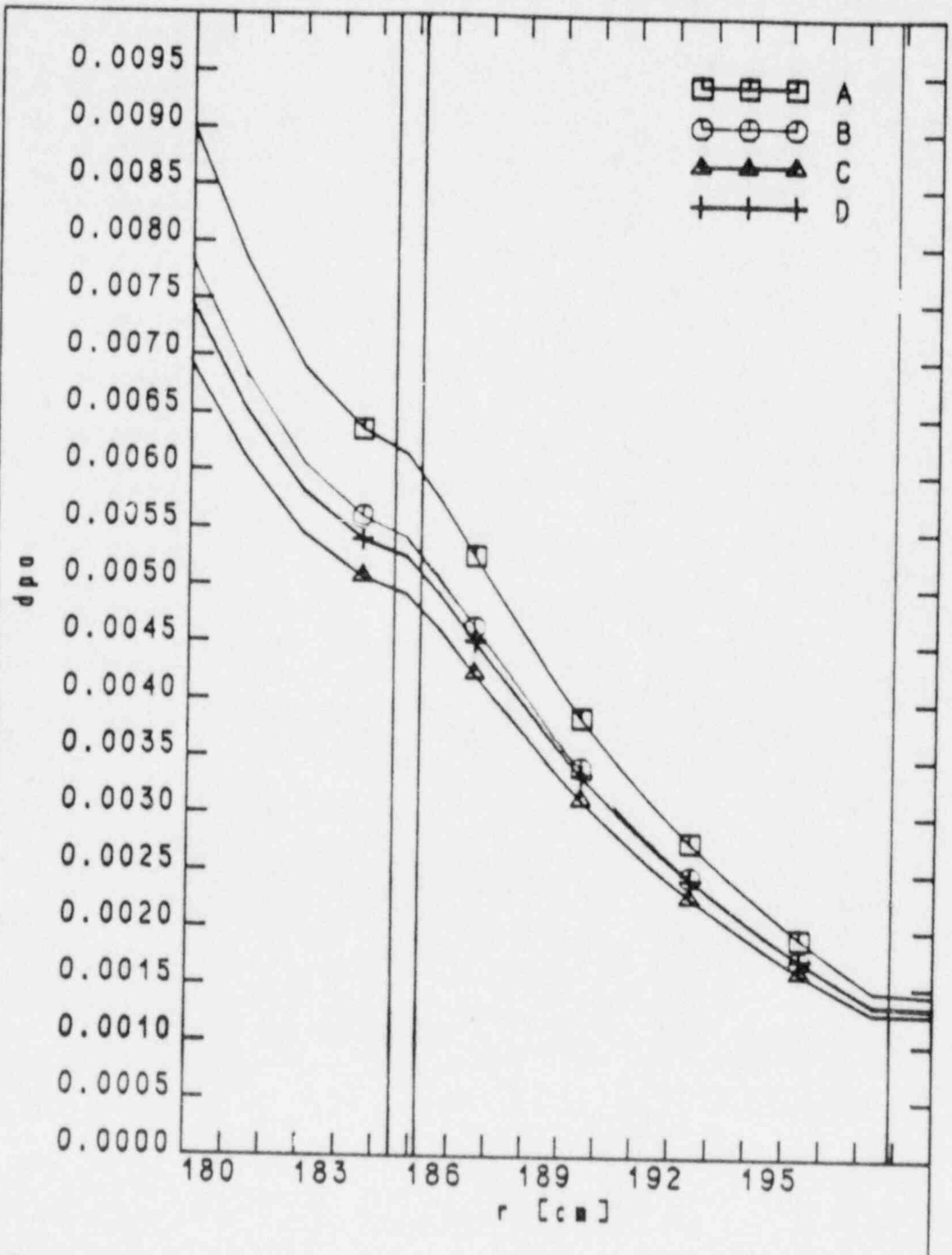

Fig.10: displacements per atom in iron trepan A,B,C,D

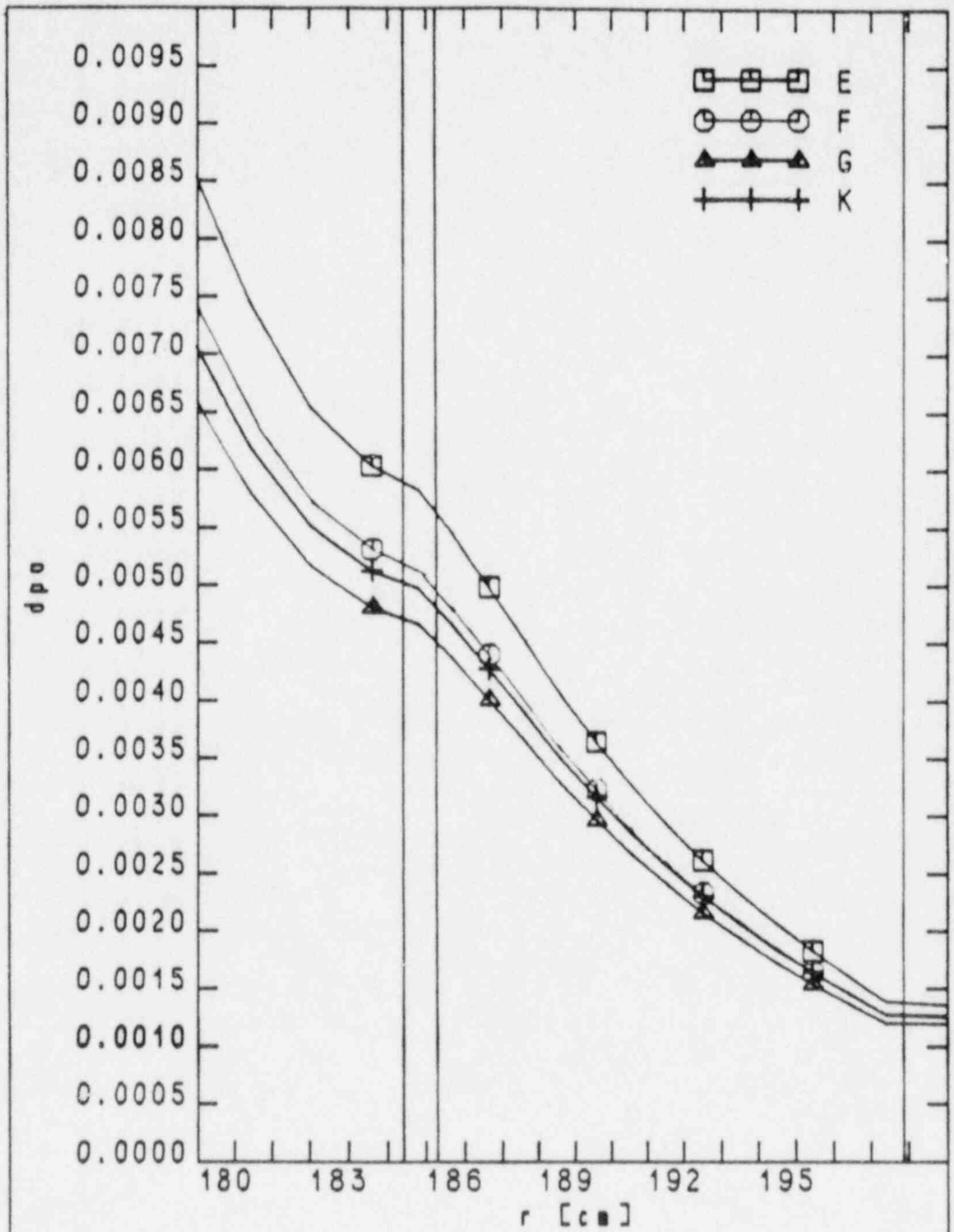

Fig.11: displacements per atom in iron trepan E,F,G,K

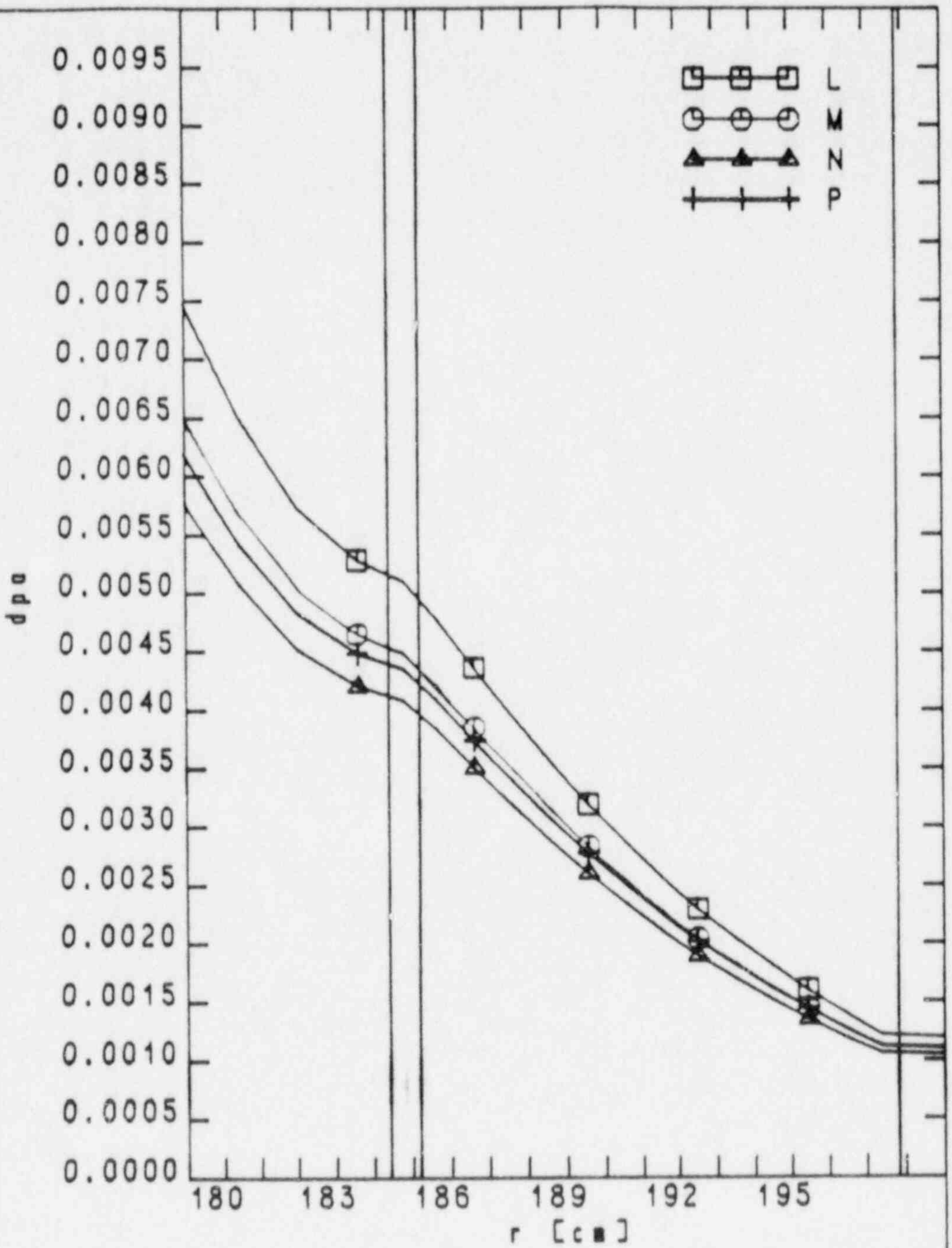

Fig.12: displacements per atom in iron trepan L,M,N,P

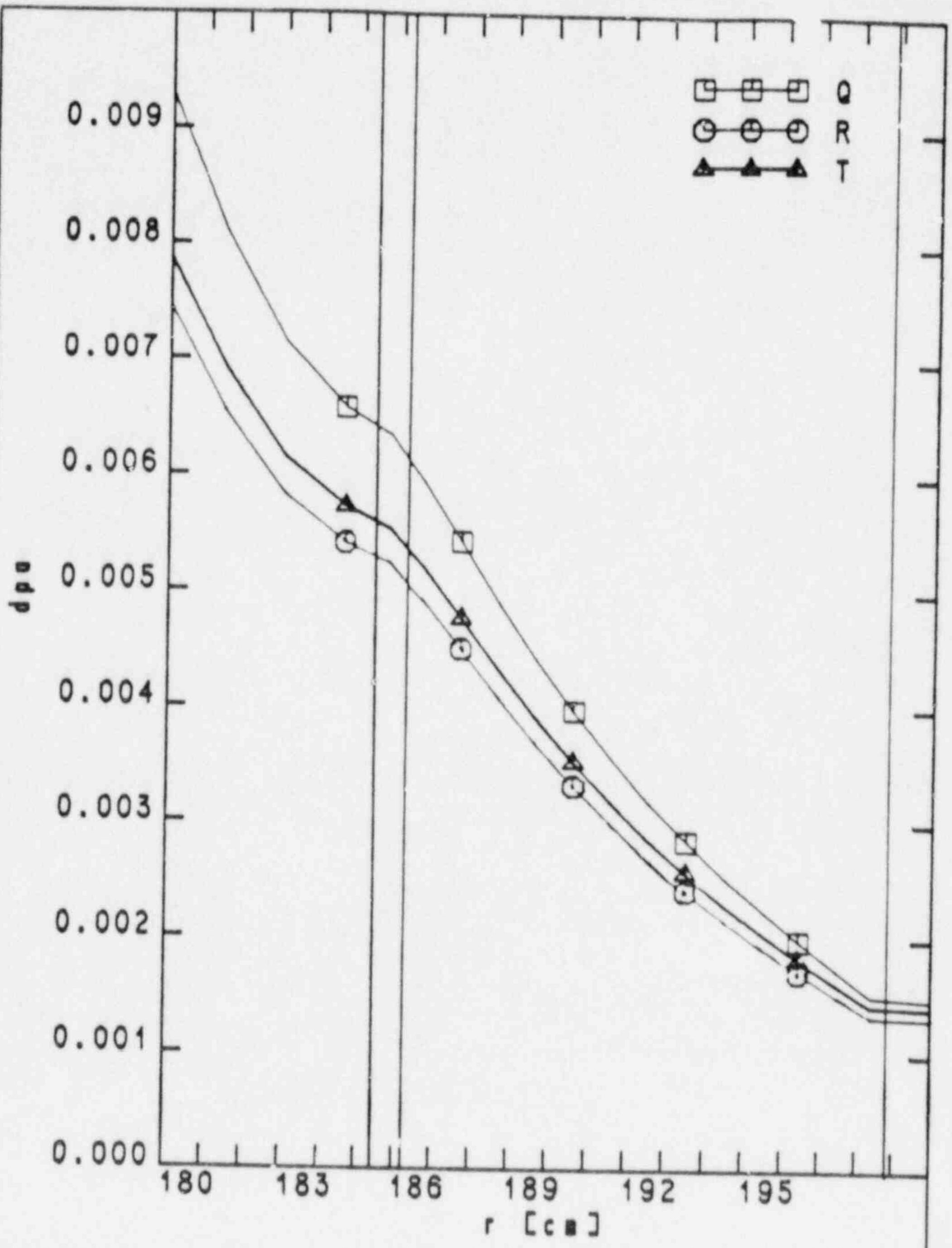

Fig.13 : displacements per atom in iron, trepan Q,R,T

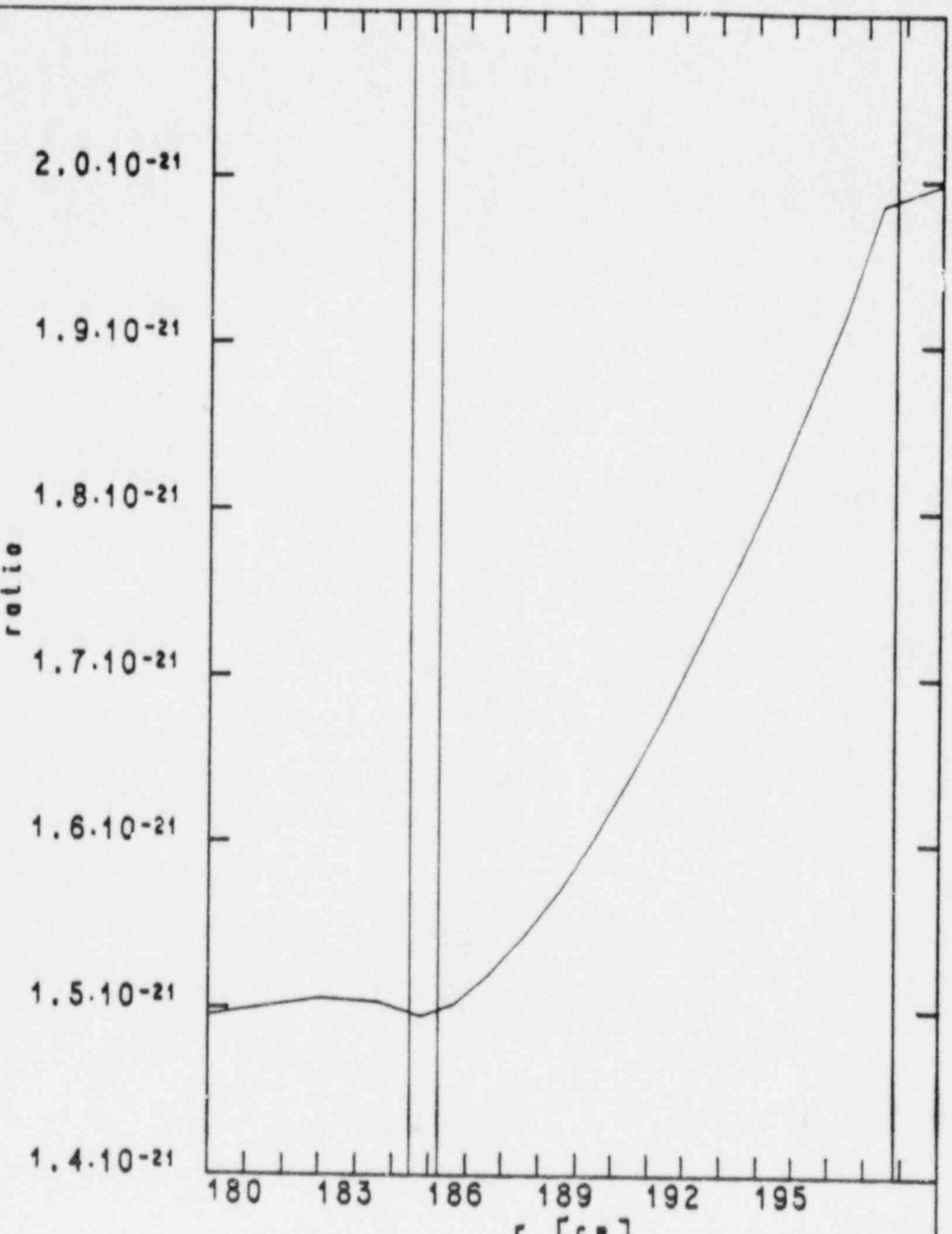

Fig.14 : dpa to E>1. MeV fluence ratio (trepan A)

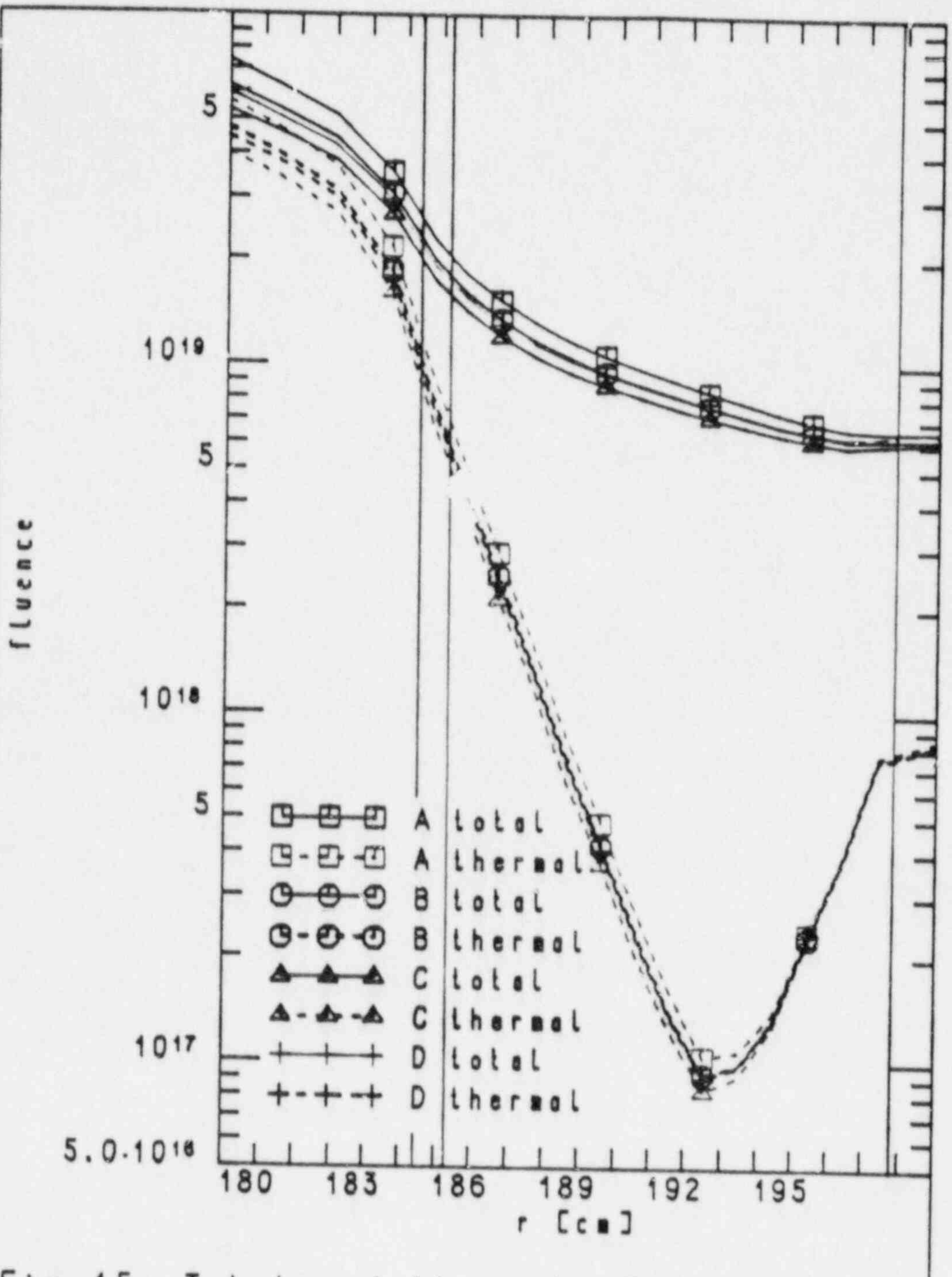

Fig.15: Total and thermal (E<0.414eV) fluence, trepan A,B,C,D

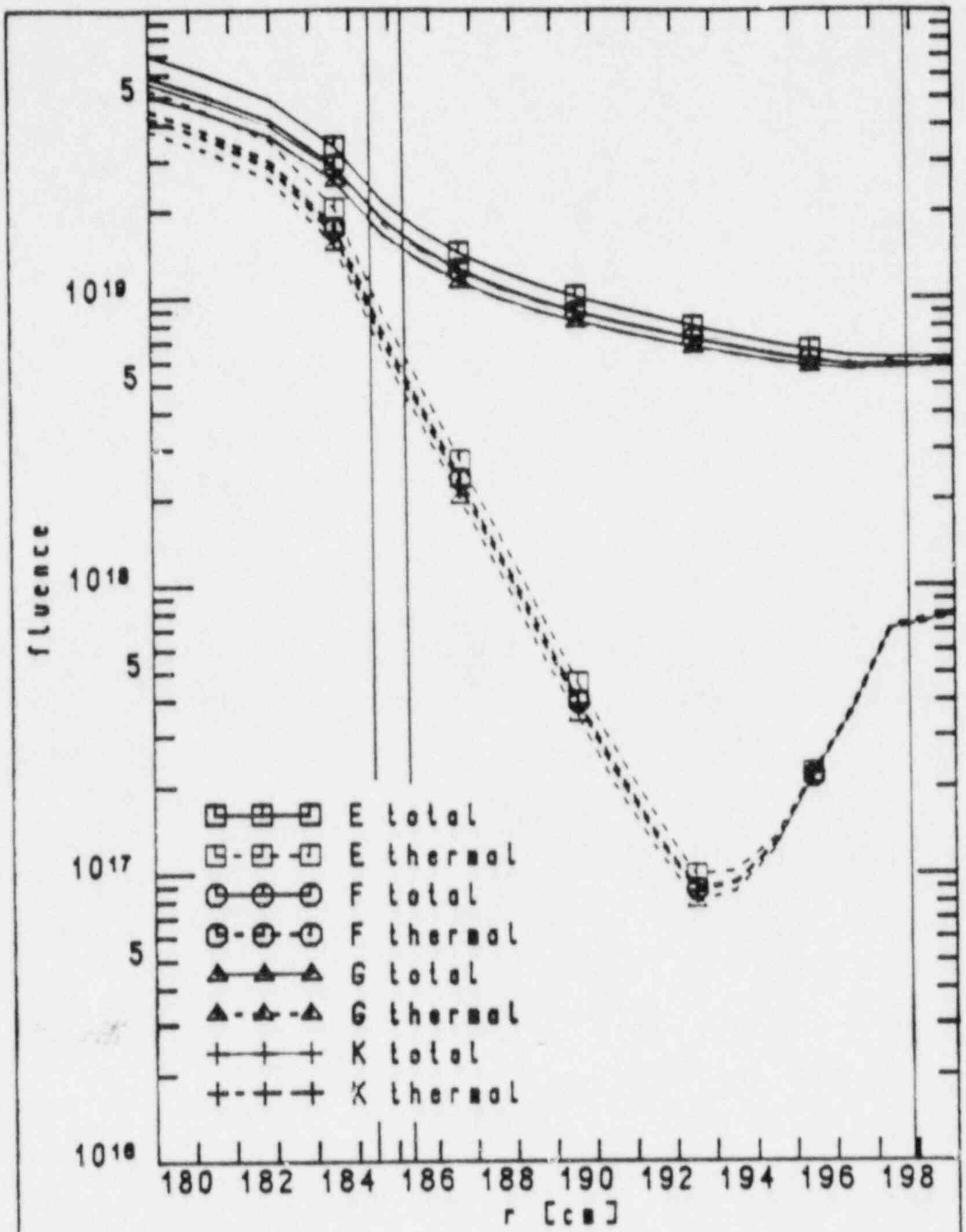

Fig.16: Total and thermal (E<0.414eV) fluence, trepan E,F,G,K

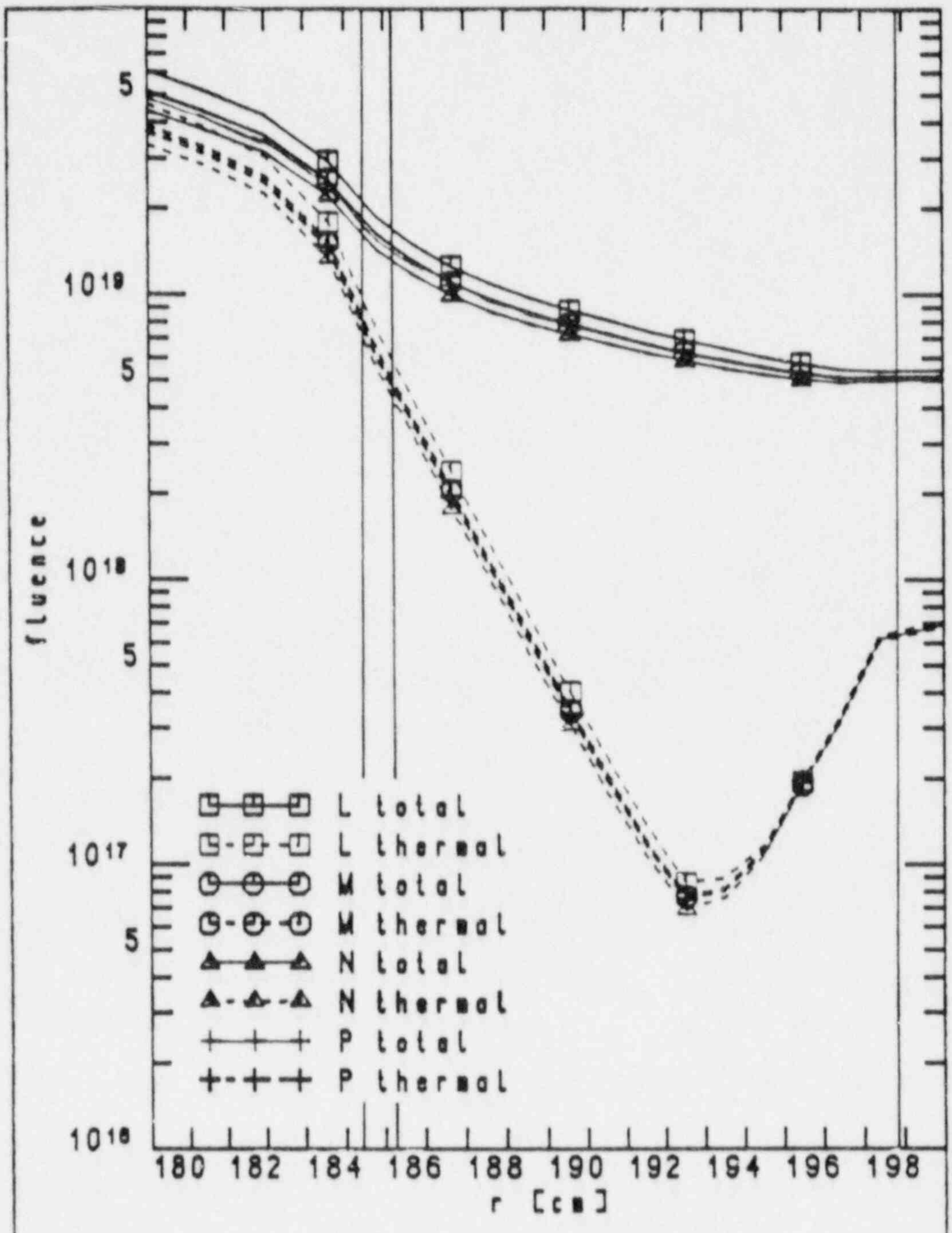

Fig.17: Total and thermal (E<0.414eV) fluence, trepan L,M,N,P

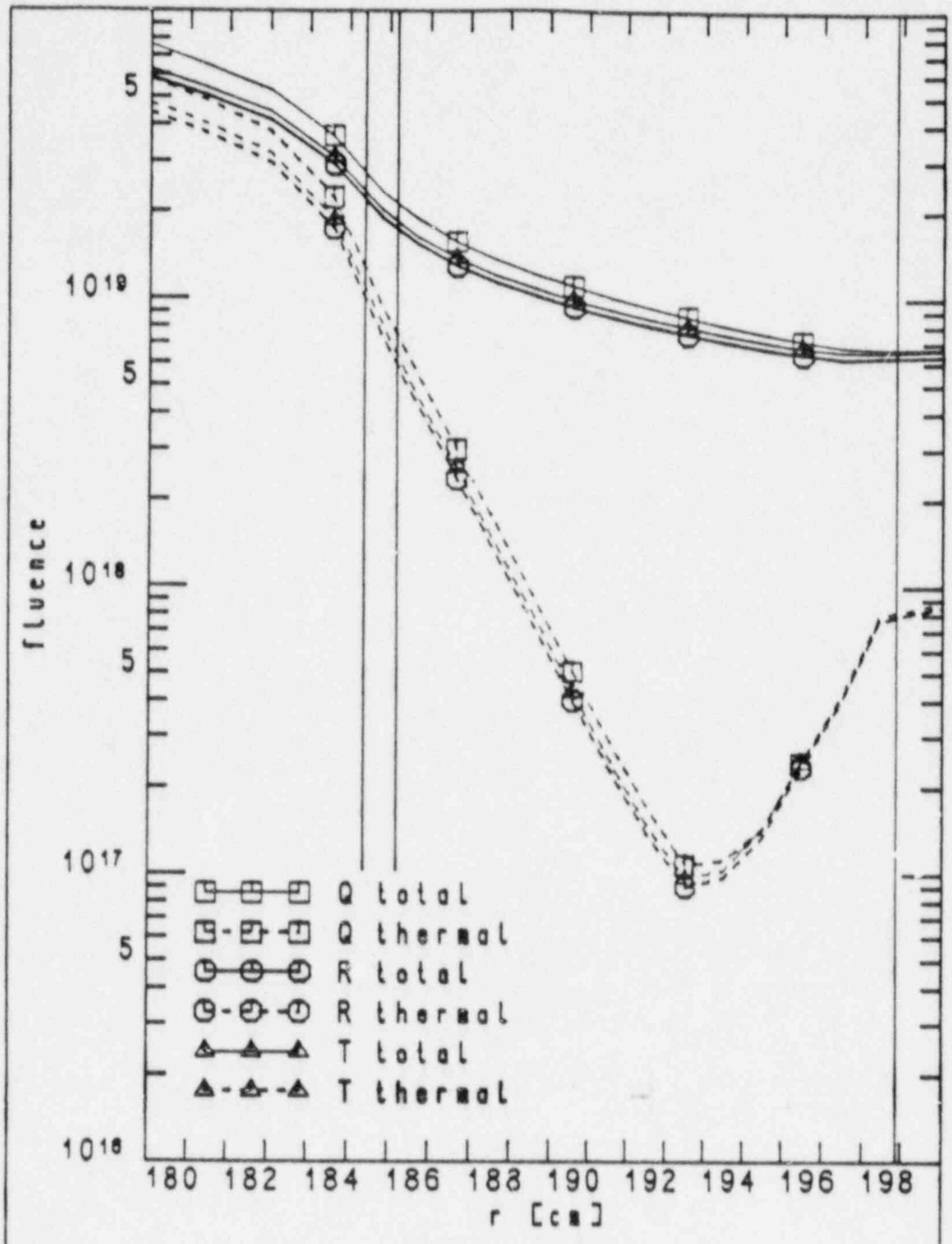

Fig.18 : Total and thermal (E<0.414eV) fluence, trepan Q,R,T

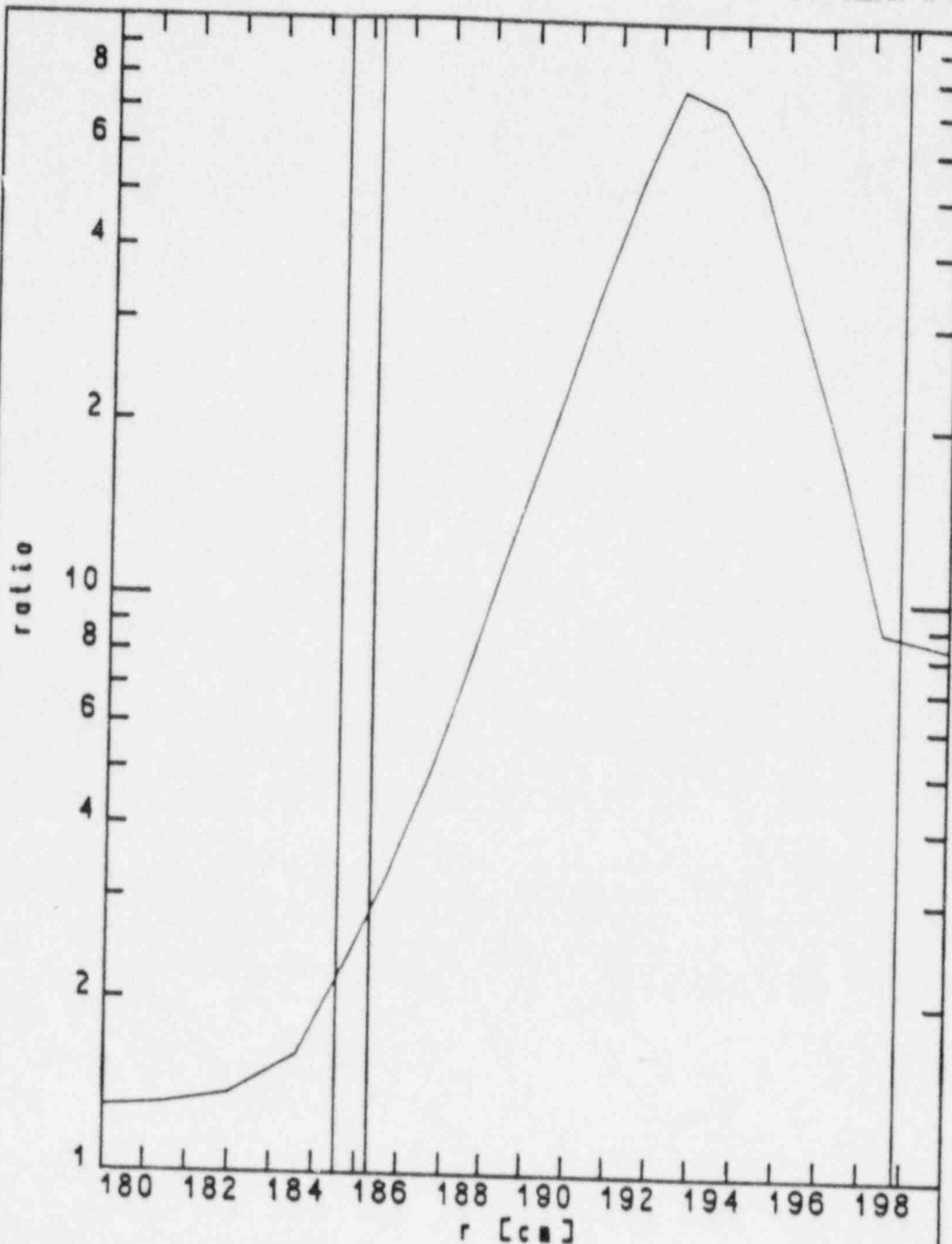

Fig.19 : total to thermal fluence ratio
(trepan A)

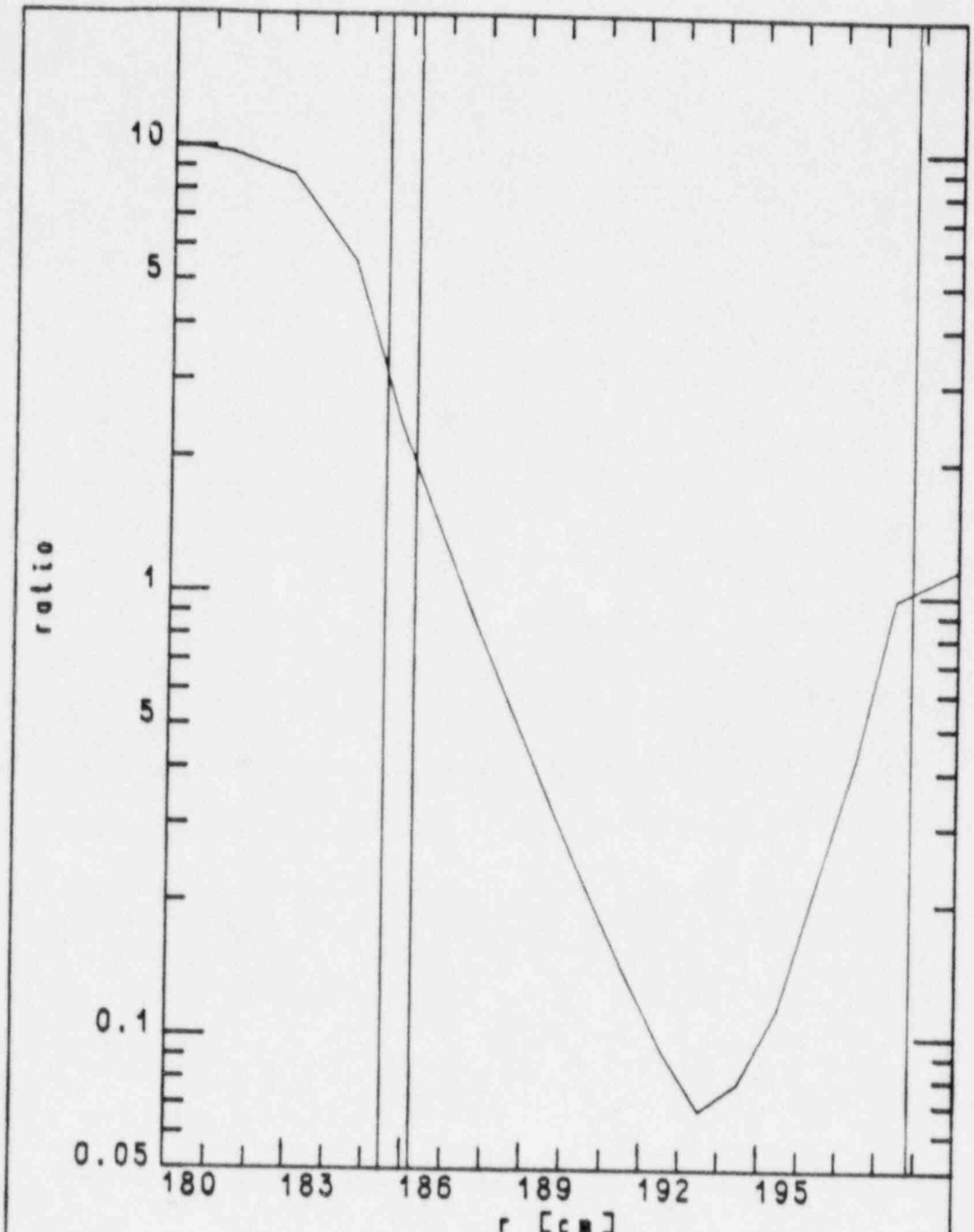

Fig.20 : thermal to E>1. MeV ratio
(trepan A)

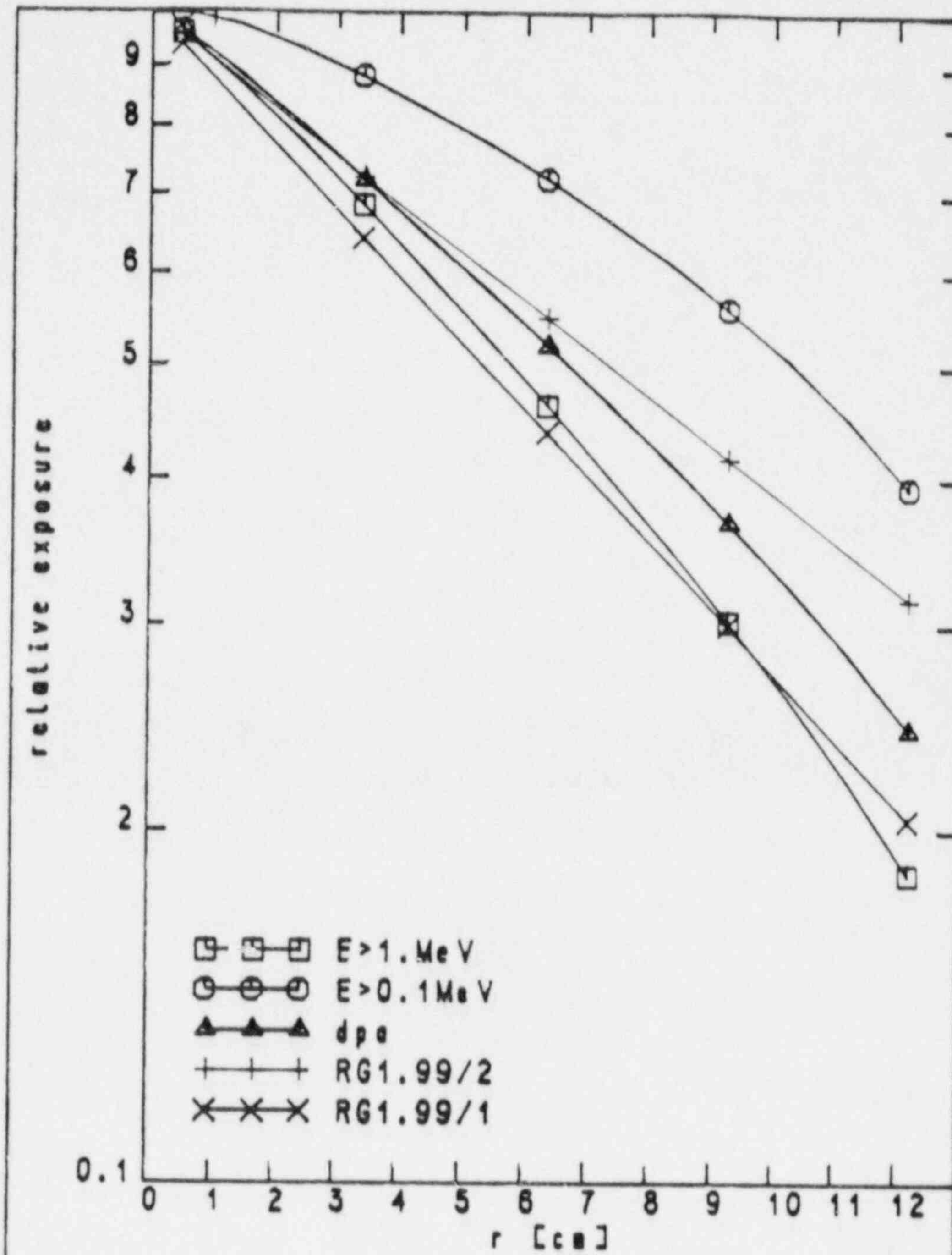

Fig.21: attenuation through vessel wall (trepan A)

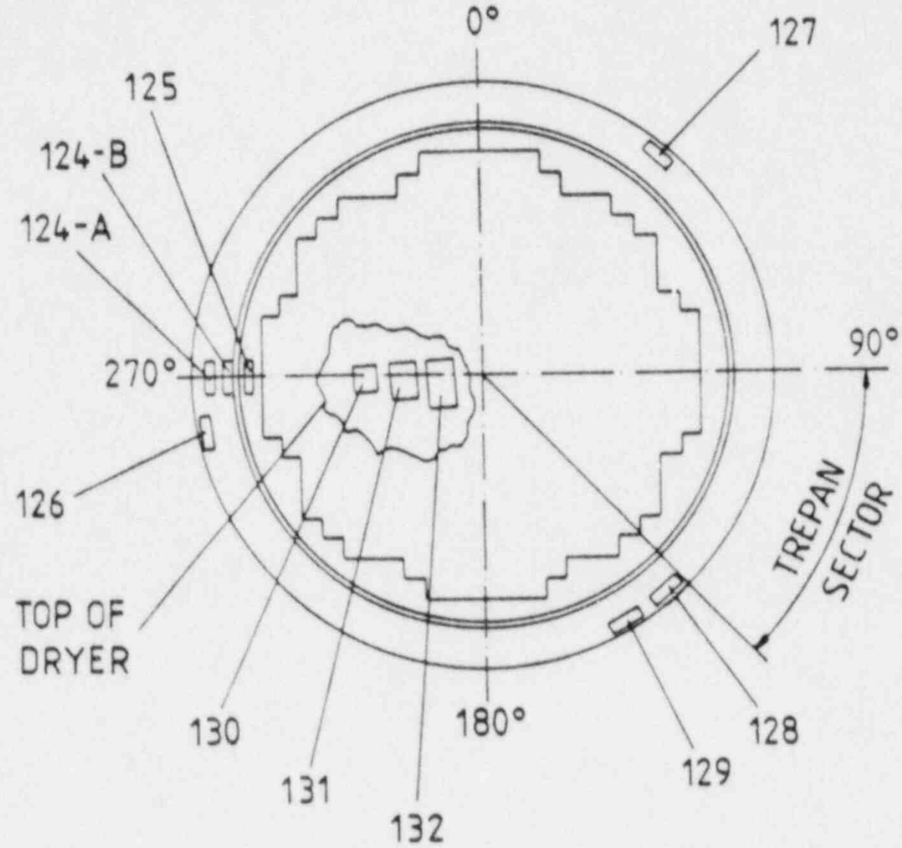

Figure 22: Location of baskets in reactor (ref. DWG-104R832)

Distribution List

Internal:

IKE:	G. Prillinger (5)	
	G. Hehn	
	D. Emendörfer	

External:

HEDL:	W.N. McElroy (20)	
	R. Gold	
	L. Kellogg	
NTIS:	(10 copies)	
NRC:	Division of Engineering Technology:	C.Z. Serpan
		A. Taboada
		M. Vagins
		5 File copies
DOE-RL/AMF:	K.R. Absher	
KFA-Jülich:	Postfach 1913, D-5170 Jülich:	W. Schneider
KGB:	Postfach 300, D-8871 Gundremmingen:	H. Flache
		Hiller
GKSS:	Postfach 160, D-2054 Geesthacht:	J. Alf
MPA:	Pfaffenwaldring 32, D-7000 Stuttgart 80:	J. Föhl
MEA:	J.W. Hawthorne	
EG&G:	J.W. Rogers	

NRC FORM 335
(2-84)
NRCM 1102
3201, 3202

U.S. NUCLEAR REGULATORY COMMISSION

BIBLIOGRAPHIC DATA SHEET

SEE INSTRUCTIONS ON THE REVERSE

1. REPORT NUMBER (Assigned by TIDC, add Vol. No., if any)
NUREG/CR-4791

2. TITLE AND SUBTITLE
NEUTRON SPECTRUM CALCULATION FOR THE GUNDREMMINGEN KRB/A REACTOR

3. LEAVE BLANK

4. DATE REPORT COMPLETED

MONTH	YEAR
October	1986

5. AUTHOR(S)
G. Prillinger

6. DATE REPORT ISSUED

MONTH	YEAR
November	1986

7. PERFORMING ORGANIZATION NAME AND MAILING ADDRESS (Include Zip Code)
Institut für Kernenergetik und Energiesysteme (IKE)
Universität Stuttgart
Pfaffenwaldring 31
D-7000 Stuttgart 80

8. PROJECT/TASK/WORK UNIT NUMBER

9. FIN OR GRANT NUMBER

10. SPONSORING ORGANIZATION NAME AND MAILING ADDRESS (Include Zip Code)
Division of Engineering Technology
Office of Nuclear Regulatory Research
U.S. Nuclear Regulatory Commission
Washington, DC 20555

11a. TYPE OF REPORT
Technical

b. PERIOD COVERED (Inclusive dates)

12. SUPPLEMENTARY NOTES

13. ABSTRACT (200 words or less)
To determine neutron exposure of several trepans taken from the pressure vessel of the nuclear power plant Gundremmingen Block A (KRB/A) a three-dimensional neutron spectrum analysis has been performed.
The trepans have been taken at different axial and azimuthal positions within the 90 - 135 degree octant of the vessel. To define neutron exposure after a more than ten years' operation-time a complete analysis of the reactor power-time history and of the three-dimensional burnup distributions at the begin and the end of each reactor cycle had to be performed. Neutron exposure parameters such as fast fluence ($E > 1.0$ and $E > 0.1$ MeV) and dpa have been calculated using the DOT 4.2 code.
To confirm the results of the transport calculations, calculated and measured Mn-54 activities of the trepans have been compared. Additionally dosimetry results from surveillance capsules have been analysed.
The attenuation of neutron exposure within the KRB/A vessel wall is discussed in context with the formulas proposed in Regulatory Guide 1.99 Revision 1 and 2.

14. DOCUMENT ANALYSIS - a. KEYWORDS/DESCRIPTORS
LWR pressure vessel surveillance
Neutron spectrum calculation
Dosimetry reevaluations

b. IDENTIFIERS/OPEN-ENDED TERMS

15. AVAILABILITY STATEMENT
Unlimited

16. SECURITY CLASSIFICATION
(This page)
Unclassified
(This report)
Unclassified

17. NUMBER OF PAGES

18. PRICE